MULTI-BAND OFDM UWB RECEIVER
WITH NARROWBAND INTERFERENCE SUPPRESSION

A Dissertation

by

BURAK KELLECİ

Submitted to the Office of Graduate Studies of
Texas A&M University
in partial fulfillment of the requirements for the degree of

DOCTOR OF PHILOSOPHY

December 2007

Major Subject: Electrical Engineering

MULTI-BAND OFDM UWB RECEIVER
WITH NARROWBAND INTERFERENCE SUPPRESSION

A Dissertation

by

BURAK KELLECİ

Submitted to the Office of Graduate Studies of
Texas A&M University
in partial fulfillment of the requirements for the degree of

DOCTOR OF PHILOSOPHY

Approved by:

Chair of Committee,	Aydın İlker Karşılayan
Committee Members,	Edgar Sánchez-Sinencio
	Laszlo Kish
	Ricardo Gutierrez-Osuna
Head of Department,	Costas N. Georghiades

December 2007

Major Subject: Electrical Engineering

ABSTRACT

Multi-Band OFDM UWB Receiver
with Narrowband Interference Suppression. (December 2007)
Burak Kelleci, B.S., Istanbul Technical University;
M.S., Istanbul Technical University
Chair of Advisory Committee: Dr. Aydın İlker Karşılayan

A multi band orthogonal frequency division multiplexing (MB-OFDM) compatible ultra wideband (UWB) receiver with narrowband interference (NBI) suppression capability is presented. The average transmit power of UWB system is limited to -41.3 dBm/MHz in order to not interfere existing narrowband systems. Moreover, it must operate even in the presence of unintentional radiation of FCC Class-B compatible devices. If this unintentional radiation resides in the UWB band, it can jam the communication. Since removing the interference in digital domain requires higher dynamic range of analog front-end than removing it in analog domain, a programmable analog notch filter is used to relax the receiver requirements in the presence of NBI. The baseband filter is placed before the variable gain amplifier (VGA) in order to reduce the signal swing at the VGA input. The frequency hopping period of MB-OFDM puts a lower limit on the settling time of the filter, which is inverse proportional to notch bandwidth. However, notch bandwidth should be low enough not to attenuate the adjacent OFDM tones. Since these requirements are contradictory, optimization is needed to maximize overall performance. Two different NBI suppression schemes are tested. In the first scheme, the notch filter is operating for all sub-bands. In the second scheme, the notch filter is turned on during the sub-band affected by NBI. Simulation results indicate that the UWB system with the first and the second suppression schemes can handle up to 6 dB and 14 dB more NBI power, respectively.

The results of this work are not limited to MB-OFDM UWB system, and can be applied to other frequency hopping systems.

To My Family

ACKNOWLEDGMENTS

First and foremost, I would like to acknowledge Dr. Aydın İlker Karşılayan, for his precious encouragement and guidance during my work at Texas A&M University. I have benefited from his foresight, creativity and technical insight. His constant assistance made this work possible.

I would also like to thank to my committee members for their help and review of this work. I am also grateful to Dr. Edgar Sánchez-Sinencio for his helpful suggestions and support. I have benefited many times from his years of experience in analog design. I want also to thank Dr. Laszlo Kish, who helped me to build solid noise background. I would also thank Dr. Erchin Serpedin for his help and valuable discussion during weekly meetings.

I owe special thanks to Kai Shi for the discussion on communication systems. I would also like to pay tribute to the analog designers of MB-OFDM UWB, Timothy Wayne Fisher for low-pass and band-reject filter, Haitao Tong for synthesizer, Sivasankari Krishnanji for variable gain amplifier, Choonghoon Lee for analog-to-digital converter and Pushkar Sharma for low noise amplifier and mixer.

I am honored to be a member of Analog and Mixed Signal group, and I want to thank everybody for their friendship.

I am also indebted to Dr. Selim Günçer for his technical support.

I want to thank my friends in College Station, Sönmez and Jessica Şahutoğlu, Fatih Çakıroğlu, Salih Bariş Öztürk, Ozan Özener, Güven Yapıcı and his brother Murat for their friendship.

Finally, I must reserve special thanks to my family; my wife Ülker, my parents Aslışen and Hüseyin Avni and my brother Orçin. Their love and support gives me strength all my life.

TABLE OF CONTENTS

CHAPTER Page

CHAPTER Page

LIST OF TABLES

TABLE Page

LIST OF FIGURES

FIGURE Page

FIGURE Page

FIGURE Page

FIGURE Page

FIGURE Page

FIGURE Page

CHAPTER I

INTRODUCTION

The increasing demand of higher communication rate is answered by increasing modulation complexity and bandwidth. Dividing signal space into smaller pieces increases number of information points, which results in higher bit-rate communication in the expense of being susceptible to noise. To achieve reliable and error-free communication, either signal power is increased or communication distance is reduced. Increasing precious bandwidth without increasing frequency of operation is usually less desired due to coexistence with existing systems. Frequency allocation of wireless systems is controlled by national and international institutes. For example, in USA Federal Communications Commission (FCC) regulates any wireless communication. Currently, frequencies from 9 Hz to 275 GHz are allocated by different wireless systems. Historically, the upper frequency is increased when there is a need for new operating frequencies and technology exists to utilize high frequency operation. Therefore, applications that require higher bandwidth operate also at higher frequencies. In 2002, this rule is changed by FCC by opening the frequency band from 3.1 GHz to 10.6 GHz for ultra-wideband (UWB) communication under the restrictions that the transmit power should not exceed the existing -41.3 dBm/MHz limit for unintentional radiation of FCC Class-B compatible electronic devices [1]. In response, the IEEE formed a committee to release a standard for UWB communication. Currently, there are two different proposals. One is based on spread spectrum [2] and the other is based on the frequency hopping orthogonal frequency division multiplexing (MB-OFDM) [3].

FCC limits the transmit power of UWB system to -41.3 dBm/MHz to guarantee

---

This dissertation follows the style of *IEEE Journal of Solid-State Circuits*.

existing narrowband systems are not affected. However, the unintentional radiation of FCC Class-B compatible devices are also limited to -41.3 dBm/MHz. Since this FCC limit is higher than proposed UWB sensitivity, any equipment can pass FCC regulations and degrade UWB communication, if this unwanted disturbance is in the UWB band. The amount of degradation depends on the signal level, interference power and frequency. The frequency and power levels of interferences are found in the electromagnetic compatibility (EMI) reports submitted to FCC. For example, the EMI report of a local area network card shows emissions of -49.8 dBm at 3.75 GHz [4], which is directly in the UWB band. NBI sources are not limited to computer components, even common household devices such as electric shavers and hair dryers emit radiation that can jam UWB communication [5]. Therefore, the suppression of this unwanted blocker is crucial for reliable operation of UWB communication.

A. Background and Motivation

Interference suppression is widely used in spread spectrum systems. Its inherent processing gain provides interference rejection capability. However, if the interfering signal is powerful, even spreading the spectrum may not be enough for reliable communication. Since spread spectrum systems use the entire dedicated band, blocking by an in-band interference is more likely than conventional narrowband systems. Therefore, narrowband in-band interference (NBI) rejection techniques for spread spectrum were well examined in the literature. The rejection algorithms are based on adaptive notch filtering. Since NBI is characterized by spikes in the spectrum, the adaptive notch filter places a notch at the NBI location. The suppression schemes are classified in two main categories, one is based on estimation-type filters and the other is based on transform domain filtering. Estimation type filters make the samples

uncorrelated by whitening the received signal [6], [7]. In [8], a digital whitening filter is used to improve receiver performance. Filter coefficients are selected by Wiener or maximum entropy algorithm. The results indicate 12 dB SNR improvement when the signal-to-interference ratio is lower than 0 dB. Continuous wave interference rejection technique for spread spectrum system is analyzed in [9]. The presented method is based on tracking interference using a PLL and generates an estimate of interfering signal. This estimate is then used to remove the interfering signal. In transform domain filtering, the received signal is converted to frequency domain using real-time Fourier transform. The interference is detected by comparing the peak level of the spectrum with a predetermined level and removed by forcing the affected bins to zero. After that, the time domain data is obtained by inverse Fourier transform. The effect of bandpass and notch filtering of the narrowband interferer on the performance of digital communication system is examined in [10].

Interference rejection for frequency hopping systems is not as well examined as interference rejection for spread spectrum systems. Since frequency hopping is performed among multiple bands within the allocated band, the signals are instantaneously narrowband. Therefore, NBI affects only limited bands. If the number of hopping frequencies is large enough, the unwanted effect of NBI will be negligible. For example, in the presence of one powerful interference occupied less than the channel bandwidth, only one channel will be destroyed. The other channels will carry enough information, so that the error correction algorithms can recover this information loss. In the literature, interference rejection in frequency hopping systems is often based on employing a whitening filter. In [11], a hard-limited combining receiver using fractional tap spacing transversal filters in FFH-BFSK system in the presence of stationary NBI is proposed. The filter uses a tap spacing of $T_h/4L$, where T_h is the hop duration and L is the total number of hops. Authors claim that the tap coefficients

must be updated adaptively for practical systems. Simulation results show that the receiver with transversal filter does not limit the bit-error rate as the receiver without filter. In [12], it is shown that NBI can be estimated independently of the desired signal using a prewhitening filter with lag values of $T_h/2L$. The filter coefficients are also recursively estimated using least mean squares algorithm, which does not require an estimate of the signal or interferer covariance.

Majority of the publications about NBI cancellation is based on digital correction. The main assumption is that the dynamic range of the receiver, especially analog-to-digital converter (ADC), does not cause any degradation on the desired signal-to-noise ratio in the presence of interferer. Since automatic gain control loop is set to provide lower gain to handle interferer, the noise floor must also be low enough not to degrade the desired signal to noise power. However, these requirements result in higher power consumption and they may even become impossible to satisfy due to technology limitations. Therefore, NBI should be attenuated within the analog domain to relax dynamic range specifications for the RF front-end, including the data converters. Digital cancellation is also required to improve overall performance further. A recent publication proposed a solution based on analog filter bank pre-processing in conjunction with maximum ratio combining and generalized matching filter for spread spectrum UWB systems [13]. The received signal is split into N band-pass channels of filter banks. The signal at each filter output is quantized, then correlated with the template signal by a rake receiver. The outputs of rake receivers are then combined according to the generalized matched filter weighting algorithm.

The motivation of this dissertation is suppression of narrow-band interference for multi-band OFDM based UWB systems. The proposed solution is based on suppression of interference within the analog domain before it reaches analog-to-digital converter (ADC). Therefore, the dynamic range requirement of RF-frontend

and ADC is greatly relaxed. Since the location and power level of the interference is unknown prior the communication, an adaptive NBI suppression scheme is needed. The detection is performed in digital domain using Fast Fourier Transform (FFT) processor. The frequency hopping period of MB-OFDM puts a lower limit on the notch filter's settling time, which is inverse proportional to notch bandwidth. On the other hand, the notch bandwidth should be small enough not to attenuate the adjacent OFDM tones. Since these requirements are contradictory, optimization of notch bandwidth is required for maximum communication performance.

B. Dissertation Overview

In the next chapter, MB-OFDM UWB proposal [3] is discussed. Its frequency allocation and operation properties related to this work are presented. Fundamental concepts in receiver architectures are presented in Chapter III. In Chapter IV, noise, nonlinearity and simulation techniques are presented, with special attention to system level integration of all nonidealities. In Chapter V, the design of MB-OFDM compatible UWB receiver with narrow-band interference rejection is presented. The modeling and circuit design issues are discussed in Chapter VI. Experimental, transistor-level and behavioral simulation results are presented in Chapter VII. Finally, concluding remarks are discussed in Chapter VIII.

CHAPTER II

MULTI-BAND OFDM UWB PROPOSAL

On February 14, 2002 the FCC opened up 7.5 GHz of spectrum depicted in Fig. 1 (from 3.1 GHz to 10.6 GHz) for ultra-wideband (UWB) communications. The maximum transmit power is restricted to the existing -41.3 dBm/MHz limit for unintentional radiation of FCC Class-B compatible electronic devices [1]. In response, the IEEE formed a committee to release a standard for UWB communication. Currently, there are two different proposals. One is based on direct sequence spread spectrum (DS-CDMA) [2] and the other is based on the multi-band orthogonal frequency division multiplexing (MB-OFDM) [3].

Multi-Band OFDM proposal specifies the physical entity for a UWB system that utilizes the unlicensed 3.1 – 10.6 GHz UWB band. The system provides a wireless communication with data-rates of 53.3, 80, 110, 160, 200, 320, 400, and 480 Mb/s. Only data-rates of 53.3, 110, and 200 Mb/s are mandatory. MB-OFDM UWB system is based on orthogonal frequency division multiplexing (OFDM) using 128 subcarriers. Only 122 modulated and pilot subcarriers are used for data communication. The rest is not used to relax receiver design. For example, the subcarriers close to DC are not used in order to relax DC offset correction requirements. Since the average transmitted power is limited by FCC, frequency hopping is performed to increase the instantaneous transmitted power. For reliable transmission, error correction is performed using convolutional coding with a rate of 1/3, 11/32, 1/2, 5/8, and 3/4. To obtain time and frequency diversity, the data is also interleaved over subcarriers and three frequency bands, which are called band group. The total allocated band is divided into four band groups with three bands each, and one band group with two bands. Band group one, which is the three lowest frequency bands, is mandatory for

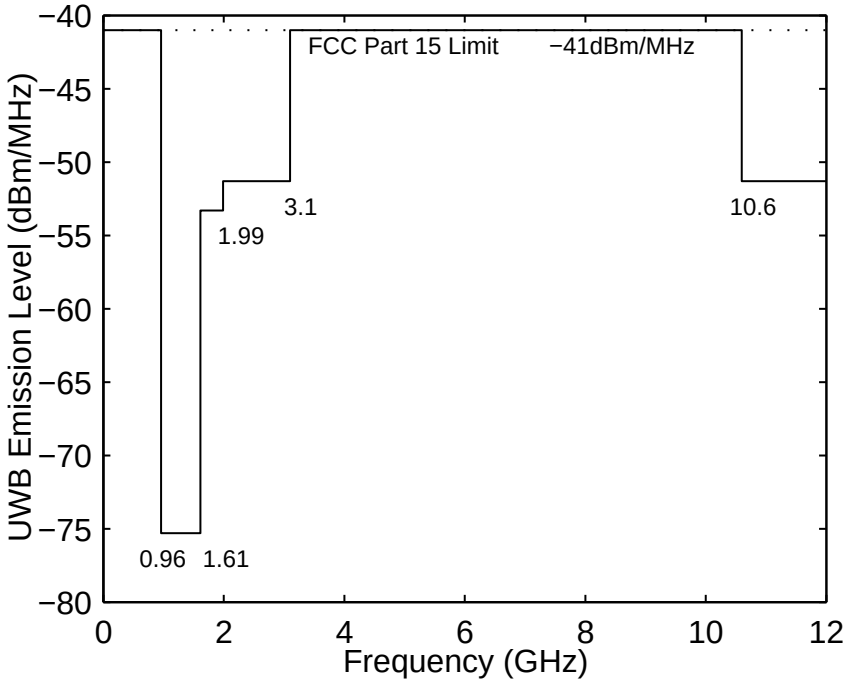

Fig. 1. UWB Spectrum.

all MB-OFDM compatible devices.

A. Frequency Band

The relationship between center frequency f_{bc} and band number n_b is given by the following equation:

$$f_{bc} = 2904 + 528 \cdot n_b, \quad n_b = 1 \cdots 14 \tag{2.1}$$

where f_{bc} is in MHz. This definition gives a unique numbering system for all channels within the band 3.1 – 10.6 GHz. The band allocation is summarized in Table. I.

B. Digital Baseband

The block level diagram of the digital part of the transmitter is illustrated in Fig. 2. The digital information is first encoded using convolutional encoder, which is depicted

Table I. MB-OFDM Band Allocation.

Band Group	Band ID	Lower Frequency	Center Frequency	Upper Frequency
1	1	3168 MHz	3432 MHz	3696 MHz
	2	3696 MHz	3960 MHz	4224 MHz
	3	4224 MHz	4488 MHz	4752 MHz
2	4	4752 MHz	5016 MHz	5280 MHz
	5	5280 MHz	5544 MHz	5808 MHz
	6	5808 MHz	6072 MHz	6336 MHz
3	7	6336 MHz	6600 MHz	6864 MHz
	8	6864 MHz	7128 MHz	7392 MHz
	9	7392 MHz	7656 MHz	7920 MHz
4	10	7920 MHz	8184 MHz	8448 MHz
	11	8448 MHz	8712 MHz	8976 MHz
	12	8976 MHz	9240 MHz	9504 MHz
5	13	9504 MHz	9768 MHz	10032 MHz
	14	10032 MHz	10296 MHz	10560 MHz

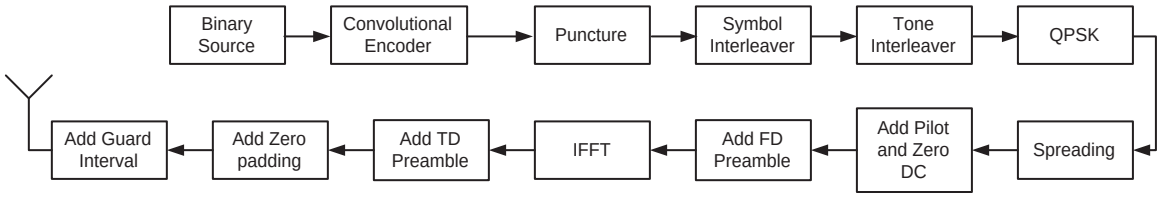

Fig. 2. Digital Baseband Transmitter.

in Fig. 3, for error correction. The information is transmitted through linear shift registers, whose output is summed according to the generator polynomial. The number of output bits for each k-bit input sequence is n bits and the code rate is defined as $R = k/n$. In MB-OFDM, the code rate is selected as 1/3 with generator polynomials, $g_0 = 1338$, $g_1 = 1658$, and $g_2 = 1718$. The first generated bit is denoted as "A", followed by the bit denoted as "B", and the last bit is denoted as "C". Different coding rates are generated by omitting some of the encoded bits in the transmitter and inserting a dummy zero bit into the convolutional decoder on the receive side in place of the omitted bits. This procedure is called puncturing. For example, the puncturing pattern for 5/8 coding rate is shown in Fig. 4.

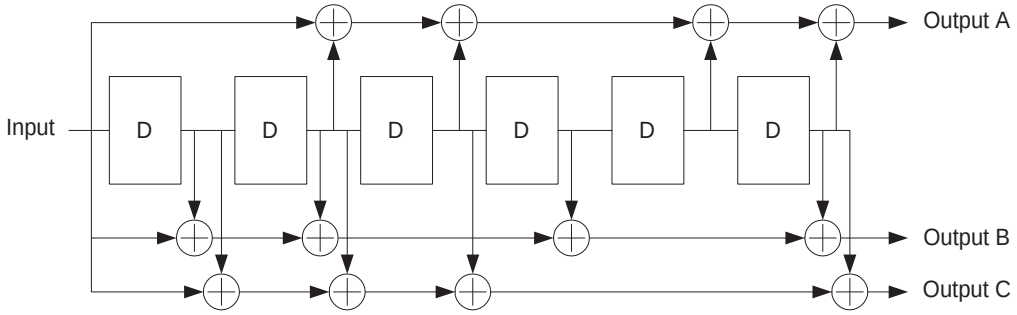

Fig. 3. Convolutional Encoder.

To provide robustness against burst errors, the coded bits are interleaved prior to modulation. Interleaving spreads out the burst errors in time so that errors within a received code word appear to be independent. First, the symbol interleaving across the OFDM symbols is performed. It permutes the bits across OFDM symbols to exploit frequency diversity across the sub-bands. Then, tone interleaving is applied to permute the bits across the data tones within an OFDM symbol. This exploits frequency diversity across tones and provides robustness against narrow-band interference.

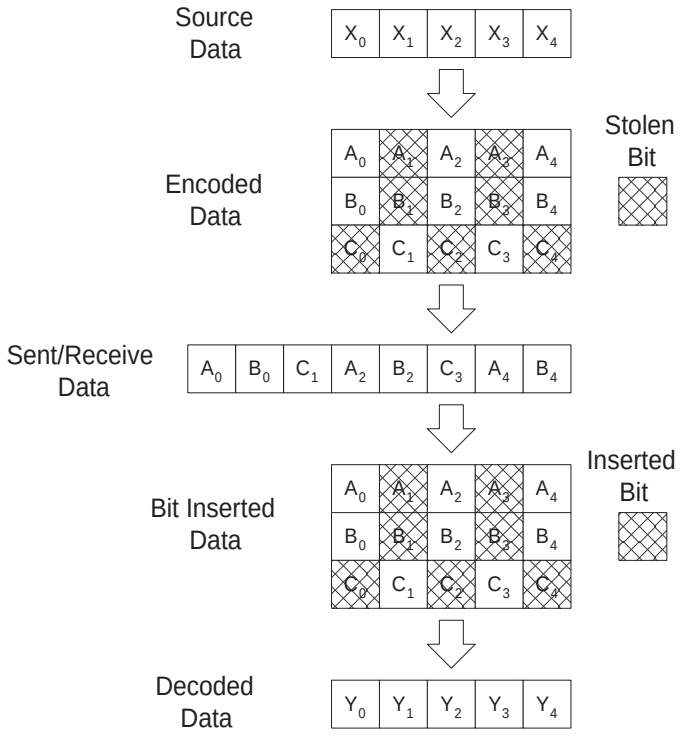

Fig. 4. Puncturing Procedure (R=5/8).

Following the interleaving, the binary data is divided into groups of two bits and converted into complex numbers, which are representing QPSK constellation points. The conversion illustrated in Fig. 5 is performed according to the Gray-coded constellation mapping.

For data rates of 53.3, 80, 110, 160 and 200 Mb/s, a spreading operation is performed in order to improve frequency diversity by transmitting the same information over two OFDM symbols. Following spreading the guard tones and pilot tones are added. The guard tones are used to relax the specifications of transmit and receive filters. The tone at DC is also not used to relax the offset and flicker noise requirements. The twelve pilot tones are dedicated to make the detection robust against frequency offsets and phase noise. Before IFFT, the frequency domain preamble symbols are added for carrier synchronization and channel estimation.

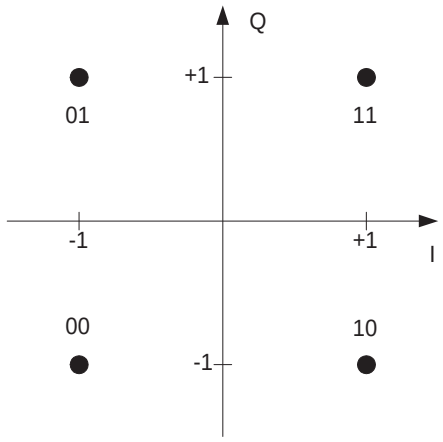

Fig. 5. QPSK Constellation.

The time-domain OFDM symbols $r_k(t)$ are constructed using an inverse Fast Fourier Transform (IFFT) using the following equation

$$r_k(t) = \sum_{n=-N/2}^{N/2} C_n e^{j2\pi n \Delta_f t}, \quad t \in [0, T_{FFT}] \tag{2.2}$$

where C_n is the nth tone value. Δf and N are defined as the tone frequency spacing and the number of total tones used, respectively. The resulting waveform has a duration of $T_{FFT} = 1/\Delta f$. In MB-OFDM N is selected as 128. For 53.3 and 80 Mb/s data rates, the complex conjugate of the tones 1 to 61 are copied to 67 to 127, as illustrated in Fig. 6. The guard tones 62 to 66 and the 0 (DC) are set to zero. After performing the IFFT, a zero-padded suffix of length 37 is appended to the IFFT output to mitigate the effects of multipath as well as to provide a guard period to allow for switching between the different bands. The final number of samples is 165.

In the receiver illustrated in Fig. 7, first 5 samples that correspond to guard interval is removed, since they are not reliable. Then the first 32 samples of remaining 160 samples are added to the last 32 samples to mitigate the multipath effects. The remaining 128 samples are then converted to frequency domain using Fast Fourier

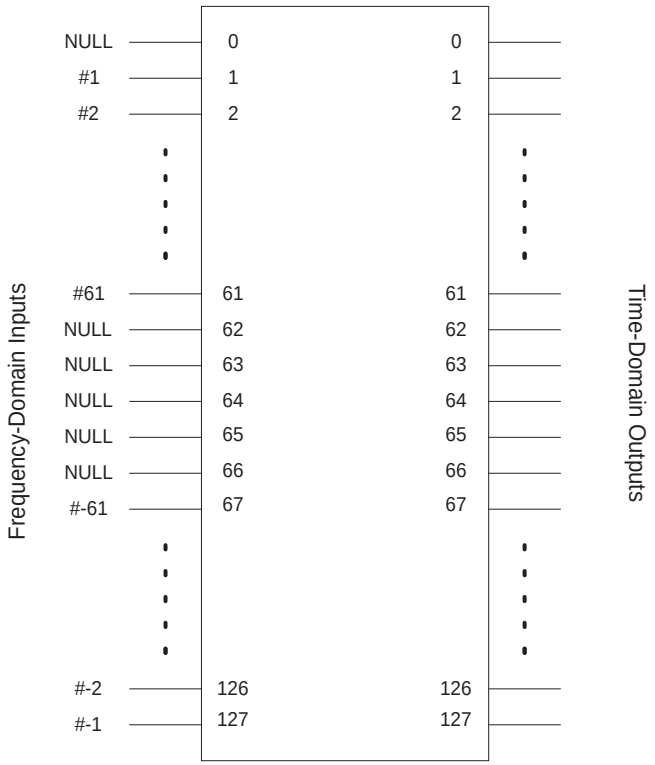

Fig. 6. Inputs and Outputs of IFFT.

Transform (FFT). After the effect of the channel is compensated by channel estimation, despreading is performed. Then the tones are obtained by demodulation. Following tone and symbol deinterleaving, the binary data is recovered using Viterbi decoder.

C. MB-OFDM Parameters

The rate and timing parameters of MB-OFDM are summarized in Tables. II and III, respectively. The data rate is calculated using the following formula

$$\text{Data Rate} = \frac{R \cdot E_M \cdot N_{CBPS}}{SR} \cdot \frac{1}{T_{SYM}} \tag{2.3}$$

Table II. MB-OFDM Rate Parameters.

Data Rate (Mb/s)	Modulation	Coding Rate (R)	Conjugate Symmetric Input to IFFT	Spreading Factor	Coded bits per OFDM symbol (N_{CBPS})
53.3	QPSK	1/3	Yes	4	100
80	QPSK	1/2	Yes	4	100
110	QPSK	11/32	No	2	200
160	QPSK	1/2	No	2	200
200	QPSK	5/8	No	2	200
320	QPSK	1/2	No	1	200
400	QPSK	5/8	No	1	200
480	QPSK	3/4	No	1	200

Table III. MB-OFDM Timing Parameters.

Parameter	Value
N_{SD}: Number of data subcarriers	100
N_{SDP}: Number of defined pilot carriers	12
N_{SG}: Number of guard carriers	10
N_{ST}: Number of total subcarriers used	122 ($= N_{SD} + N_{SDP} + N_{SG}$)
Δf: Subcarrier frequency spacing	4.125 MHz (= 528 MHz/128)
T_{FFT}: IFFT/FFT period	242.42 ns (Δf)
T_{ZP}: Zero pad duration	70.08 ns (= 37/528 MHz)
T_{SYM}: Symbol Interval	312.5 ns ($= T_{ZP} + T_{FFT}$)

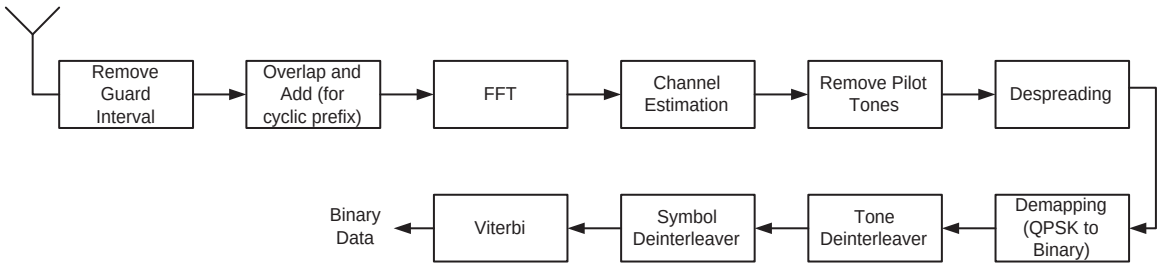

Fig. 7. Digital Baseband Receiver.

where R and SR are the coding rate and spreading rate, respectively, and E_M is modulation efficiency, which is equal to $\log_2 4$ for QPSK. N_{CBPS} is the number of data tones and equals to 100 in MB-OFDM. For instance, for 200Mb/s data rate, the coding rate is 5/8 and spreading factor is 2. The coded bits per OFDM symbol is 100, therefore, the data rate is calculated as

$$\frac{5/8 \cdot \log_2 4 \cdot 100}{2} \cdot \frac{1}{312.5\ ns} = 200\ Mb/s \tag{2.4}$$

D. Sensitivity

Sensitivity is defined as the minimum acceptable signal level for the desired performance. The criteria of performance depend on the application and acceptable loss of the data. For example, in audio communication more data loss can be acceptable than data communication. Few number of losses during audio transfer does not degrade overall audio quality. However, any loss during data communication can make the data unusable. The parameters to determine the link quality are signal-to-noise ratio for analog communications, and bit-error-rate (BER) or packet-error-rate (PER) for digital communications. PER is usually used for communication systems, where data is transferred in packets. The number of packet errors depends on not only the bit errors but also location of errors. Therefore two extreme cases are defined. In one

case, all the bit errors are only in one packet. The result is high BER but low PER. In the other case, every packet has one bit error. The result is total loss of transmitted packages but low BER. In practical cases, bit errors are spread across the packets and PER can not be directly calculated using BER information of the channel without knowing statistical distributions of bit errors.

The IEEE 802.15 group issued the sensitivity criteria to evaluate UWB systems. According to the criteria, the system must satisfy PER less than 8% for 1024 byte packets when the received signal is at the sensitivity level [14]. The sensitivity is defined relative to additive white Gaussian channel (AWGN).

BER of digital modulation schemes as a function of bit energy to noise ratio (E_b/N_0) is well defined in the literature [15]. When no error-correction coding is used and the channel is AWGN, the BER as a function of E_b/N_0 of QPSK modulation is

$$\text{BER} = \frac{1}{2}\text{erfc}\left(\sqrt{\frac{E_b}{N_0}}\right) \tag{2.5}$$

where erfc is the complementary error function and is defined by

$$\text{erfc}(u) = \frac{2}{\sqrt{\pi}}\int_u^\infty e^{-x^2}dx \tag{2.6}$$

Equation 2.5 is valid if error-correction is not used, in other words if no coding is applied. However, when error-correction is applied, the same BER performance can be obtained for lower E_b/N_0. Error-correction is a nonlinear process, and it is more successful for higher bit energy-to-noise ratios. Therefore, the coding gain is also a function of uncoded E_b/N_0. For convolutional codes, the upper bound of coding gain of 1/3 code rate for soft decision Viterbi decoding is given as 5.7 dB for 9.6 dB E_b/N_0, which corresponds 10^{-5} BER [16]. If each packet has only one bit error, the required BER for 8% PER is 0.977×10^{-5}, which is approximated to 10^{-5}. Therefore, the required E_b/N_0 is (9.6 dB-5.7 dB) 3.9 dB.

Table IV. Sensitivity Requirement for Mode 1.

Data Rate	Average Noise per Bit	E_b/N_0	Minimum Sensitivity
53.3 Mb/s	−96.7 dBm	3.6 dB	−83.6 dBm
80 Mb/s	−95.0 dBm	3.9 dB	−81.6 dBm
110 Mb/s	−93.6 dBm	3.6 dB	−80.5 dBm
160 Mb/s	−92.0 dBm	3.9 dB	−78.6 dBm
200 Mb/s	−91.0 dBm	4.3 dB	−77.2 dBm
320 Mb/s	−88.9 dBm	3.9 dB	−75.5 dBm
400 Mb/s	−88.0 dBm	4.3 dB	−74.2 dBm
480 Mb/s	−87.2 dBm	4.6 dB	−72.6 dBm

The derivations presented above do not take the puncturing, interleaving and fading channels into account. When these effects are also included, it is not possible to derive an analytical formula. The performance of the link should be derived numerically. In Table IV, required E_b/N_0 and corresponding sensitivity values for different data rates are shown. PER performance vs. E_b/N_0 curves for AWGN and 2 fading channels CM1 and CM2 are shown in Figs. 8, 9 and 10, respectively. The results for AWGN channel is very close to the predicted values. In fading channels the required E_b/N_0 is 5-6 dB higher than AWGN channel.

Another performance measure for MB-OFDM is the maximum communication distance. For AWGN channel the communication distance is shown in Fig. 11. The simulation results show that 110 MB/s data rate can be used at almost twice the communication distance of 200 MB/s.

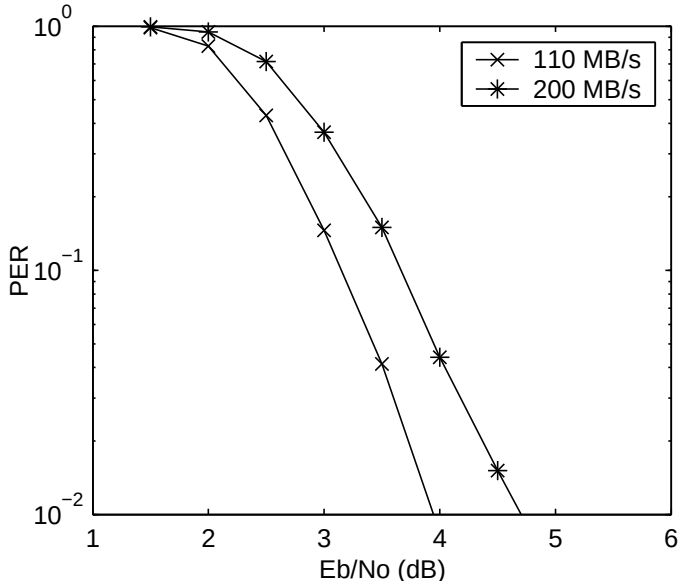

Fig. 8. E_b/N_0 (AWGN).

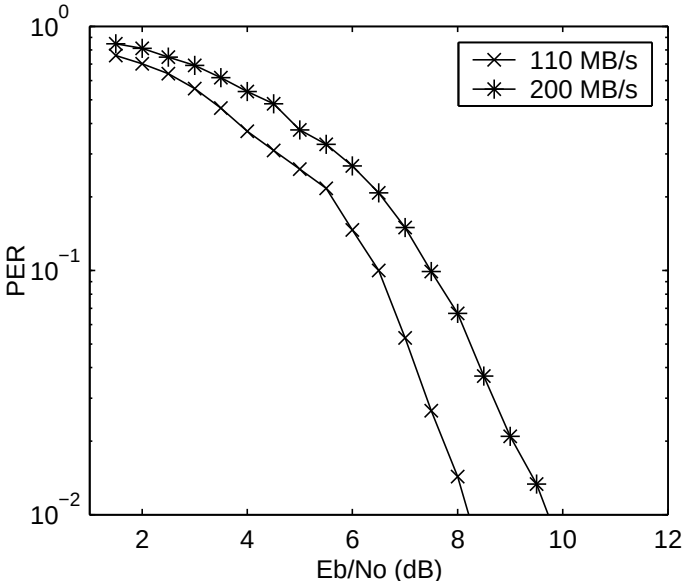

Fig. 9. E_b/N_0 (CM1).

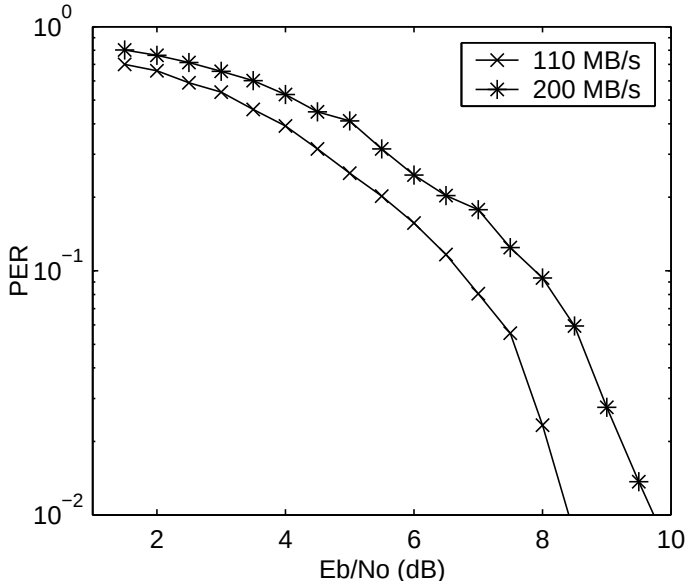

Fig. 10. E_b/N_0 (CM2).

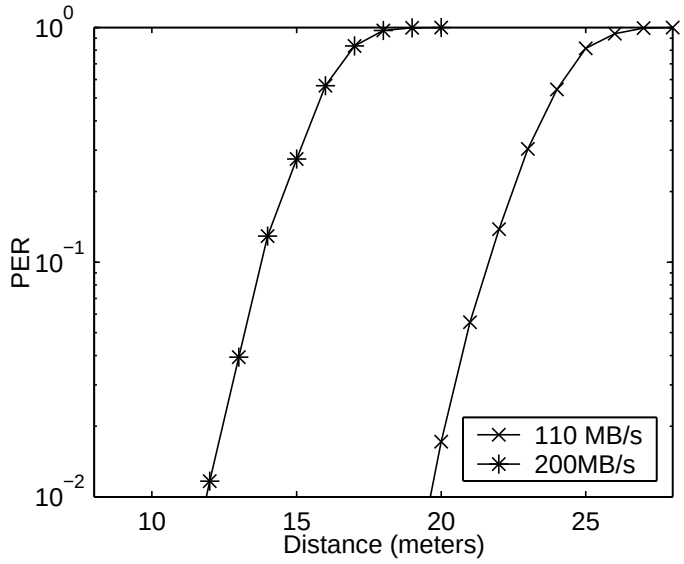

Fig. 11. Distance (AWGN).

CHAPTER III

RECEIVER ARCHITECTURES

The radio era started when Marconi first had experimented wireless telegraphy in 1894. In the following century, the radio receivers evolved from the simple discrete design to integrated receivers. Although many different architectures are reported during this period, they can be categorized as heterodyne and homodyne receivers, respectively. In heterodyne receivers, the signal is first downconverted to intermediate frequencies (IF). If the downconversion is performed in two or more steps, this type of architecture is called superheterodyne receiver. If the IF frequency is close to DC and lower than the signal band, it is referred as low-IF receiver. In zero-IF receivers, the signal is downconverted directly to baseband. Currently, zero-IF receivers allow high integration without requiring complex or external blocks, since they do not need high-Q IF filters. In this chapter, first superheterodyne receivers are examined. The advantages and disadvantages of zero-IF receivers are presented in the second section.

A. Superheterodyne Receivers

Superheterodyne receivers were invented by Edwin Armstrong in 1918 [17]. Although there are numerous improvements in electronics since 1918, it has been in use and basis for most modern receivers. As depicted in Fig. 12, superheterodyne receiver downconverts the RF signal to baseband in two or more steps. This allows selecting local oscillator frequency different than the RF frequency. Therefore, the local oscillator leakage to antenna is attenuated by the channel select filter. Since in-phase and quadrature signals are generated at lower frequency than RF, the IQ mismatch problem is less serious than direct conversion receivers.

Although superheterodyne receivers have many advantages, they require high-Q

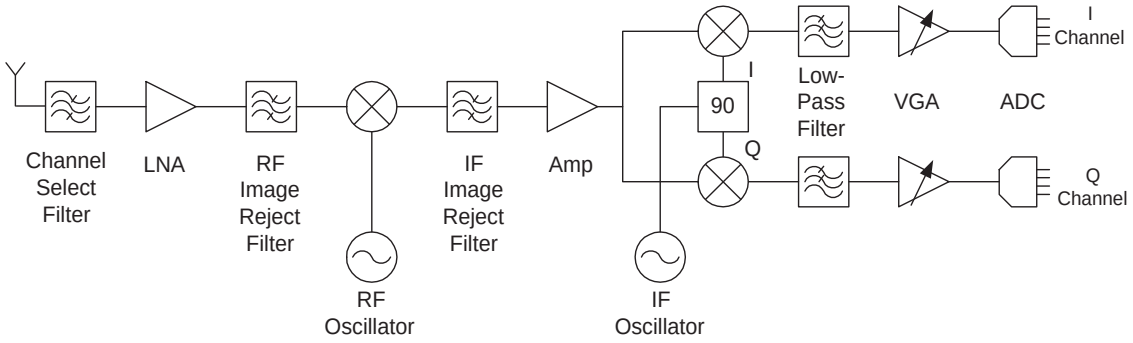

Fig. 12. Architecture of Superheterodyne Receiver.

filters to suppress the unwanted image signals. The integration of these filters in current IC technologies is not feasible due to the requirement of extra process steps. If external high-Q filters, such as SAW or ceramic, are used, extra pins and buffers are required. Due to demand for low-power and minimum cost, superheterodyne receivers are not preferred in current highly integrated receivers. On the other hand, low-IF receivers are chosen in highly integrated receivers for narrowband applications. To increase integration, the intermediate IF section is not used, and the RF signal is directly downconverted to low frequency, where analog-to-digital converters operate with low power and high accuracy. The downconversion is performed in digital domain with complex mixing. Since the image is removed by complex downconversion, the IQ mismatch determines the image rejection performance. Usually for practical systems, IQ mismatch estimation and correction algorithms are used to guarantee image rejection. DC offset, due to self-mixing of LO, is less serious problem, because DC can be removed by high pass filtering.

B. Zero-IF Receivers

Zero-IF receivers, also called direct conversion or homodyne receivers, convert the desired signal directly to baseband. As depicted in Fig. 13, the image signal is a part

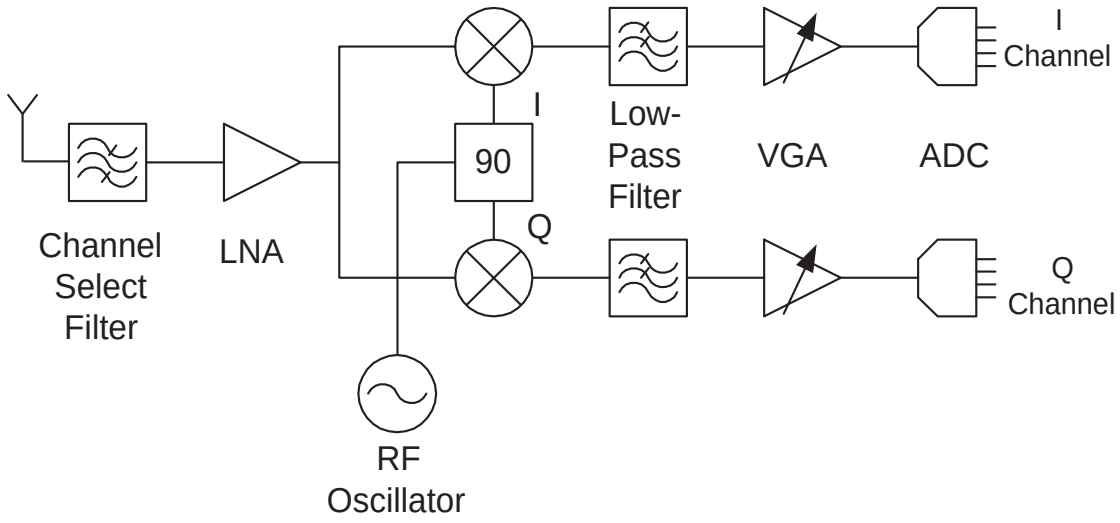

Fig. 13. Architecture of Zero-IF Receiver.

of the desired signal. Since the desired and image signals are mirror images of each other, the lower and upper sidebands are failing on top each other. This problem is solved by performing the down-conversion with sine and cosine waveforms. The transmitted signal is

$$RF = I(t)\cos(\omega_c t) + Q(t)\cos(\omega_c t) \tag{3.1}$$

At the receiver side, the quadrature signal are recovered by

$$2 \cdot RF\cos(\omega_c t) = I(t) + I(t)\cos(2\omega_c t) + Q(t)\sin(2\omega_c t) \tag{3.2}$$

$$2 \cdot RF\sin(\omega_c t) = Q(t) - Q(t)\cos(2\omega_c t) + I(t)\sin(2\omega_c t) \tag{3.3}$$

The frequency components at $2\omega_c$ are removed by a low-pass filter. Although zero-IF receivers are simpler than superheterodyne, they have drawbacks, such as DC Offset, LO Leakage, and IQ mismatch.

1. DC Offset

Self mixing of local oscillator signal and mismatch of the mixers or following stages generates DC offset at the baseband. In zero-IF receivers, the mixer is usually followed by a low-pass filter and high gain stages. Therefore, even a small level of DC offset can saturate the stages following these high gain stages. The DC offset is a sum of two components, a constant and time varying offset. Since the mismatch is independent of the signal level, it creates a constant offset. Self-mixing of the LO causes time varying offset.

DC offset can be removed by AC coupling. However, this technique will not only remove DC offset, but at the same time will attenuate the signals near DC. Therefore, zero-IF receiver is not feasible for modulation with DC components. This problem can be solved by using DC-free modulation schemes, but not using the spectrum close to DC reduces the spectral efficiency. Another problem of high pass filtering is the need for large settling time since the cutoff frequency is close to DC. If a low settling time is required, the offset cancellation is performed using a mixed-mode approach. The DC offset is estimated at the ADC output in digital domain, and is corrected at the VGA input by adding or subtracting current or voltage to the signal. Since the correction data is generated in digital domain, the detected DC-offset is quantized to a level. Therefore, with this technique it is not possible to totally remove DC offset. There will be some residual DC offset smaller than the least significant level.

2. Local Oscillator Leakage

When the local oscillator leaks to the input of receiver, it radiates out in the receive band. This is not a problem in superheterodyne receivers, since the LO leakage is removed by the channel select filter. However, in zero-IF receiver this radiation can

saturate the RF front end operating in the same band [18]. Most wireless standards have LO leakage radiation specifications less than −80 dBm, which would require more than 80 dB isolation between the local oscillator and the antenna. Another problem of LO leakage arises if LNA is not well matched to the antenna. The leaked LO power will reflect back to LNA input due to the mismatch. This reflected signal is than mixed with LO itself and creates DC offset.

3. I/Q Mismatch

Zero-IF receivers rely on the quadrature demodulation to solve the image problem. This is accomplished by using two downconverters operating in parallel with 90° of phase difference. Any error on the 90° of phase shift, and mismatch between the amplitudes, degrades the signal to noise ratio of the received signal.

The baseband I and Q voltages with the amplitude and phase mismatch of ϵ and θ are defined as

$$V_I = \left(1 + \frac{\epsilon}{2}\right)\left[I(t)\cos\left(\frac{\epsilon}{2}\right) - Q(t)\sin\left(\frac{\epsilon}{2}\right)\right] \tag{3.4}$$

$$V_Q = \left(1 - \frac{\epsilon}{2}\right)\left[I(t)\sin\left(\frac{\epsilon}{2}\right) + Q(t)\cos\left(\frac{\epsilon}{2}\right)\right] \tag{3.5}$$

According to the (3.4) and (3.5), the amplitude mismatch appears as a non unity scale factor, and the phase mismatch creates cross talk between I and Q channels. The bounds of amplitude and phase mismatch depend on the type of modulation. For instance, it is required to achieve amplitude mismatch below 1 dB and phase mismatch below 5° for $\pi/4$-DQPSK modulated signal [19].

4. Even Order Distortion

Zero-IF receivers are also susceptible to even order intermodulations. For example, consider the case depicted in Fig. 14. If the mixer is linear, the interferers will be

out-of band after downconversion, and will be removed by low-pass filter. However, if the mixer has even-order nonlinearity, it will create low-frequency beat in the baseband. The low-noise amplifier's (LNA) second order nonlinearity can also generate low frequency beat at the LNA output. This low-frequency beat will be fed through the mixer to baseband due to finite isolation between mixer's IF and RF ports. The even-order nonlinearity problem can be mitigated by using fully differential and double balanced mixer. Although fully differential structures double the power consumption and thermal noise, they are widely used to remove second order nonlinearity and increase supply and substrate noise rejection.

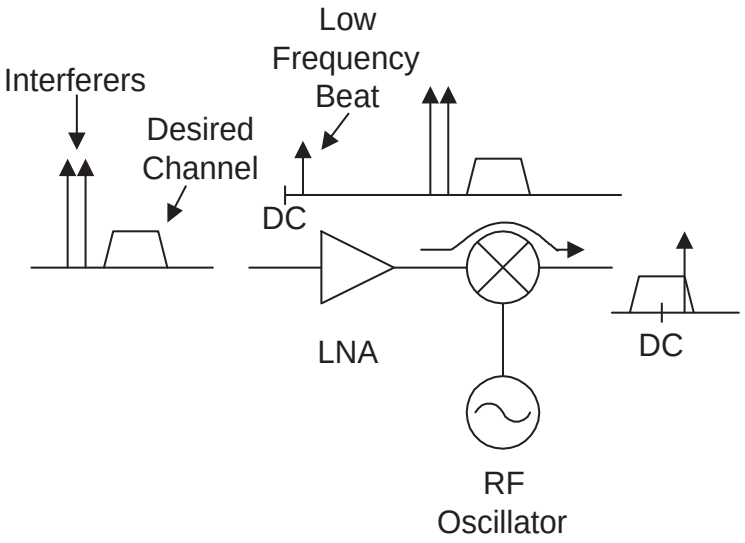

Fig. 14. Low Frequency Beat Due to Even Order Distortion.

5. Flicker Noise

Flicker noise (also known as 1/f noise) is observed in every electronic device. Its level depends on the device type, device parameters and the process which is used to manufacture it. Among the integrated processes, MOS gives high integration and yield, and is currently driving technology of low cost high integration. However, typical

MOSFET shows higher flicker noise than bipolar transistors. Flicker noise affects overall system performance at two different blocks. The first one is the synthesizer. The voltage controlled oscillator (VCO) used in the synthesizer upconverts flicker noise and shows higher phase noise. To increase overall synthesizer performance, the loop bandwidth is selected high enough so that VCO's close-in phase noise is attenuated. However, the loop bandwidth is not only determined by the overall phase noise requirement, but also other parameters, such as crystal frequency. Flicker noise of RF frontend is not a major problem, because the received signal is at higher frequency than the flicker noise corner, where flicker noise level equals to thermal noise level. However, when the signal is downconverted to baseband, the flicker noise determines the noise floor for the signals close to DC. Overall degradation on signal-to-noise ratio can be mitigated by increasing the gain at RF stages. However, this technique increases the linearity requirements of the receiver, since the low-pass filter, VGA, and ADC should handle signals with higher voltage swings.

CHAPTER IV

RF SYSTEM LEVEL DESIGN

The decision of receiver architecture is the first step in receiver design. The choice depends on the requirements such as bandwidth, frequency of operation, modulation type and etc. Once the architecture is determined, individual block specifications are derived using system level requirements. These initial derivations are based on gain formulas, noise and linearity calculations. Although formula-based approach gives good insight of the whole system, it is not adequate to model every nonideality and transient behavior. If some of the block properties are not modeled analytically, they are usually ignored or approximated. Therefore, the accuracy of overall design is reduced. With the help of computer-based simulations, the nonidealities that are ignored during formula-based approach are modeled. This allows designers to verify the performance of complex communication systems during the design phase.

In this chapter, sources of analog circuit nonidealities, such as noise and nonlinearity are discussed. Thermal, flicker and phase noise are presented in the first section. The section on nonlinearity is divided into three parts, based on single-tone, two-tone and multi-tone input. Simulation techniques for these nonidealities are discussed in the last section.

A. Noise

Noise is defined as the unwanted random disturbance which interferes with the signal of interest. The source of disturbance can be internal such as thermal, and flicker noise, or external such as electrostatic or electromagnetic coupling between the circuit and other circuits, power lines or radio transmitters. The important property of noise is that it is a stochastic signal. It consists of frequency components random in

amplitude and phase.

1. Thermal Noise

Thermal noise is the random fluctuations of the charge particles in the conductor in which the signal is traveling. This phenomenon is first observed by J. B. Johnson in 1927, and its theory is established by H. Nyquist in 1928. This noise is called Johnson noise or Nyquist noise because of their work.

Electrons in a conductor are in random motion above absolute zero. When the voltage on a conductor is observed for infinite period, the average voltage will be zero. However, instantaneously the voltage will be nonzero due to current fluctuations, where the available noise power is proportional to absolute temperature and system bandwidth, and is expressed as,

$$P_N = kT\Delta f \tag{4.1}$$

where k is Boltzmann's constant ($1.38 \times 10^{-23} Ws/K$), T is the temperature of the conductor in Kelvin (K) and Δf is the noise bandwidth of the system. At room temperature ($290^o K$) for a 1 Hz bandwidth, (4.1) gives -174 dBm. This power level is often referred as noise floor or minimum noise that can be achieved at room temperature. Thermal noise is also called white noise, since it has many frequency components and its spectrum shows flat response with respect to frequency. It is one of the main limitations of any communication system. Even if the system is built noise-free, the resistance of the antenna still adds noise.

Although noise is usually expressed in terms of its power level, using noise voltage or current instead of noise power eases the measurement and circuit design. Since thermal noise is defined on a conductor with finite resistance, the maximum power transfer can be obtained by terminating the conductor with a resistor, which has the

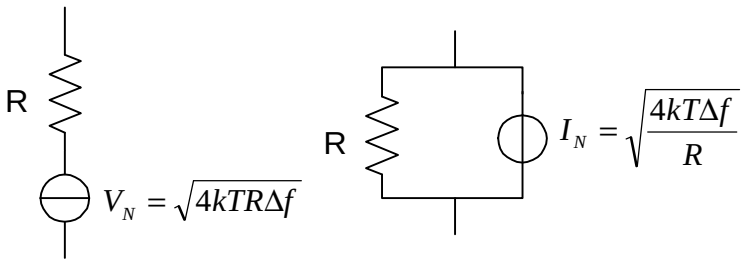

Fig. 15. Equivalent Circuits for Thermal Noise.

same resistance. The noise voltage of a resistor R is

$$V_N = \sqrt{4kTR\Delta f} \tag{4.2}$$

where V_N is in V. The same approach is used to obtain noise current, which is

$$I_N = \sqrt{\frac{4kT\Delta f}{R}} \tag{4.3}$$

For analysis, the noisy resistor is substituted with noiseless resistor and equivalent voltage or current source. These equivalent circuits are depicted in Fig. 15.

When uncorrelated noise sources are connected, their power is added together. For two series connected noise voltage sources, the total noise voltage is

$$V_{N,T}^2 = V_{N,1}^2 + V_{N,2}^2 \tag{4.4}$$

where $V_{N,1}$ and $V_{N,2}$ are noise voltages of the first and second noise sources, respectively. If the noise sources are partially correlated, the sum of noise voltages is

$$V_{N,T}^2 = V_{N,1}^2 + V_{N,2}^2 + 2CV_{N,1}V_{N,2} \tag{4.5}$$

where C is the correlation coefficient and can have any value between -1 and +1, including 0. For uncorrelated noise sources C equals 0, (4.5) gives the same result as (4.4).

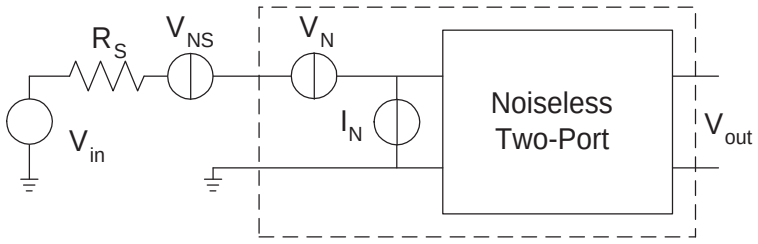

Fig. 16. Equivalent Circuit for Two-Port.

2. Flicker Noise

Flicker noise is a phenomenon observed for the signals close to DC. It is also called 1/f noise due to its $1/f^{\alpha}$ spectral characteristic. Usually α is unity, but it can vary from 0.8 to 1.3. The noise spectral density increases without a limit as frequency decreases. Flicker noise is defined using an empirical formula as follows

$$V_{N,F}^2 = \frac{K}{f^{\alpha}}\Delta f \tag{4.6}$$

where $V_{N,F}$ is the rms noise voltage, K is device dependent empirical parameter. Since flicker noise and thermal noise are present in every device, they intersect at a corner frequency, where flicker noise density equals thermal noise density. In MOSFETs, flicker noise is due to the random trapping of the charges at the oxide-silicon interface, and it is dominant below a few megahertz.

3. Noise of a Two-Port

The noise model of a two-port network is well established. The noise sources are considered as external noise sources and the network itself is considered as noise-free. The external noise sources are generally simplified to two noise sources, one noise voltage generator and the other is noise current generator. There can be a correlation between these two sources. The noise model of two-port is shown in Fig. 16. The

total input referred noise voltage is

$$V_{Ni}^2 = V_{NS}^2 + V_N^2 + I_N^2 R_S^2 \tag{4.7}$$

where V_{NS} is the noise voltage due to the source resistance, V_n is two-port's input referred noise voltage and I_n is the input referred noise current. Note that the contribution of noise current decreases when R_S decreases. Integrated circuits are usually optimized for voltage amplification. An ideal voltage amplifier shows infinite input impedance and zero output impedance. Therefore, when a voltage amplifier is driven by another voltage amplifier, the noise current of the second amplifier will not contribute any noise.

According to IEEE standards, the noise factor of a two-port device is defined as

$$F = \frac{N_O}{GN_i} \tag{4.8}$$

where N_O is the available output noise power, N_i is the noise due to the source, and G is the available power gain of the two-port. (4.8) can also be written as the ratio of input SNR to output SNR as

$$F = \frac{N_O}{GN_i} = \frac{S_i/N_i}{GS_i/N_O} = \frac{S_i/N_i}{S_O/N_O} \tag{4.9}$$

where S_i is the signal power at the input and S_O is the signal power at the output. When the noise factor is expressed in decibels, the ratio is called noise figure (NF), which is defined as

$$NF = 10 \log F \tag{4.10}$$

For an noiseless two-port noise factor will be 1 and noise figure will be 0. Noise figure can also be expressed in terms of V_N and I_N as

$$NF = 10 \log \frac{V_{NR}^2 + V_N^2 + I_N^2 R_S^2}{V_{NR}^2} \tag{4.11}$$

If the source impedance is resistive and contributes only thermal noise, (4.11) is written as

$$NF = 10\log\left(1 + \frac{V_N^2 + I_N^2 R_S^2}{4kTR_S\Delta f}\right) \tag{4.12}$$

When the noise of a two-port has flat spectrum in the band of interest, (4.12) is further simplified as

$$NF = 10\log\left(1 + \frac{\overline{V_N^2} + \overline{I_N^2} R_S^2}{4kTR_S}\right) \tag{4.13}$$

where $\overline{V_N^2}$ and $\overline{I_N^2}$ are noise voltage and current densities in V^2/Hz and A^2/Hz, respectively. Since noise simulations calculate noise density rather than noise power, (4.13) is very useful to compute the noise figure.

4. Noise of Cascaded Stages

In a communication system, the SNR at the output of the RF front end is wanted to be maximized. Since an RF chain incorporates many blocks, it is useful to derive an noise expression for cascaded networks. A simple case is two cascaded two-port networks. The noise at the output due to the input source and the first stage's input referred noise are amplified by the two stages. However, the second stage's noise is amplified only by the second stage. Therefore, the total output noise power N_{OT} is

$$N_{OT} = G_2\left(G_1 N_i + N_{O,1}\right) + N_{O,2} \tag{4.14}$$

where $N_{O,1}$, $N_{O,2}$, G_1 and G_2 are the output noise power and the available power gain of the first and the second stages, respectively. Using (4.8), (4.14) is written in terms of noise factors as

$$F_{12} = F_1 + \frac{F_2 - 1}{G_1} \tag{4.15}$$

where F_{12} is the total noise factor, F_1 and F_2 are the noise factors of the first stage and the second stage, respectively. A general formulation is written as

$$F_T = F_1 + \frac{F_2 - 1}{G_1} + \frac{F_3 - 1}{G_1 G_2} + \cdots + \frac{F_N - 1}{G_1 G_2 \cdots G_{N-1}} \tag{4.16}$$

This equation is also called the Friis equation [20]. It indicates the noise contributed by each stage. Since the noise factor is divided by the previous stage's gain, the contribution of noise is reduced as the gain preceding the stage increases. Therefore, the noise of the first stage is important on the overall noise figure.

In integrated circuit design, voltage gain is a more commonly used parameter than power gain. If the noise factor of each stage is calculated with respect to the source impedance driving that stage, (4.16) is written as

$$F_T = 1 + \frac{\overline{V_{N,1}^2} + \overline{I_{N,1}^2} R_{S1} + \frac{\overline{V_{N,2}^2} + \overline{I_{N,2}^2} R_{S2}}{G_1} + \frac{\overline{V_{N,3}^2} + \overline{I_{N,3}^2} R_{S3}}{G_1 G_2} + \cdots + \frac{\overline{V_{N,M}^2 I_{N,M}^2} R_{SM}}{G_1 G_2 \cdots G_{M-1}}}{4kTR_{S1}} \tag{4.17}$$

where $\overline{V_{N,M}^2}$ and $\overline{I_{N,M}^2}$ are the input referred voltage and current noise densities of $\mathrm{M^{th}}$ stage, and R_{SM} is the source impedance driving $\mathrm{M^{th}}$ stage. If the input referred noise current density is negligible compared to input referred noise voltage density, and the input of each stage is perfectly matched to driving impedance, (4.17) is written as follows,

$$F_T = 1 + \frac{\overline{V_{N,1}^2} + \frac{\overline{V_{N,2}^2}}{A_1} + \frac{\overline{V_{N,3}^2}}{A_1 A_2} + \cdots + \frac{\overline{V_{N,M}^2}}{A_1 A_2 \cdots A_{M-1}}}{4kTR_{S1}} \tag{4.18}$$

where A_M is the voltage gain of the $\mathrm{M^{th}}$ stage. Equation (4.18) eases to determine block level noise specifications for integrated receivers, since noise figure is calculated using noise densities and voltage gains of the stages.

5. Phase Noise

Noise in oscillators appears on the amplitude and the phase of the output signal. The amplitude noise is unimportant or negligible in most cases, since amplitude perturbations are removed by limiting the oscillator output. However, random variations of the phase can not be removed. This random variation can also be seen as a time-dependent frequency deviation, (differentiation of phase with respect to time is frequency), which can be characterized in time-domain or frequency domain. In time domain, it is an undesired perturbation or uncertainty in the timing of zero crossings, also known as jitter. In frequency domain, the spectrum shows skirts near the oscillating frequency due to random frequency deviations. Jitter is preferred for the performance analysis of the circuits such as sample-and-hold and analog-to-digital converters. On the other hand, phase noise is preferred to analyze overall blocker performance of receivers due to mixing phase noise with blocker. Jitter is quantified in RMS second and phase noise is quantified by calculating the noise power in a unit bandwidth at an offset with respect to nominal oscillator frequency.

For narrowband systems, phase noise downconverts any interferer that resides in the skirts of local oscillator spectrum. Phase noise in broadband systems also causes self-mixing of the in-band signal. For instance, consider an OFDM signal with 1 MHz tone spacing. The phase noise at 1 MHz offset mixes the adjacent tones and downconverts them on the desired tone frequency. This results in degradation of overall signal-to-noise ratio.

For oscillators, the sideband depicted in Fig. 17 has four regions. Close to nominal frequency the noise increases at a rate $1/f^4$ due to the random walks [21]. $1/f^3$ region is due to flicker noise. The slope reduces to $1/f^2$ between f_c and f_o due to the thermal noise, and above f_o the noise is constant due to the external noise sources.

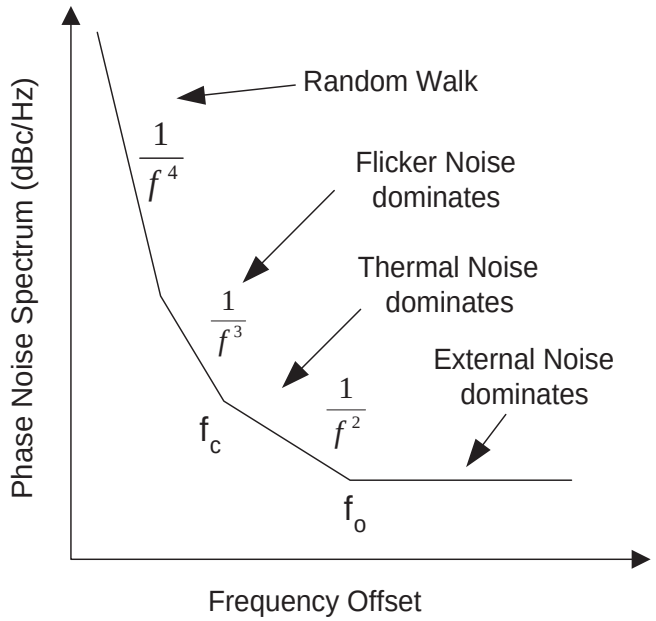

Fig. 17. Phase Noise Spectrum of Oscillator.

A typical frequency synthesizer phase noise, as depicted in Fig. 18, shows different spectral density than free-running oscillator. Close to the output frequency, the crystal oscillator (XTAL) noise dominates. The spectral density becomes flat, and above the noise bandwidth of the synthesizer, the voltage control oscillator (VCO) noise is the dominant noise source.

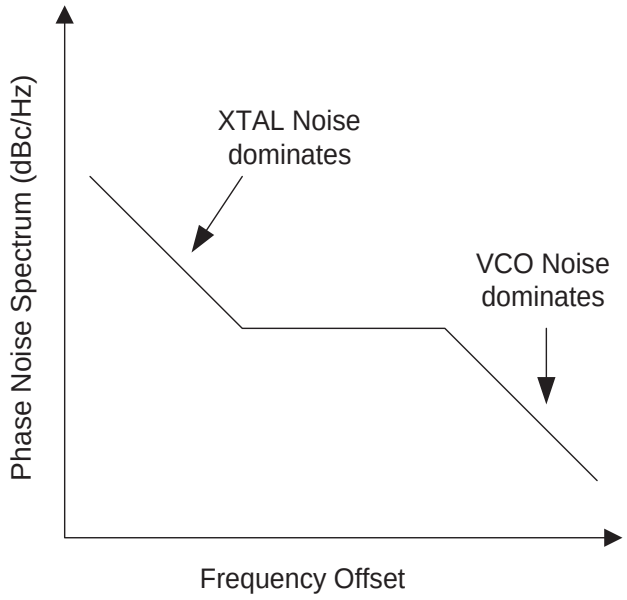

Fig. 18. Phase Noise Spectrum of Frequency Synthesizer.

B. Nonlinearity

A system is defined as linear if its parameters do not change with time and its output is the superposition of the responses to individual inputs. The linear relationship of a system with input $x(t)$ and output $y(t)$ is

$$y(t) = a \cdot x(t) \tag{4.19}$$

where a is the gain. The output has only frequency components, which also exist at the input. Although (4.19) is a good approximation, it is not possible to realize a pure linear system. A system is time-variant if its parameters change with time. A typical example of a time variant system is a switch, where its resistance changes if it is on or off. If the system output does not follow the input linearly and does not depend on the past values of the input, it is called a memoryless nonlinear system. A memoryless nonlinear system's transfer function can be expanded based on Taylor

series and written as a polynomial,

$$y(t) = a_0 \cdot x(t) + a_1 \cdot x^2(t) + a_2 \cdot x^3(t) + \cdots \tag{4.20}$$

where a_0 is the linear gain, a_1 and a_2 are the second and third order nonlinearity coefficients, respectively. Usually the first three terms in (4.20) are used to achieve a practical linearized model.

1. Single Tone Input

The basic test method for linearity is applying a single sinusoidal signal, and checking the harmonics at the output. The input $x(t)$ is selected as

$$x(t) = A\cos(\omega t) \tag{4.21}$$

where ω is the input frequency in radians. Inserting (4.21) into (4.20) and neglecting the terms higher than the third results in,

$$\begin{aligned} y(t) &= a_1 A\cos(\omega t) + a_2 A^2\cos^2(\omega t) + a_3 A^3\cos^3(\omega t) \\ &= a_1 A\cos(\omega t) + \frac{a_2 A^2}{2}\left[1+\cos(2\omega t)\right] + \frac{a_3 A^3}{2}\left[3\cos(\omega t)+\cos(3\omega t)\right] \\ &= \frac{a_2 A^2}{2} + \left[a_1 A + \frac{3a_3 A^3}{4}\right]\cos(\omega t) + \frac{a_2 A^2}{2}\cos(2\omega t) + \frac{a_3 A^3}{4}\cos(3\omega t) \end{aligned} \tag{4.22}$$

According to (4.22), even order nonlinearity causes a DC term and harmonic at twice the input signal frequency. Third order nonlinearity causes a term at 3ω. Since harmonics are unwanted terms, a figure of merit for the nonlinearity is defined as the ratio of the second and third harmonic to the fundamental response. The second order harmonic distortion is defined as

$$HD_2 = \frac{1}{2}A\left|\frac{a_2}{a_1}\right| \tag{4.23}$$

The third order harmonic distortion is expressed as

$$HD_3 = \frac{1}{4}A^2 \left| \frac{a_3}{a_1} \right| \tag{4.24}$$

The third order nonlinearity at the signal frequency causes gain compression or expansion. This property can also be used as an indication of the nonlinearity of the system. The 1-dB gain compression point is defined as the input level where the gain is 1-dB less than its linear value. Therefore, input referred 1-dB gain compression point is written as

$$x_{1dB} = \sqrt{0.145 \left| \frac{a_1}{a_3} \right|} \tag{4.25}$$

In single tone analysis, HD_2 and HD_3 are useful for wideband systems, where the harmonics are not attenuated due to the frequency response of the system. For narrowband systems, where second and third order harmonics are out-of the band, these results are not meaningful. Although 1-dB compression point can be used to test the nonlinearity, the system should be driven to very nonlinear region, where the nonlinear coefficients higher than three affect the result.

2. Two Tone Input

Characterization systems using single tone input requires the harmonics to be in the system band and not attenuated due to limited bandwidth. This requirement is not satisfied for RF systems, unless the system occupies so large bandwidth that the harmonics are in the band. To test the linearity without being affected by limited bandwidth, the system is excited with sum of two sinusoidal signals, which is

$$x(t) = A_1 \cos(\omega_1 t) + A_2 \cos(\omega_2 t) \tag{4.26}$$

where A_1 and A_2 are amplitude of the first and second signals, respectively. ω_1 and ω_2 are selected close to each other so that their intermodulation products are also in the band. Inserting (4.26) into (4.20) gives

$$\begin{aligned} y(t) &= \frac{a_2 A_1^2}{2} + \frac{a_2 A_2^2}{2} \\ &+ a_2 A_1 A_2 \cos((\omega_1 - \omega_2)t) \\ &+ \frac{3a_3 A_1^2 A_2}{4}\cos((2\omega_1 - \omega_2)t) + \frac{3a_3 A_1 A_2^2}{4}\cos((2\omega_2 - \omega_1)t) \\ &+ \left(a_1 A_1 + \frac{3a_3 A_1 A_2^2}{2} + \frac{3a_3 A_1^3}{4}\right)\cos(\omega_1 t) \\ &+ \left(a_1 A_2 + \frac{3a_3 A_1^2 A_2}{2} + \frac{3a_3 A_2^3}{4}\right)\cos(\omega_2 t) \\ &+ \frac{a_2 A_1^2}{2}\cos(2\omega_1 t) + \frac{a_2 A_2^2}{2}\cos(2\omega_2 t) \\ &+ a_2 A_1 A_2 \cos((\omega_1 + \omega_2)t) \\ &+ \frac{a_3 A_1^3}{4}\cos(3\omega_1 t) + \frac{a_3 A_2^3}{4}\cos(3\omega_2 t) \\ &+ \frac{3a_3 A_1^2 A_2}{4}\cos((2\omega_1 + \omega_2)t) \\ &+ \frac{3a_3 A_1 A_2^2}{4}\cos((2\omega_2 + \omega_1)t)) \end{aligned} \tag{4.27}$$

For a narrowband system the terms except ω_1, ω_2, $2\omega_1 - \omega_2$ and $2\omega_2 - \omega_1$ are out-of band and are attenuated by a low-pass filter. For simplicity, A_1 is selected equal to A_2, which is A. Under these assumptions (4.27) reduces to

$$\begin{aligned} y(t) &= \frac{3a_3 A^3}{4}\cos((2\omega_1 - \omega_2)t) + \frac{3a_3 A^3}{4}\cos((2\omega_2 - \omega_1)t) \\ &+ \left(a_1 A + \frac{9a_3 A^3}{4}\right)\cos(\omega_1 t) + \left(a_1 A + \frac{9a_3 A^3}{4}\right)\cos(\omega_2 t) \end{aligned} \tag{4.28}$$

Since the frequency components at $(2\omega_2 - \omega_1)$ and $(2\omega_1 - \omega_2)$ are not desired, the ratio of the third order intermodulation products to the fundamental response can be used as a figure of merit for the systems with low input drive. The third order

intermodulation distortion is given by

$$IM_3 = \frac{3}{4}\left|\frac{a_3}{a_1}\right| A^2 \tag{4.29}$$

Note that there is a relationship between IM_3 and HD_3, which is

$$IM_3 = 3HD_3 \tag{4.30}$$

Although the response at the fundamental frequency changes linearly with input level, the response at $(2\omega_2 - \omega_1)$ increases with A^3. Since their slopes are different, they will cross at a point, which is called third order intercept point. It can be found by determining the input amplitude for which the third order intermodulation distortion equals to one. This gives

$$IP_3 = \sqrt{\left|\frac{4a_1}{3a_3}\right|} \tag{4.31}$$

If the second order terms are in the band, the second order intermodulation distortion will be defined as

$$IM_2 = \left|\frac{a_2}{a_1}\right| A \tag{4.32}$$

Similar to the third order intercept point definition, the second order intercept point is the input amplitude for which the second order intermodulation distortion equals to one.

$$IP_2 = \left|\frac{a_1}{a_2}\right| \tag{4.33}$$

Since the calculation of cascaded systems are performed using intercept points, most of the time they are used to specify the nonlinearity performance of receivers.

3. Multi Tone Input

Modern communication systems require highly spectral efficient modulation schemes or wide bandwidth to increase the data rate. Although IP3 is a good figure of merit

for narrowband systems, it is not for systems with multi tone modulation formats, such as OFDM. Since the tone spacing of each OFDM symbol is smaller than overall OFDM bandwidth, the intermodulation products and harmonics of the tones are in the band.

The multi tone tests are separated as baseband tests and RF tests. In RF tests, the signal is at high frequency; therefore its bandwidth is lower than the channel center frequency. Since the distortion products except third order intermodulation products are out-of band, multi tone tests can be analytically calculated using the IM3 [22]. At the baseband, the second and third order harmonics and intermodulation products are in the band; therefore, multi tone test specifications are determined numerically.

a. Adjacent Channel Power Ratio (ACPR)

ACPR shown in Fig. 19 is a measure of signal spreading into the adjacent channel due to the system nonlinearities. It is

$$ACPR = \frac{P_{adj1} + P_{adj2}}{P_{sig}} \tag{4.34}$$

where P_{adj1} and P_{adj2} are adjacent channels integrated power and P_{sig} is the signal power, respectively. The relationship between IM3 and ACPR is given by

$$ACPR = IM_3 + 10\log\left(\frac{n^3}{16N_1 + 4M_1}\right) \tag{4.35}$$

where n is the number of input tones, $N1$ and $M1$ are defined as

$$N_1 = \frac{2n^3 - 3n^2 - 2n}{24} \cdot \frac{\mathrm{mod}(n/2)}{8} \tag{4.36}$$

$$M_1 = \frac{n^2 - \mathrm{mod}(n/2)}{4} \tag{4.37}$$

Note that $\mathrm{mod}(n/2)$ is defined as the remainder when n is divided by 2.

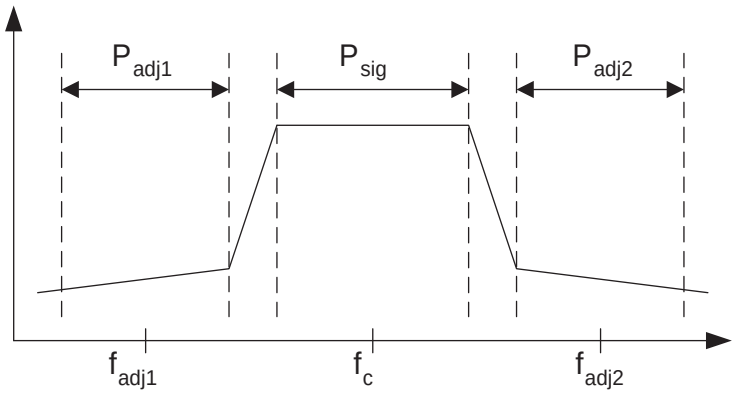

Fig. 19. Adjacent Channel Power Ratio.

b. Multi Tone Intermodulation Ratio (MIMR)

MIMR shown in Fig. 20 is a measure of the nonlinearity with a multi tone input signal. It is the ratio between a tone power and the highest distortion tone power outside, but closest to the signal band. The relationship between IM3 and MIMR is derived as

$$MIMR = IM3 - 6 + 10\log\left(\frac{n^2}{4N_2 + M_2}\right) \tag{4.38}$$

where n is the number of input tones, $N2$ and $M2$ are defined as

$$N_2 = \left(\frac{n-r}{2}\right)^2 - \frac{\mathrm{mod}((n+r)/2)}{4} \tag{4.39}$$

$$M_2 = \left(\frac{n-r}{2}\right)^2 + \frac{\mathrm{mod}((n+r)/2)}{4} \tag{4.40}$$

where r is the tone number corresponding to the highest distortion component outside the band. Most of the time r is selected as 1, since it is the nearest tone outside the band and expected the highest distortion tone.

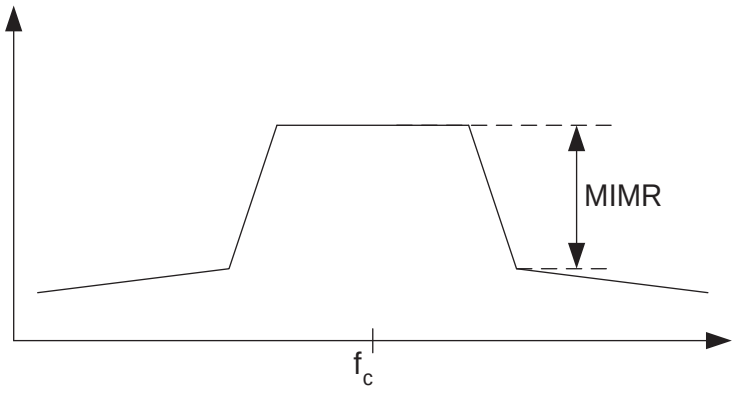

Fig. 20. Multi Tone Intermodulation Ratio.

c. Missing Tone Power Ratio (MTPR)

MTPR shown in Fig. 21 is a measure of the in-band distortion power due to the nonlinearity. It is the ratio between the in-band distortion and signal spectral densities when an in-band noise spectrum slice is removed. The relationship between IM3 and MTPR is defined as

$$MTPR = IM3 - 6 + 10\log\left(\frac{n^2}{4N_3 + M_3}\right) \tag{4.41}$$

where n is the number of input tones, $N3$ and $M3$ are defined as

$$\begin{aligned} N_3 &= \left(\frac{n-b-2}{2}\right)^2 - \frac{\mathrm{mod}((n+b)/2)}{4} \\ &\quad + \left(\frac{b-1}{2}\right)^2 - \frac{\mathrm{mod}((b+1)/2)}{4} + b(n-b-2) \end{aligned} \tag{4.42}$$

$$\begin{aligned} M_3 &= \left(\frac{n-b-2}{2}\right) + \frac{\mathrm{mod}((n+b)/2)}{4} \\ &\quad + \left(\frac{b-1}{2}\right) + \frac{\mathrm{mod}((b+1)/2)}{4} \end{aligned} \tag{4.43}$$

where b is the number of removed tones.

When all tones are applied, the phases of tones determine the time domain

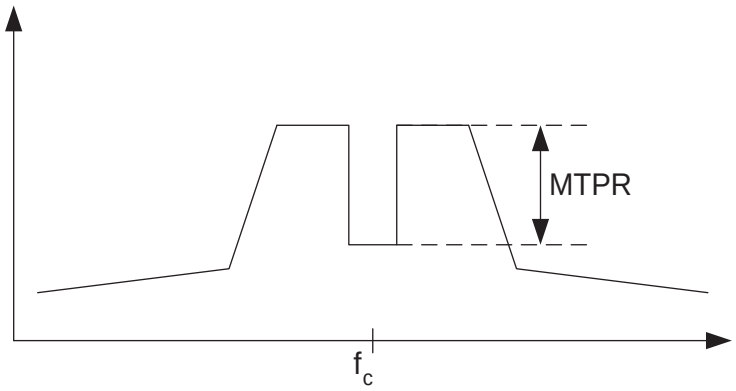

Fig. 21. Missing Tone Power Ratio.

waveform. If every tone has the same phase, the sum will give a signal with a very high peak. However, in real situation the phases are random, and practically the peak to average ratio of the signal is constant. Having random phases creates also random MTPR results for the system with fixed IP3 and IP2. When the test signal is created, the signal with the worst MTPR should be used to guarantee proper operation. For example, a multi tone signal is applied to a system with 20 dBVrms IIP2 and 0 dBVrms IIP3. The signal occupies the band from DC to 264 MHz. The band between 165 MHz and 206.25 MHz is removed. The input time domain waveform is shown in Fig. 22. The worst case MTPR is 15.5 dB an depicted in Fig. 23. Since the phases have Uniform distribution, the MTPR histogram is shown in Fig. 24. The Matlab code is added in Appendix C.

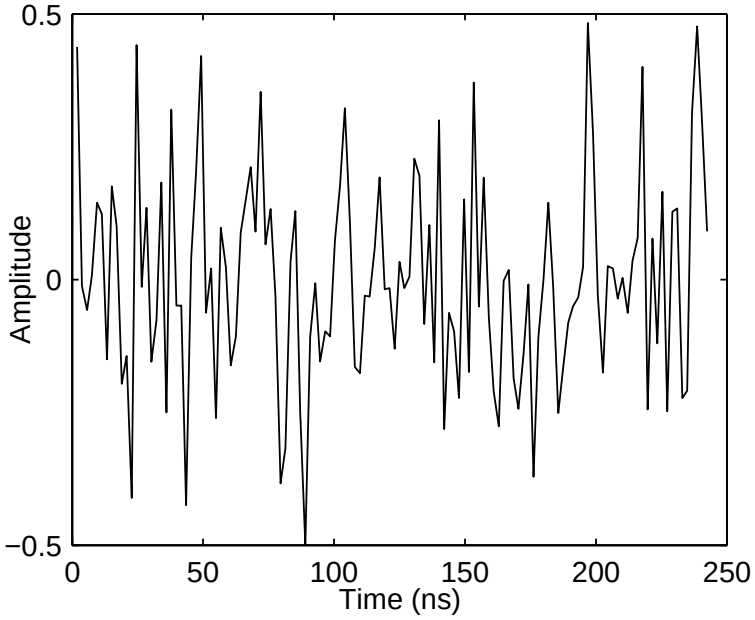

Fig. 22. MTPR Input Signal.

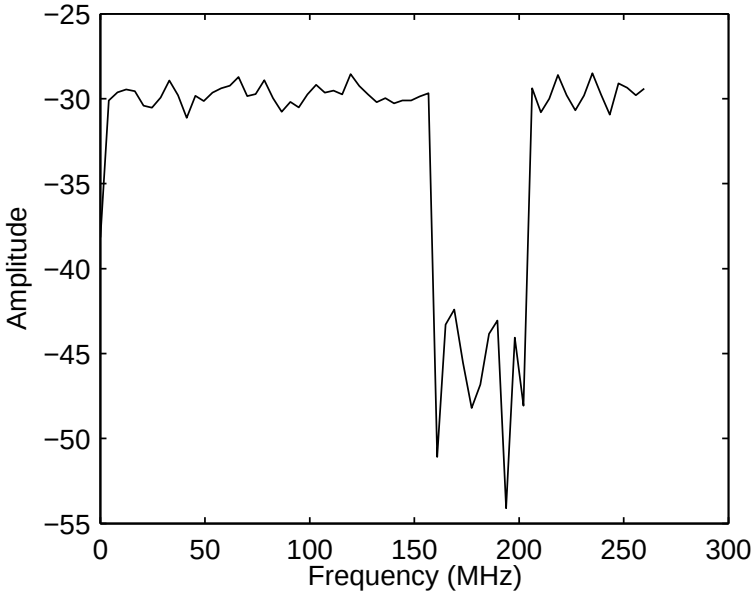

Fig. 23. MTPR Output Spectrum.

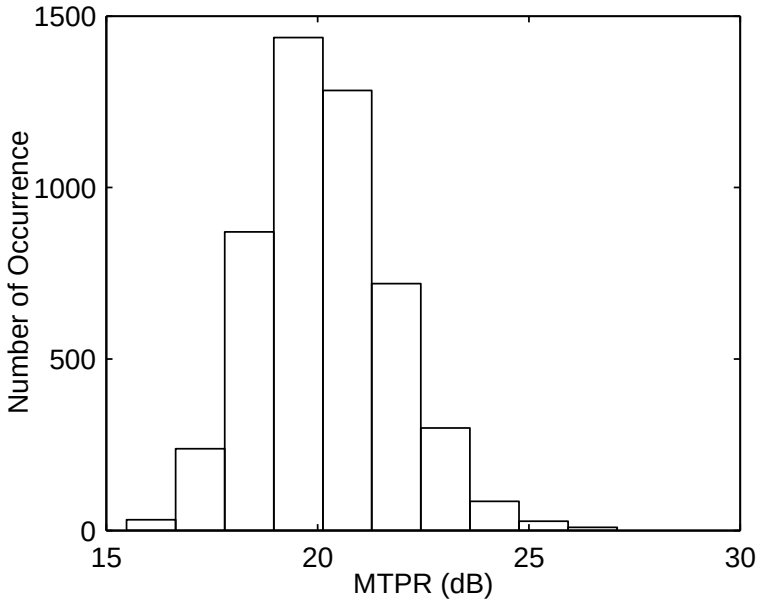

Fig. 24. Histogram of MTPR.

4. Nonlinearity of Cascaded Stages

The level of intermodulation products at the output of a memoryless nonlinear system is given by

$$IIP_n = P_{in} + \frac{IM_n}{n-1} \tag{4.44}$$

where n is the order of IM product, IIP_n is the nth order input referred intercept point and P_{in} is the input power. All power levels in (4.44) are in dBVrms or dBm. (4.44) indicates that nth order IM product increases n dB for every 1 dB increase in P_{in}.

When the systems are cascaded, the calculation of overall intercept point is problematic. IM products generated in the first stage are amplified or attenuated by the following stages and new IM products are generated. These newly generated IM products are at the same frequency as the previous stage but their phases are not determined. Therefore, the IM products may be added in a way to increase or reduce

their magnitudes. An upper bound can be determined by assuming that IM products generated by the stages are added in phase [23]. Under this worst case assumption, the input referred intercept point is

$$\frac{1}{A_{IIPn}^{(n-1)}} = \frac{1}{A_{IIPn,1}^{(n-1)}} + \frac{a_{1,1}^{(n-1)}}{A_{IIPn,2}^{(n-1)}} + \cdots + \frac{(a_{1,1}a_{1,2}\cdots a_{1,M-1})^{(n-1)}}{A_{IIPn,M}^{(n-1)}} \tag{4.45}$$

where A_{IIPn} is the input referred nth order intercept point in Volts, $a_{1,M}$ is the Mth stage linear voltage gain. This general formula is written for second order and third order cascaded intercept point as follows

$$\frac{1}{A_{IIP_2}} = \frac{1}{A_{IIP_2,1}} + \frac{a_{1,1}}{A_{IIP_2,2}} + \cdots + \frac{(a_{1,1}a_{1,2}\cdots a_{1,M-1})}{A_{IIP_2,M}} \tag{4.46}$$

$$\frac{1}{A_{IIP_3}^2} = \frac{1}{A_{IIP_3,1}^2} + \frac{a_{1,1}^2}{A_{IIP_3,2}^2} + \cdots + \frac{(a_{1,1}a_{1,2}\cdots a_{1,M-1})^2}{A_{IIP_3,M}^2} \tag{4.47}$$

C. Simulation Techniques

System level simulations are widely used to gain insight into the system behavior. If the simulation setup is properly built, the results will be similar to real implementation of the system. System measurements are easily performed at various points. Parametric studies such as filter bandwidth, signal-to-noise ratio sweep, are easily conducted. Furthermore, time domain waveforms and signal spectra are easily generated. Although computer simulations give good insight of the system, the time domain waveforms can not be continuous or real valued signals due to discrete-time processing and finite precision of signals in computers. These requirements put some limitation on computer analysis, such as spectrum, noise, and linearity.

1. Spectrum Analysis

The spectra of signals are obtained by discrete fourier transform (DFT), where discretization requires sampling a continuous-time signal and assuming it is constant between the consecutive samples. Real time signals are rounded to the nearest quantization level to obtain a finite-precision number. DFT parameters must be carefully selected to ensure accuracy of the result. For instance, improper selection of the sampling frequency causes numerical problems resulting in substantial differences between the calculated spectrum and the actual spectrum. Also, sampling the signal at a lower frequency than the signal or signal harmonics causes aliasing of the signals above $f_s/2$ to the band, which is from $-f_s/2$ to $f_s/2$.

a. Definition of Discrete Fourier Transform and its Inverse

The DFT of a discrete signal $x(n)$ is defined by

$$X(k) = \sum_{n=0}^{N-1} x(n) e^{-j2\pi kn/N} \qquad k = 0, \cdots, N-1 \tag{4.48}$$

where $X(k)$ is the kth coefficient of the DFT and $j = \sqrt{-1}$. The $x(n)$'s can be complex numbers and the $X(k)$'s are always complex. The inverse of the DFT has a form that is very similar to that of the DFT and is given by

$$x(n) = \frac{1}{N} \sum_{k=0}^{N-1} X(k) e^{j2\pi kn/N} \qquad n = 0, \cdots, N-1 \tag{4.49}$$

This relationship is called the Inverse Discrete Fourier Transform (IDFT). It is easy to show that this inversion is valid by inserting (4.48) into (4.49).

$$x(n) = \sum_{k=0}^{N-1} \sum_{n=0}^{N-1} \left(x(n)/N\right) e^{-j2\pi kn/N} \qquad n = 0, \cdots, N-1 \tag{4.50}$$

Interchanging the order of summation of the indices n and k in (4.50), and using the orthogonality relation

$$\begin{aligned} \sum_{k=0}^{N-1} e^{-j2\pi k(n-m)/N} &= N, \qquad \text{if } n = m \bmod N \\ &= 0, \qquad \text{otherwise} \end{aligned} \tag{4.51}$$

the right side of (4.50) is in fact equal to $x(n)$. Since (4.51) gives the same result for any n of modulo N, it is useful to extend the range of $X(k)$ to all integers (positive and negative). Within this definition it follows that

$$X(k) = X(N+k) = X(2N+k) = \cdots \tag{4.52}$$

Similarly,

$$x(n) = x(N+n) = X(2N+n) = \cdots \tag{4.53}$$

According to (4.52), the spectrum repeats itself every N samples, and (4.53) shows that the signal is periodic in time.

If $x(n)$ is also a real function, the following relation holds

$$X(k) = X^*(N-k) \tag{4.54}$$

where $*$ indicates the complex conjugate. This relation implies that only the first $N/2$ values of $X(k)$ are unique, which is verified by Nyquist's sampling theorem.

b. DFT of a Sinusoidal Wave

To calculate the spectrum of a sinusoidal wave using (4.48), the continuous-time sinusoidal signal is discretized as follows

$$\begin{aligned} x(t) &= A\cos(2\pi f_0 t) \\ x(n) &= A\cos(2\pi f_0 n\Delta t) \\ &= A\cos(2\pi r\Delta f n\Delta t) \\ &= A\left[e^{2\pi nr\Delta f\Delta t} + e^{-2\pi nr\Delta f\Delta t}\right]/2 \\ &= A\left[e^{2\pi nr/N} + e^{-2\pi nr/N}\right]/2 \end{aligned} \tag{4.55}$$

where Δt (sampling period) and Δf (frequency resolution) are the time difference between two consecutive samples and the minimum distinguishable frequency, respectively. The input frequency is chosen in the form $f_0 = r\Delta f$, where r is not necessarily an integer. Substituting $x(n)$ into (4.48),

$$\begin{aligned} X(k) &= A\sum_{n=0}^{N-1} e^{-j2\pi kn/N}\left(e^{2\pi nr/N} + e^{-2\pi nr/N}\right)/2 \\ &= \frac{A}{2}\sum_{n=0}^{N-1}\left[e^{2\pi n(r-k)/N} + e^{-2\pi n(r+k)/N}\right] \end{aligned} \tag{4.56}$$

Finally, (4.56) is a geometric series and is evaluated in closed form as,

$$X(k) = \frac{A}{2}\left[\frac{e^{j2\pi(r-k)} - 1}{e^{j2\pi(r-k)/N} - 1} + \frac{e^{-j2\pi(r+k)} - 1}{e^{-j2\pi(r+k)/N} - 1}\right] \tag{4.57}$$

The power spectra $P(k) = X(k)X^*(k)$ reduces to a simpler form near f_0 and $-f_0$;

$$P(k) \approx \frac{A^2}{4}\left[\frac{\sin^2(\pi(r-k))}{\sin^2(\pi(r-k)/N)} + \frac{\sin^2(\pi(r+k))}{\sin^2(\pi(r+k)/N)}\right] \tag{4.58}$$

Consider the case where r is an integer and $r \neq k$. Then $X(k) = 0$ since k is also an integer. When $r = k$, both numerator and denominator are 0 and the limiting

result is $X(r) = (A \cdot N)/2$. Thus, when r is an integer, the digital spectra produces the intuitive result that $X(k) = 0$ everywhere except at the input signal frequency $f_0 = r\Delta f$.

When a DC signal is evaluated, in other words $r = 0$, (4.57) reduces to

$$X(k) = A\frac{e^{-j2\pi k} - 1}{e^{-j2\pi k/N} - 1} \tag{4.59}$$

For $k = 0$, (4.59) gives $A \cdot N$ at the limit, and if $k \neq 0$ the result will be zero.

c. Non-Integer Multiple of Frequency Resolution

If the input signal frequency is not selected as an integer multiple of the frequency resolution, the spectrum is different than expected. As an example, the sampling frequency and frequency resolution are selected as 16 Hz and 0.01 Hz, respectively. The input signal frequency is 2.555 Hz, which is 255.5 times the frequency resolution. The spectrum for these parameters is shown in Fig. 25, which shows a modulation that should not exist. When the frequency resolution is decreased and the input signal frequency is an integer multiple of the frequency resolution, the spectrum shown in Fig. 26, is obtained as expected.

The problem is why the spectrum shows some modulation when the input signal is selected as a non-integer multiple of frequency resolution. Although there is no modulation on the signal, the spectrum is correct. Fig. 25 shows what is called bin splatter or spectral leakage [24]. This result is verified by an analytical expression. To obtain a physical picture, the basic analog Fourier transform should be evaluated for the same sine wave. The spectra is

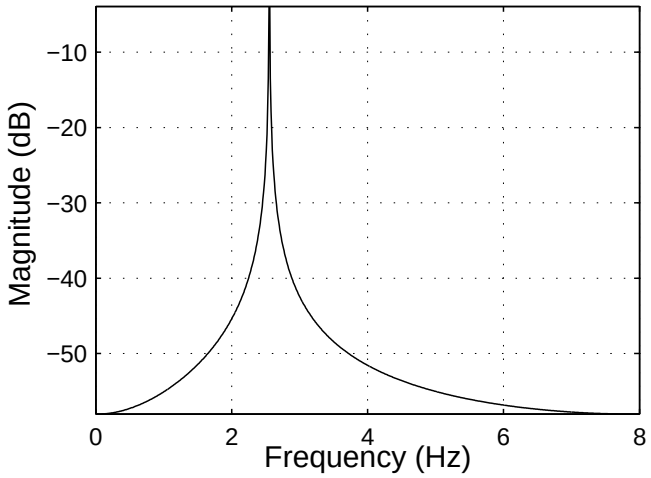

Fig. 25. Spectrum for Non-integer Multiple of Δf (Δf=0.01Hz).

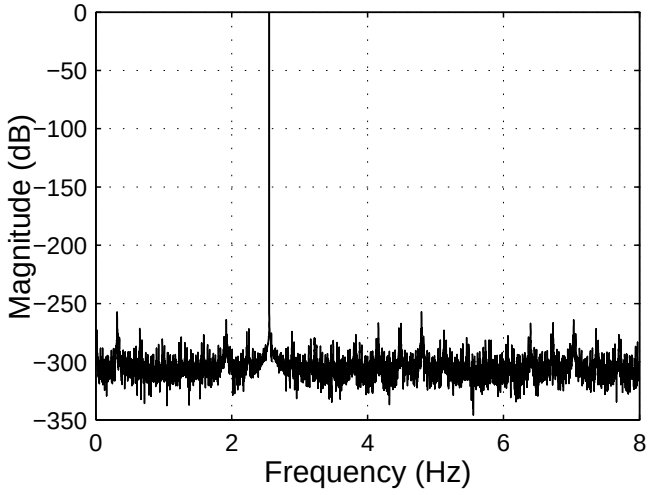

Fig. 26. Spectrum for Integer Multiple of Δf (Δf=0.001Hz).

$$P(f) = \frac{A^2}{4}\left[\frac{\sin^2(\pi(f_0-f)/\Delta f)}{\sin^2(\pi((f_0-f)/\Delta f)/N)} + \frac{\sin^2(\pi(f_0+f)/\Delta f)}{\sin^2(\pi((f_0+f)/\Delta f)/N)}\right] \quad (4.60)$$

Near f_0, (4.60) is simplified using the assumption $\sin(x) \approx x$ for small x values.

$$P(f) \approx \frac{A^2}{4}\left[\frac{\sin(\pi(f_0-f)/\Delta f)}{(\pi((f_0-f)/\Delta f)/N)}\right]^2 \quad (4.61)$$

This expression has a maximum at $f = f_0$, and the nulls are separated at integer multiples of Δf from this maxima. If $P(f)$ is evaluated for discrete frequencies, which are multiples of Δf , the maxima of the peak is sampled, while any other sample is zero [25]. Note that near f_0 the spectrum decreases with $1/f^2$, which appears as a modulation in the simulations.

d. Aliasing

In the previous sections, the signal is assumed to be band-limited and does not have any spectral components above $f_s/2$. If this assumption is violated, the signals above $f_s/2$ are down-converted to the band from $-f_s/2$ to $f_s/2$.

A typical example is the DFT of a signal with abrupt changes, such as a square wave. Due to the sharp changes of the square wave, the required bandwidth to represent the signal is infinite. Another example is a distorted signal sampled at a frequency lower than its maximum distortion product. The result is depicted in Fig. 27 where the 6^{th} and higher harmonics are down-converted to the band and the harmonics between $f_s/2$ and f_s are mirrored across $f_s/2$. The following formula gives

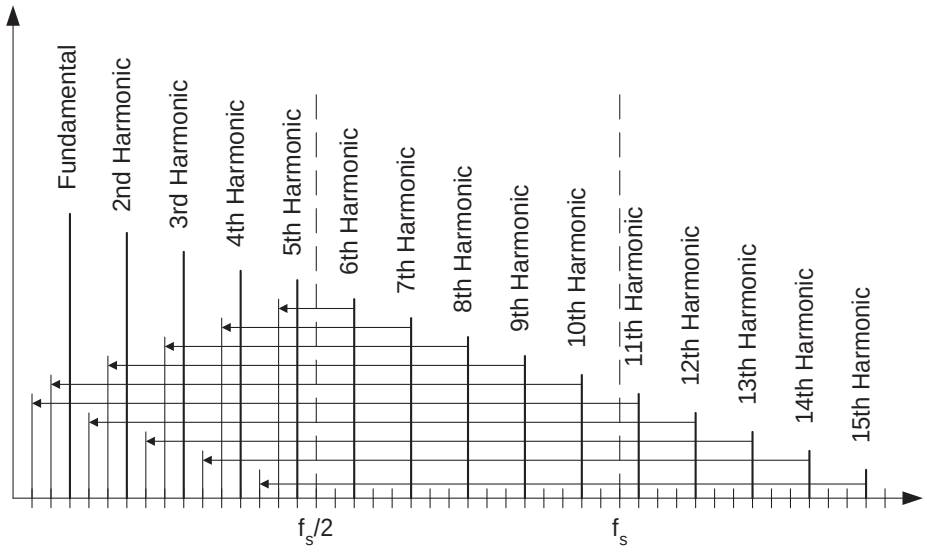

Fig. 27. Spectrum Due to Aliasing.

the frequency of the down-converted signal f_{down}

$$f_{down} = |n \cdot f_s - f_{signal}| \quad \text{n: integer from } -\infty \text{ to } \infty$$
$$-f_s/2 \leq f_{down} < f_s/2 \tag{4.62}$$

For example, the harmonic at 9 Hz with a sampling frequency of 16 Hz will be down-converted to 7 Hz.

To reduce the aliasing problem, the signal must be band-limited before taking the DFT. A low-pass filter serves very well to limit the band of the signal. However, filtering introduces frequency-dependent group delay, which usually increases with filter order. An equalizer can also be used to compensate the group delay variations, but this technique adds extra complexity and design effort. Another method is to increase the sampling frequency and use a low-order low-pass filter with a high cut-off frequency to minimize the group delay variations in the band of interest. The drawback of this method is for the same frequency resolution, a higher sampling

frequency results in higher computational time.

e. Quantization Noise

Analog-to-digital converters connect the analog world to the digital domain. They sample and quantize real valued continuous signals and represent them as finite precision digital words. Since some information is lost during this procedure, it creates an error called quantization noise [26], which has the RMS voltage

$$V_Q = \frac{V_{LSB}}{\sqrt{12}} \tag{4.63}$$

where V_{LSB} is the least significant bit voltage level. Since the signal is sampled at f_s, the noise is spread from $-fs/2$ to $fs/2$. Because the spectrum is not continuous, the noise power is distributed over the frequency bins and the DFT output shows a noise density equal to $V_Q/\sqrt{N/2}$. To spread the quantization noise homogeneously over all bins, the input signal frequency bin and the number of DFT samples should be co-prime and the signal should not be symmetrical. Otherwise, the quantization noise power will be concentrated on the bins numbered with the greatest common divisor of the input signal frequency bin and N.

For example, the output spectrum of an 8-bit ADC with 1 KHz sampling frequency is depicted in Figs. 28 and 29 for 101 Hz and 100 Hz input signals, respectively. V_{LSB} is selected as $2/2^8$ and frequency resolution is 1 Hz, therefore, N is 1000 and the quantization noise density is at -80 dB in Fig 28. However, Fig. 29 indicates bins at -60 dB, which is $10 \cdot \log(100)$ dB higher than Fig. 28, since the greatest common divisor of 100 and N is 100. Note that, the integrated quantization noise power is independent from sampling frequency and input signal frequency, and for both cases the integrated power is the same.

To obtain a proper noise density plot, the following procedure is used. In Matlab,

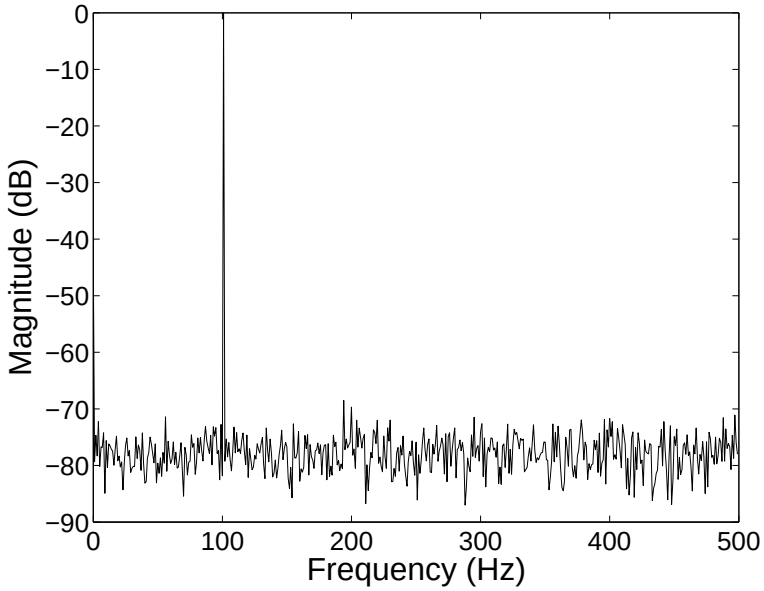

Fig. 28. Quantization Noise Density (f_{in} =101 Hz).

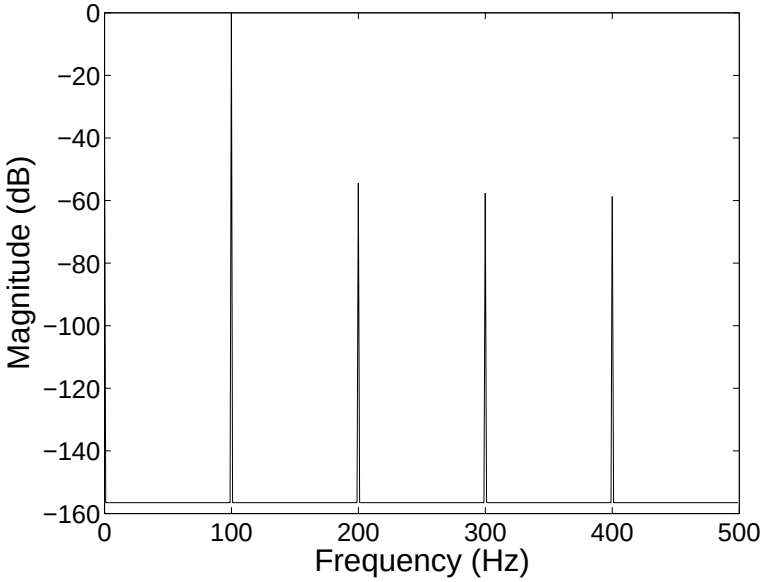

Fig. 29. Quantization Noise Density (f_{in} =100 Hz).

run *primes(N)* and *factors(N)* commands to obtain primes smaller than N and factors of N. Then, select one prime number (p_n) which is not any of the factor's of N and apply the input signal at the frequency $p_n \cdot \Delta f$. The resulting plot gives the spectrum of the quantization noise spreading homogeneously over the entire band.

f. Window Technique

The time required for circuit or system level simulations is reduced by decreasing sampling frequency or increasing the frequency resolution. However, sampling frequency determines the upper edge of the band, therefore, its minimum value is fixed according to the bandwidth requirements. Decreasing frequency resolution reduces the dynamic range of DFT and reduces the number of frequency bins. If the signal frequency is not exactly on the frequency bin, the spectral leakage corrupts the spectrum. The situation worsens in the presence of two signals with different power levels. The weaker signal can be buried under the spectral leakage of the larger signal, if the stronger signal is not integer multiple of frequency resolution. In these cases, the signals power is estimated by applying an appropriate window to the data.

Basically, the aim of the window is to reduce the abrupt changes of the signal due to finite observation time. In the literature, there are many different windows for different applications [27, 28, 29, 24]. However, there is no general approach to select an optimum window for any application. The best window can be found by comparing different windows' performance. As a start, rectangular window is used since it has the best spectral resolution. The widely-used window functions and their properties are summarized in Table. V. The windows are distinguished according to the following properties depicted in Fig. 30.

- Peak Side-lobe Level: It is the indication of the dynamic range of the window.

Table V. Window Properties.

Window	Peak Sidelobe (dB)	Rolloff Rate (dB/oct)	3dB Bandwidth	Coherent Gain
Rectangle	-13	-6	$0.86 \cdot \Delta f$	1
Hamming	-42	-6	$1.3 \cdot \Delta f$	0.54
Hanning (cosine4)	-47	-30	$1.86 \cdot \Delta f$	0.38
Kaiser ($\beta = 11$)	-82	-6	$1.83 \cdot \Delta f$	0.37
Blackman-Harris	-92	-6	$1.9 \cdot \Delta f$	0.36

That is, how small can the signal be and still be detected in the presence of a large signal and its side-lobes.

- Rolloff Rate: This parameter describes the amplitude fall off of side-lobe peaks. This indicates the available dynamic range.

- 3 dB Bandwidth: The resolution of the window, for instance, the ability to distinguish two closely spaced sinusoids from a single sinusoid, is dictated by the 3 dB Bandwidth.

- Coherent Gain: This is a measure of the window that takes into account data sequence weighting. The coherent gain G_C is given by

$$G_C = \frac{1}{N} \sum_{n=0}^{N-1} w(n) \tag{4.64}$$

where $w(n)$ is the window function.

Since the 3 dB bandwidth and peak side-lobe are inversely proportional, high

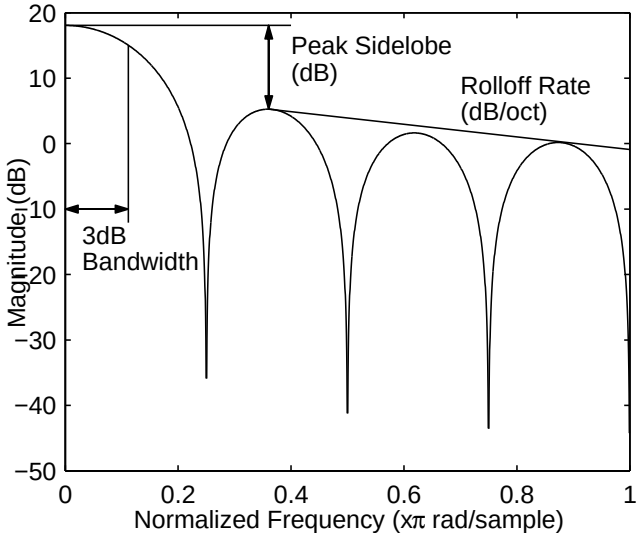

Fig. 30. Window Properties.

dynamic range and high resolution can not be obtained at the same time without decreasing frequency resolution. The rectangular window has the smallest 3 dB bandwidth and thus the best spectral resolution. However, its spectral leakage, as indicated by the peak side-lobe level and rolloff rate, is poor. The bandwidths of the last three windows are almost the same and are distinguished only by their leakage properties. In particular, the Blackman-Harris window has the lowest side-lobe level while the Hanning has the steepest rolloff rate, and the Kaiser window has a parameter to set the side-lobe height. To achieve a side-lobe height of $-\alpha$ dB, the β parameter is

$$\beta = \begin{cases} 0.1102(\alpha - 8.7), & \alpha > 50 \\ 0.5842(\alpha - 21)^{0.4} + 0.07886(\alpha - 21), & 50 \leq \alpha \leq 21 \\ 0, & \alpha < 21 \end{cases} \tag{4.65}$$

As a general rule of thumb, β is selected as 0.11 times the required side-lobe height.

The spectrum of a signal with two spectral components at 2 Hz and 2.55 Hz is calculated using rectangular and Kaiser windows. The signal power at 2 Hz is 40 dB

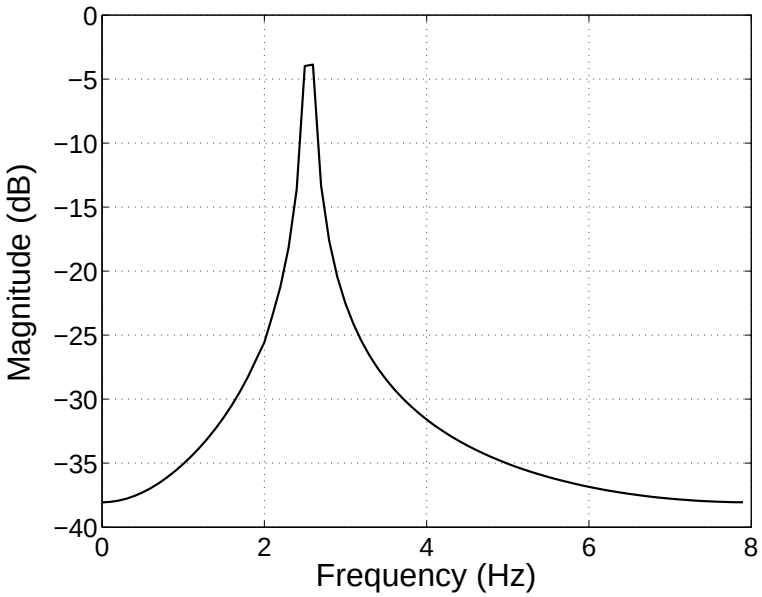

Fig. 31. Spectrum with Rectangular Window.

lower than the signal power at 2.55 Hz, and the frequency resolution and the sampling frequency are selected as 0.1 Hz and 16 Hz, respectively. Although the signal at 2 Hz is an integer multiple of the frequency resolution, the other one is not. In Fig. 31, the rectangular window's side-lobe is 21 dB lower than its main-lobe at 0.55 Hz for 16 Hz sampling frequency, the 2 Hz signal is buried under the side-lobe of the 2.55 Hz signal. Using a different window, the side-lobe level is decreased and the weaker signal is detected. For example, a Kaiser window ($\beta = 10$) gives a side-lobe level 83 dB lower than the signal itself. Now, the signal at 2 Hz is distinguished as shown in Fig. 32.

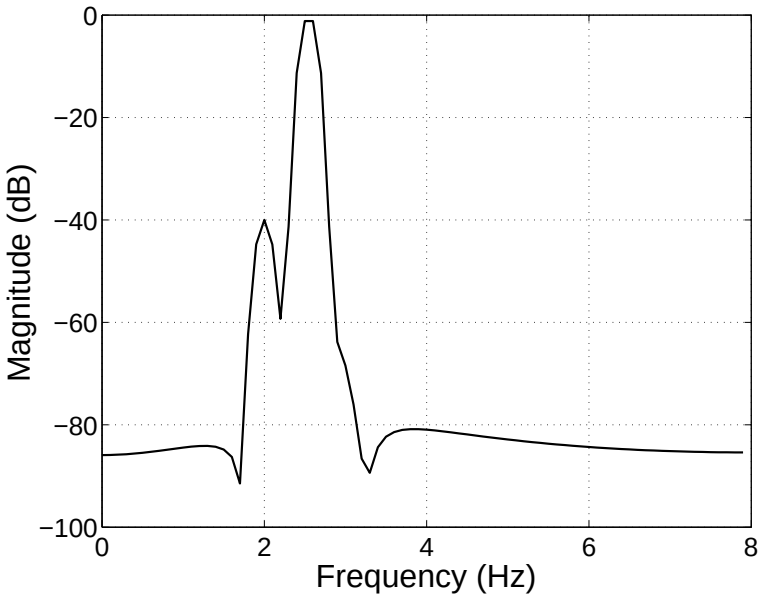

Fig. 32. Spectrum with Kaiser Window.

g. Systematical Approach to DFT

Equation (4.48) is the basic equation, however it is not clear how to select its parameters, such as N and the sampling interval. From the design viewpoint, the sampling frequency and minimum distinguishable frequency are the main parameters to determine. To distinguish the signals, which are very close or close to DC, the signal must be observed for one period of the lowest frequency or minimum difference frequency of two signals of interest. Since simulation time is limited, it must be equal to or longer than the required observation time, T_{obs}. The sampling frequency f_s dictates the upper edge of the band of interest because of the Nyquist theorem. Therefore, the total number of samples is,

$$N = \frac{T_{obs}}{\Delta t} = \frac{f_s}{\Delta f} \tag{4.66}$$

where Δt (sampling period) and Δf (frequency resolution) are the time difference between two consecutive samples and the minimum distinguishable frequency, re-

spectively. Using (4.66) the following important relations are derived,

$$\text{Sampling Frequency} \quad f_s = 1/\Delta t = N\Delta f \tag{4.67}$$

$$\text{Frequency Resolution} \quad \Delta f = 1/T_{obs} = 1/(N\Delta t) \tag{4.68}$$

To test whether correct samples are obtained from a periodic signal, the samples should be repeated. The newly constructed signal should show the same time domain behavior as the original periodic signal. For example, a sinusoidal signal shown in Fig. 33 is first sampled, and then repeated. This new signal should show the same time domain behavior as the original sinusoidal signal. The spectrum shown in Fig. 34 consists of frequency bins separated by frequency resolution.

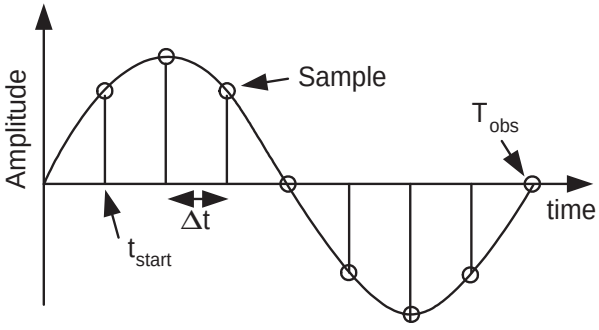

Fig. 33. Time Domain Waveform.

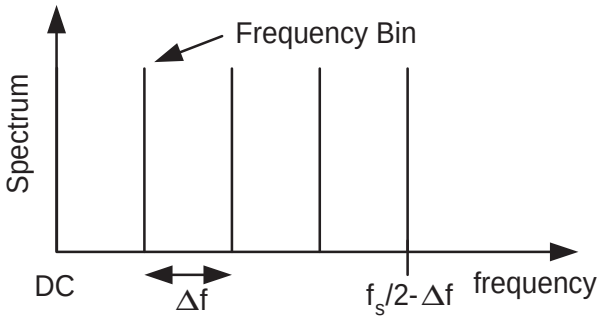

Fig. 34. Frequency Domain Waveform.

2. Noise

Thermal noise is modeled as a zero-mean stationary, Gaussian random process. The distribution is defined mathematically as

$$f(x) = \frac{1}{\sigma\sqrt{2\pi}} \exp\left[-\frac{x^2}{2\sigma^2}\right] \tag{4.69}$$

where σ is the standard deviation or root mean square value of the variable x. If there is no correlation between samples, Gaussian distribution has a flat spectral density, which is defined as

$$S_N(f) = \frac{\eta}{2}, \quad -\infty < f < \infty \tag{4.70}$$

where $\eta/2$ is the uniform spectral density of thermal noise. Equation (4.70) is not physically realizable, since its total integrated power is infinity. However, the bandwidths of the real systems are always finite. Therefore, (4.70) is rewritten as

$$S_N(f) = \begin{cases} \frac{\eta}{2}, & |f| < B \\ 0, & \text{elsewhere} \end{cases} \tag{4.71}$$

where B is the system bandwidth. The total power of the noise source is

$$\int_{-B}^{B} S_N(f)df = \eta B < \infty \tag{4.72}$$

Although noise is obtained when it is observed for infinite time, computer simulations must be finite. Moreover, computers can not process continuous signals; all the signals must be discrete. These put two limitations on the computer simulation of the noise sources. First the noise bandwidth is limited with half of the sampling frequency. Second, noise bandwidth starts from minimum frequency resolution which is determined by simulation time.

Since the bandwidth of sampled systems is limited to half of the sampling fre-

quency, the power of the noise source is $\eta f_s/2$, which is equal to the σ^2 for Gaussian distribution.

Flicker noise has a power spectral density that decreases with $1/f^{\alpha}$. This noise is generated by passing the white noise through a filter having the transfer function

$$H(f) = \frac{K}{\sqrt{f^{\alpha}}} \tag{4.73}$$

This transfer function is implemented using an IIR filter [30]. The numerator of the filter equals to 1 and the denominator coefficients are calculated recursively using the following algorithm

$$\begin{aligned} a_0 &= 1 \\ a_k &= \left(k - 1 - \frac{\alpha}{2}\right) \frac{a_{k-1}}{k} \end{aligned} \tag{4.74}$$

where α is 1 for most cases. A typical noise spectrum for 1 MHz corner frequency, $1nV/\sqrt{Hz}$ thermal noise density and 200 MHz sampling frequency is shown in Fig. 35.

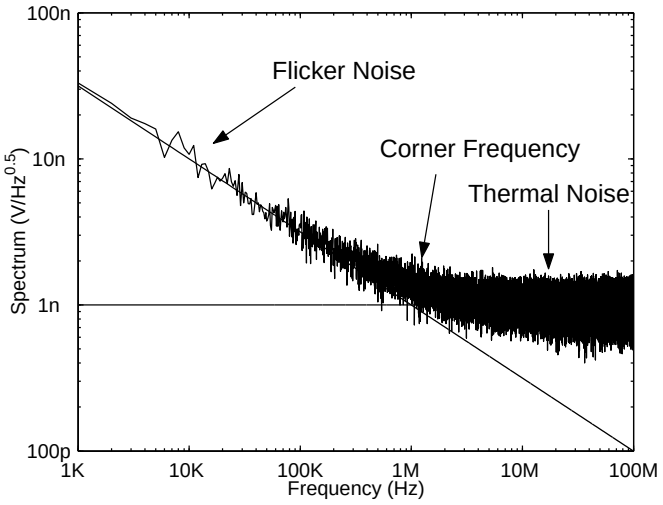

Fig. 35. Thermal and Flicker Noise Spectrum.

3. Phase Noise

Generating phase noise which matches the desired response is the main challenge in phase noise simulations. The methods are whether filtering white Gaussian noise or generating exact phase noise response by summing of sinusoidal signals. First approach generates signals without repetitive pattern and is simulation efficient. However, if the phase noise response is approximated to a known filter response, accuracy of the model is degraded. On the other hand, any arbitrary phase noise response can be modeled using the second approach in the expense of increased simulation time and accuracy for limited bandwidth. Therefore, there is no general approach that works for every possible phase noise response.

The sinusoidal oscillator output $V_O(t)$ is modeled as

$$V_O(t) = \cos(2\pi f_O t + \Delta\theta(t)) \tag{4.75}$$

where f_O is oscillator output frequency in Hz, and $\Delta\theta(t)$ is random phase fluctuations due to phase noise. To simplify the model, oscillator amplitude is assumed 1, and amplitude noise is neglected. $\Delta\theta(t)$ has also spectral density, denoted as $\Delta\theta(f)$, which is also the spectral density of phase noise at the baseband. Although spectral density of phase noise is used during receiver design, the time domain simulations require $\Delta\theta(t)$. Therefore, modeling of phase noise is reduced to conversion of $\Delta\theta(f)$ to $\Delta\theta(t)$. The simplest phase noise spectrum is an impulse, which is a sinusoidal signal in time domain. The integrated phase noise is concentrated in this single impulse. Therefore, oscillator output becomes

$$V_O(t) = \cos(2\pi f_O t + \beta \sin(2\pi f_m t)) \tag{4.76}$$

where β is the amplitude or modulation index and f_m is the frequency of the sinusoidal

phase noise impulse. To determine the spectrum of $V_O(t)$, (4.76) is rewritten as

$$\begin{aligned} V_O(f) &= \Re\left\{e^{j(2\pi f_O t+\beta\sin(2\pi f_m t))}\right\} \\ &= \Re\left\{e^{j2\pi f_O t}e^{j\beta\sin(2\pi f_m t)}\right\} \end{aligned} \tag{4.77}$$

The second part of (4.78) is written as sum of Bessel series.

$$e^{j\beta\sin(2\pi f_m t)} = \sum_{n=-\infty}^{\infty} J_n(\beta_m)e^{j2\pi f_m t} \tag{4.78}$$

By inserting (4.78) into (4.78), the oscillator output voltage is written as

$$V_O(f) = \frac{1}{2}\sum_{n=-\infty}^{\infty} J_n(\beta)\left[\delta\left(f+f_O+nf_m\right)+\delta\left(f-f_O-nf_m\right)\right] \tag{4.79}$$

where δ is the Dirac function.

Equation 4.79 indicates that there are infinite number of impulses, although phase noise spectral density has only one impulse. However, for small values of the modulation index β, Bessel coefficients are approximated as

$$\begin{aligned} J_0(\beta) &\approx 1 \\ J_1(\beta) &\approx \frac{\beta}{2} \\ J_n(\beta) &\approx 0 \quad n>2 \end{aligned} \tag{4.80}$$

Inserting (4.80) into (4.79), time-domain signal for small modulations is derived as

$$V_O(f) = \cos[2\pi f_O t] + \frac{\beta}{2}\left(\cos[(f_O+f_m)t] + \cos[(f_O-f_m)t]\right) \tag{4.81}$$

Equation 4.81 indicates that phase noise is at the sideband of oscillator output. Random phase noise has a spectral shape, and approximating it as an impulse does not give enough detail from the design perspective. The desired spectral shape can be obtained whether shaping a white Gaussian noise source with a filter, which has the

desired frequency response, or summing multiple impulses to match the desired spectrum. Filter method has shorter simulation-time than summing method, but it is harder to model the desired spectrum unless the spectrum matches a known filter response.

a. Summing Impulses Method

The random phase fluctuation is defined as the sum of infinite number of sinusoidal signals. Substituting $\sum_{m=0}^{\infty} \beta_m \sin(2\pi f_m t)$ into (4.75) and rewriting it similar to (4.78) gives

$$\begin{aligned} V_O(t) &= \cos\left[2\pi f_O t + \sum_{m=0}^{\infty} \beta_m \sin(2\pi f_m t)\right] \\ &= \Re\left\{e^{j\left(2\pi f_O t + \sum_{m=0}^{\infty} \beta_m \sin(2\pi f_m t)\right)}\right\} \\ &= \Re\left\{e^{j2\pi f_O t} \prod_{m=0}^{\infty} e^{j\beta_m \sin(2\pi f_m t)}\right\} \end{aligned} \tag{4.82}$$

The spectrum is calculated by inserting (4.78) into (4.82)

$$V_O(f) = \frac{1}{2} \prod_{m=0}^{\infty} \sum_{n=-\infty}^{\infty} J_n(\beta_m) \left[\delta\left(f + f_O + nf_m\right) + \delta\left(f - f_O - nf_m\right)\right] \tag{4.83}$$

Using (4.80) spectrum is approximated for small modulations as

$$V_O(f) = \cos(2\pi f_O t) + \frac{\beta}{2} \sum_{n=0}^{\infty} \left[\cos((f_O + nf_m)t) + \cos((f_O - nf_m)t)\right] \tag{4.84}$$

Equation (4.84) also shows that the baseband phase noise appears as sidebands. Since simulation time increases with n, phase noise is modeled only at the band of interest with finite number of n. To avoid repetitive patterns of generated data, n is selected so that the frequency difference between impulses is smaller than the frequency resolution of the simulation.

According to (4.75), the output power of the oscillator is constant regardless of

phase noise. Therefore, carrier power is the difference between the total power and the phase noise power. In the case of high noise levels, the carrier will be diminished. To avoid this case, carrier power is calculated as

$$V_O(f_c) = \frac{1}{2}\prod_{m=0}^{\infty} J_0(\beta_m)\left[\delta\left(f+f_O\right)+\delta\left(f-f_O\right)\right] \tag{4.85}$$

If the approximation in (4.80) holds, (4.85) will be approximately 1. Therefore, a boundary is determined by limiting the degradation of (4.85) to 1%. This limit number is selected arbitrary, and guarantees 99% of the oscillator output power on the carrier.

b. Filter Method

The main drawback of summing impulses is the computation time increases with number of impulses. To overcome this problem the random phase fluctuations is generated by filtering white Gaussian source in discrete domain. Since the filter is discrete, it is realized using addition and multiplication. Therefore, it does not require trigonometric calculations, which usually takes long time to compute.

The oscillator output is written for a strictly stationary random process $\phi(t)$ as

$$\begin{aligned} V_O(t) &= \cos(2\pi f_O t + \phi(t)) \\ &= \Re\left\{e^{j2\pi f_O t} e^{j\phi(t)}\right\} \\ &= \Re\left\{e^{j2\pi f_O t} v(t)\right\} \end{aligned} \tag{4.86}$$

where $v(t) = e^{j\phi(t)}$. The power spectral densities of $V_O(t)$ and $v(t)$ are Fourier transforms of their autocorrelations. Since $V_O(t)$ is the frequency conversion of $v(t)$, the power spectral density of $V_O(t)$ is

$$P_O(f) = \frac{1}{4}\left[P_v(f-f_O)+P_v(-f-f_O)\right] \tag{4.87}$$

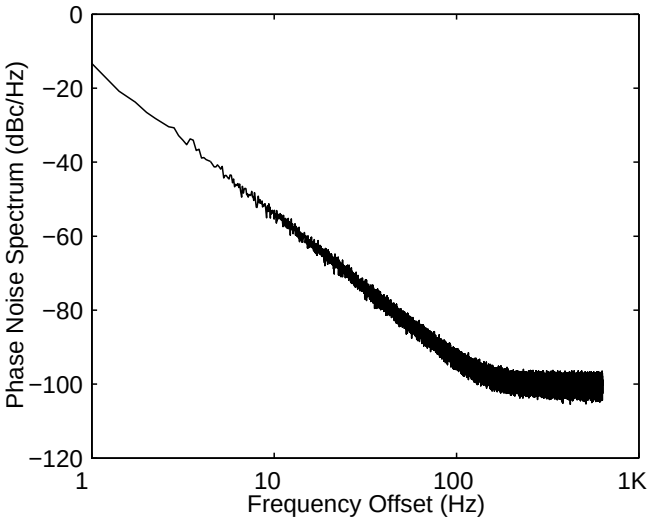

Fig. 36. Simulated Phase Noise Spectrum with $1/f^2$ Slope.

where P_v is the power spectral density of $v(t)$. Equation (4.87) indicates that $P_v(f)$ appears as sidebands. Therefore, the problem is reduced to calculating the filter function which gives the desired spectral shape. A convenient method is to determine the best fit, in the minimum mean square error sense, to the transfer function. Any arbitrary spectrum can be obtained by solving Yule-Walker equations [24]. However, Yule-walker method results in high order filters to match the required responses. For special cases, such as when the spectrum decreases at $1/f^2$ and flat for a limited range, simpler transfer functions can be obtained. If the spectrum decreases only with $1/f^2$ and does not have a flat region, the filter is a simple integrator defined as

$$H(z) = \frac{1}{z-1} \tag{4.88}$$

If the spectrum has a flat region, but the noise slope is $1/f^2$, the required spectrum is generated in analog domain and is converted to digital using bilinear or impulse invariance methods. Simulation results for noise sidebands are shown in Figs. 36 and 37 for spectrum with $1/f^2$ and flat responses, respectively.

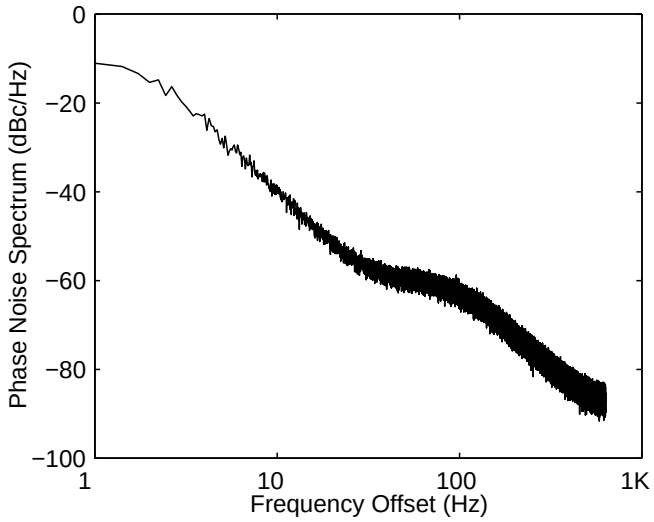

Fig. 37. Simulated Phase Noise Spectrum with a Flat Region.

4. Nonlinearity

The memoryless nonlinearity of components is modeled as weak nonlinearity using (4.20). A model is constructed by ignoring higher than third order terms. If the nonlinearity is caused by the clipping of the signal, it is called strong nonlinearity. The measures, such as third-order intercept point, harmonic distortion, assumes the component under test has only weak nonlinearity. However, under high signal levels, this assumption is not valid and strong nonlinearities should be added to the simulation model. In the model depicted in Fig. 38, the weak nonlinearity is modeled by (4.20). The strong nonlinearity is modeled by saturating the signal at a specific level, which is the maximum voltage swing allowed in the design. The third order intercept point for an amplifier with 0 dBVrms IIP3 is simulated, and the results are shown in Fig. 39. At low signal levels, the amplifier shows weak nonlinearity. When the signal starts to be clipped, the output level at fundamental frequency becomes constant.

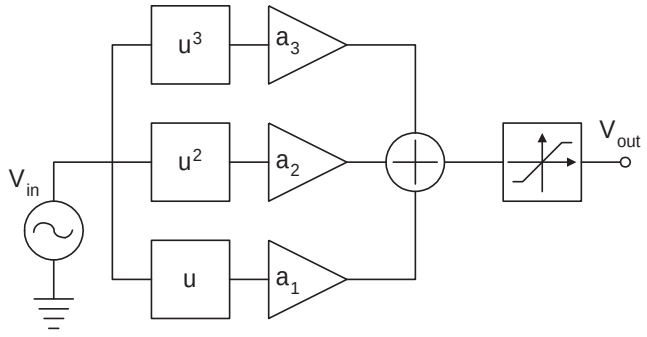

Fig. 38. Amplifier Nonlinearity Model.

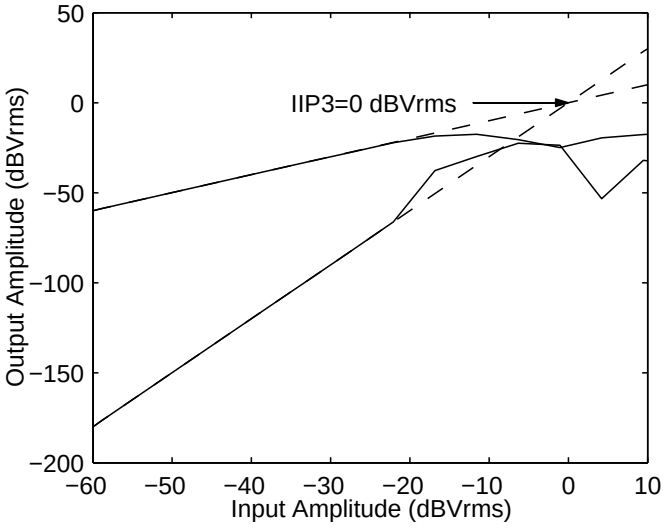

Fig. 39. IIP3 Plot.

CHAPTER V

MULTI-BAND OFDM UWB RECEIVER DESIGN

The first step in the receiver design is selecting the topology based on system analysis. Topology selection involves frequency planning, study of blockers and image frequencies. Once the topology is determined, every building block is defined by evaluating the required gain, noise and dynamic range requirements. Noise requirement is dictated by sensitivity specification. Linearity specification is derived based on the out-of band blockers, because the receiver should not degrade the desired channel in the presence of strong blockers. Overall frequency response of the receiver is determined by group delay variation specifications, desired attenuation of image and blockers.

A. Receiver Design

Topology selection starts with frequency planning. The bandwidth of multi-band OFDM is 528 MHz and the band starts at 3.168 MHz. Therefore, intermediate frequency (IF) can be between 528 MHz and 2904 MHz. If IF is selected as 1188 MHz to relax image rejection, the worst case image frequency will be 5776 MHz. However, this frequency is also in the UWB band, and it is not possible to attenuate this band without complex mixing, which is not feasible at high frequencies. Therefore, the downconversion must be performed directly to DC, which dictates zero-IF receiver topology. To relax overall noise requirements of baseband blocks, the RF signal should be amplified prior to downconversion using a low-noise amplifier (LNA). LNA gain is desired to be programmable to relax linearity requirements of baseband blocks and prevent saturation of LNA. Since the mixer down-converts also blockers, they should be removed before further amplification using a low-pass filter. Otherwise, the

baseband amplifiers must be extremely linear to handle blockers. Although LNA's gain is programmable, it is not possible to cover the whole dynamic range with LNA only. Therefore, another programmable amplifier is needed at the baseband. The location of this amplifier is between low-pass filter and analog-to-digital converter (ADC). This variable-gain amplifier (VGA) relaxes dynamic range of prior blocks in the receive chain. VGA has more number of gain steps than LNA, since it is more efficient to design small gain steps at the baseband.

Multi-band OFDM is a wideband system and susceptible to narrowband in-band interference (NBI). To suppress the NBI, a notch filter is required possibly located before the LNA or before the ADC. Placing the filter before LNA relaxes LNA's linearity requirement, but increases overall noise figure of the receiver due to filter loss. This technique also requires a very high Q filter, since the tone frequency is much smaller than the RF frequency. For example, if the NBI is in the middle of the first band and occupies only one tone, the required Q is above 800. It is not possible to obtain such high-Q levels in current IC technologies; therefore, the suppression should be done at the baseband. The direct conversion architecture with notch filter is depicted in Fig. 40. Since the low-pass filter attenuates the out-of-band interference, the voltage swing is reduced at the notch filter. Variable gain amplifier is placed after the filter to relax its swing requirement, because NBI is reduced by the notch filter. As a result, the optimum location of the notch filter is between the low-pass filter and the VGA, as in Fig. 40.

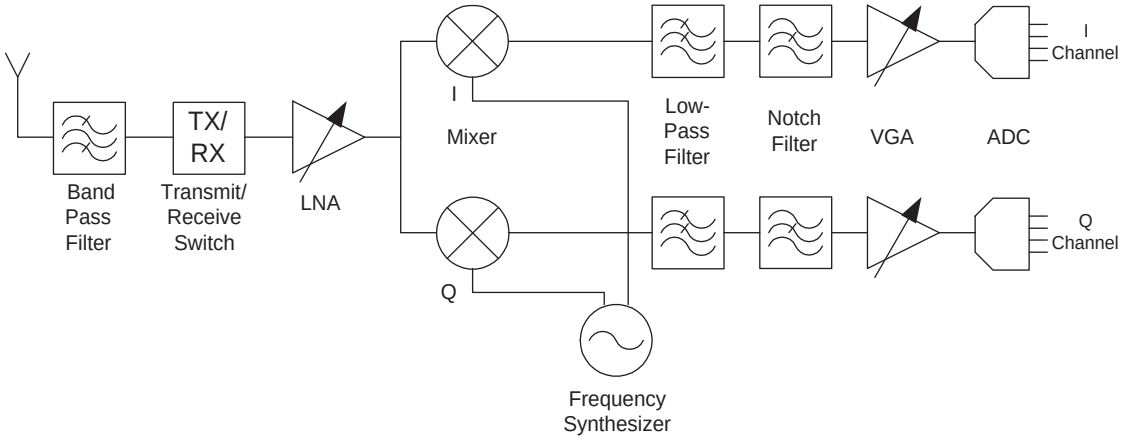

Fig. 40. Receiver Schematic.

1. Noise, Gain and Dynamic Range

The maximum gain is needed when the communication is at the minimum data rate at the sensitivity level, which is -83.6 dBm. The minimum gain is used when the receiver is very close to the transmitter. In this case the received average power is -10.3 dBm. The dynamic range, DR, is calculated as follows

$$DR = P_{max} - P_{sens} \tag{5.1}$$

where P_{max} and P_{sens} are the maximum received power and the minimum sensitivity level, respectively. Their units are in dBm, therefore, the dynamic range is obtained in dB. For MB-OFDM the required dynamic range is 73.3 dB.

Since the input is differential and UWB signal's peak-to-average ratio is 9 dB, the peak-to-peak input voltage swing is calculated as follows

$$V_{PP} = 2 \cdot \sqrt{\cdot 100 \cdot 10^{(P_{dBm}+9-30)/10}} \tag{5.2}$$

The output differential peak-to-peak voltage swing is selected as 1 V. Since supply voltage is 1.8 V, and single ended maximum peak-to-peak voltage swing is 0.5 V,

1.3 V remains for transistor biasing. Since the minimum and the maximum peak-to-peak differential voltage swing at the input are 117.8 μV and 0.54 V, the maximum and the minimum gains required are 78.6 dB and 5.3 dB, respectively.

The loss for the pre-select and transmit-receive switch is 1.1 dB and 0.6 dB. Therefore, using the (4.16) the noise figure for the rest of the blocks is 4.9 dB.

2. Out-Of Band Interferences

FCC limits the actual field intensity or power density at a given distance from a transmitter. Field intensity or power density calculations are necessary when estimating electromagnetic interference (EMI) effects, when determining potential radiation hazards (personnel safety), or in determining or verifying specifications. Field intensity (field strength) is a general term that usually means the magnitude of the electric field vector, commonly expressed in volts per meter. At frequencies above 100 MHz, and particularly above 1 GHz, power density (P_D) terminology is more often used than field strength. Power density and field intensity are related by

$$P_D = \frac{E^2}{Z_0} = \frac{E^2}{120\pi} = \frac{E^2}{377} \tag{5.3}$$

where P_D is in W/m^2 , E is the RMS value of the field in volts/meter and Z_0 is the characteristic impedance of free space. For a known transmitted power, the expected signal strength is determined at a specified distance from the transmitter. Assuming signal is radiating isotropically into a sphere, the power is evenly distributed over a surface equal to $4\pi r^2$, where r is the distance from the transmitter in meters. The power density at the receiver, expressed in watts/m^2, can be determined by

$$P_D = \frac{P_t}{4\pi r^2} \tag{5.4}$$

Table VI. Interferences.

Fundamental Frequency	Power of Fundamental	Power of Harmonics
$902 - 928$ MHz	18.75 dBm	-31 dBm
$1.910 - 1.930$ GHz	4.77 dBm	
$2.390 - 2.400$ GHz	4.77 dBm	
$2.435 - 2.465$ GHz	18.75 dBm	-31 dBm
$5.15 - 5.25$ GHz	17 dBm	
$5.25 - 5.35$ GHz	24 dBm	
$5.725 - 5.825$ GHz	30 dBm	
$5.785 - 5.815$ GHz	18.75 dBm	-31 dBm
$10.500 - 10.550$ GHz	32.73 dBm	-7.27 dBm

where P_t is the input power. Inserting (5.4) into (5.3) and solving for P_t gives

$$P_t = \frac{E^2 4\pi r^2}{377} \tag{5.5}$$

If the field intensity is given, the transmitted power is calculated using (5.5). The power levels and frequencies of interferences that can affect the UWB communication is summarized in Table. VI.

Operation within the bands $902 - 928$ MHz, $2435 - 2465$ MHz, $5785 - 5815$ MHz, $10500 - 10550$ MHz, and $24075 - 24175$ MHz is limited to intentional radiators used as field disturbance sensors, excluding perimeter protection systems. The maximum field strength at 3 meters should be below 500 mV/m except for the bands $10500 - 10550$ MHz, and $24075 - 24175$ MHz, which is limited to 2500 mV/m.

Operation within the bands $902 - 928$ MHz, $2400 - 2483.5$ MHz and $5725 -$

5850 MHz is limited to frequency hopping and digitally modulated intentional radiators. The maximum peak output power of the intentional radiator should not exceed 1 watt for frequency hopping systems operating in the $2400 - 2483.5$ MHz band employing at least 75 hopping channels, and all frequency hopping systems in the $5725 - 5850$ MHz band. For all other frequency hopping systems in the $2400 - 2483.5$ MHz band, the peak output power is 0.125 watts. In $902 - 928$ MHz band the peak power is limited to 1 watt for systems employing at least 50 hopping channels, and 0.25 watts for systems employing less than 50 hopping channels. In case of the systems using digital modulation in the $902 - 928$ MHz, $2400 - 2483.5$ MHz, and $5725 - 5850$ MHz bands the limit is 1 Watt.

FCC also puts regulations for unlicensed National Information Infrastructure (U-NII) devices operating in the $5.15 - 5.35$ GHz and $5.725 - 5.825$ GHz bands. The peak transmit power over the $5.15 - 5.25$ GHz band should not exceed 50 mW or 4 dBm + $10 \log B$, where B is the 26-dB emission bandwidth in MHz. The limit for $5.25 - 5.35$ GHz band and $5.725 - 5.825$ GHz band are 250 mW or 11 dBm + $10 \log B$ and 1 W or 17 dBm + $10 \log B$, respectively.

The typical applications operating at these frequency bands are wireless local area network (LAN) devices, such as IEEE 802.11a, 802.11b and Bluetooth, and microwave ovens. The frequency band is illustrated in Fig. 41. The MB-OFDM receiver should operate even in the presence of these interferences, which have higher power levels than maximum transmit power of UWB.

The out-of band interferences are first attenuated by external band select filter, which is typically SAW type. After the downconversion, the low pass filter attenuates them. The interference power levels at the output of band select filter are summarized in Table. VII. The frequency of 802.11a interference is closer to the sub-band 1 than the other interference sources. Therefore, for the low-pass filter attenuation of 802.11a

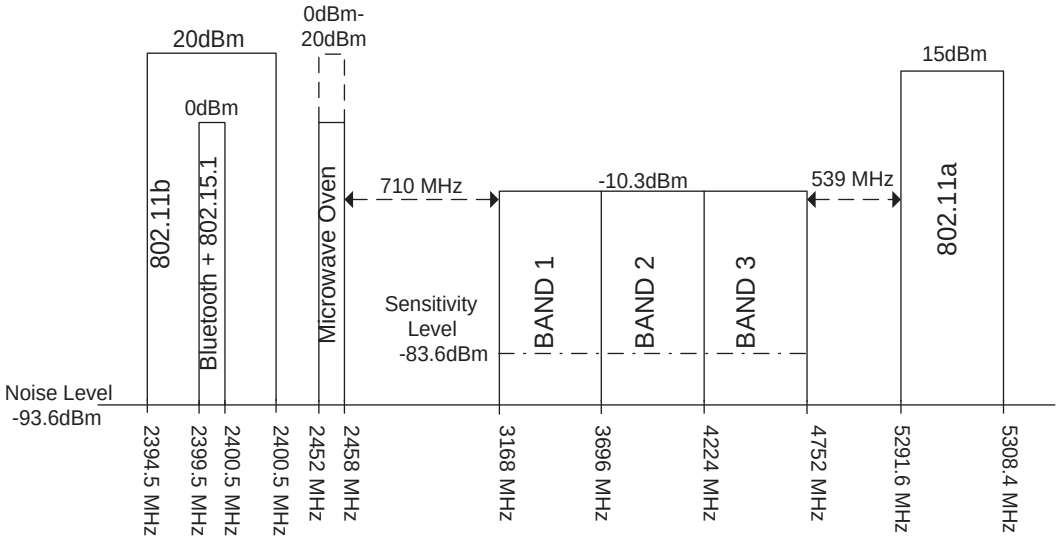

Fig. 41. Out-Off Band Interference Spectrum.

interference is the worst case.

3. Low-Pass Filter

Inherently, mixer output has also frequency components at twice of the carrier frequency. Additionally, the out-of band interference components are also downconverted. These frequency components are attenuated by the low-pass filter. The filter order and approximation are selected according to the attenuation at these frequencies. In order not to affect the receiver performance, the interference components should be at the noise level. Usually the filter order is higher than two.

A high-order filter function $H(s)$ can be realized as a cascade connection of lower-order stages, preferably first and second order. If $H(s)$ is an odd order transfer function, there will be a first order stage. For even order transfer functions, the filter can be realized by using only second order stages. The high-order transfer function

Table VII. Received Interference Power after Band Select Filter.

Fundamental Frequency	Filter Attenuation	Power after Filter
$902 - 928$ MHz	35 dB	-16.25 dBm
$1.910 - 1.930$ GHz	35 dB	-25.23 dBm
$2.390 - 2.400$ GHz	35 dB	-25.23 dBm
$2.435 - 2.465$ GHz	35 dB	-16.25 dBm
$5.15 - 5.25$ GHz	25 dB	-8 dBm
$5.25 - 5.35$ GHz	30 dB	-6 dBm
$5.725 - 5.825$ GHz	35 dB	-5 dBm
$5.785 - 5.815$ GHz	35 dB	-16.25 dBm
$10.500 - 10.550$ GHz	35 dB	2.73 dBm

$H(s)$ can be written as follows

$$H(s) = h(s) \cdot \prod_{i=1}^{N} h_i(s) \tag{5.6}$$

where $h(s)$ is the first-order term for odd-order functions and equals to unity for even-order transfer functions. The filter order is $N/2$ and $(N-1)/2+1$ for even and odd-order transfer functions, respectively. $h_i(s)$ is the second-order transfer function and is given as

$$h_i(s) = \frac{a_2 s^2 + a_1 s + a_0}{s^2 + \omega_0 s/Q + \omega_0^2} \tag{5.7}$$

where ω_0 and Q are natural frequency and quality factor of the poles, respectively. Depending on $H(s)$, one or two numerator coefficients of $h_i(s)$ may be zero. The

group delay variation of the second-order low-pass function is

$$G_d = \frac{\omega^2 + \omega_0^2}{\left(\omega_0^2 - \omega^2\right)^2 + \frac{\omega^2\omega_0^2}{Q^2}} \tag{5.8}$$

The variation is a function of the quality factor and for higher Q values the group delay variation increases. Therefore, realizing the filter using low Q biquads reduces the overall group delay variation of $H(s)$.

The attenuation of the interferences depends on the approximation of the low-pass filter. In the literature, there are mainly two different approaches for filter approximations. One is the magnitude type and the other is delay type. Typical examples for magnitude type approximation are Butterworth, Chebyshev, Inverse Chebyshev and Elliptic filter. Although delay type filters give better group delay variations than magnitude type filter, their attenuation performance is worse.

Butterworth approximation shows a flat response in band, and monotonically increasing attenuation. The amplitude function is given by

$$M(\omega) = \frac{1}{\left[1 + \omega^{2n}\right]^{1/2}} \tag{5.9}$$

where n is the filter order. At the cut-off frequency ($\omega = 1$) the amplitude is 3 dB lower than its DC value. Between DC and cut-off frequency the magnitude response is decreased monotonically. Above cut-off frequency the attenuation is $20n$ dB/decade. Butterworth filter has n poles, which are located on the unit circle on the complex plane. By increasing filter order, the poles are closer to the $j\omega$ axes. This requires higher Q factors for the biquads and results in higher group delay variation with increasing filter order.

If higher attenuation than Butterworth approximation is desired, the Chebyshev approximation can be used in the expense of ripple in the passband and worse group

delay variations. The magnitude function for Chebyshev filter is

$$M(\omega) = \frac{1}{\sqrt{1+\epsilon^2 C_n^2(\omega)}} \tag{5.10}$$

where ϵ is the maximum error in the pass band, and $C_n(\omega)$ is the Chebyshev polynomial of degree n and is defined as

$$\begin{aligned} C_n(\omega) = &\quad \cos(n\cos^{-1}\omega), \qquad 0 \le |\omega| \le 1 \\ = &\quad \cosh(n\cosh^{-1}\omega), \qquad 1 \le |\omega| \end{aligned} \tag{5.11}$$

The attenuation for $\omega \gg 1$ is $20\log(\epsilon) + 6(n-1) + 20n\log(\omega)$ dB. Compared to Butterworth approximation it has $20\log(\epsilon) + 6(n-1)$ dB advantage. However, for $\epsilon < 1$ the advantage is less significant, since $\log(\epsilon)$ becomes negative. The poles of Chebyshev approximation lie on an ellipse. For the same filter order, the required Q-factors are higher than Butterworth approximation. Therefore, it has higher group delay variations.

When high falloff rate is required near the cut-off frequency Inverse Chebyshev or Elliptic approximations can be used. By putting zeros in the passband close to the cut-off frequency, a notch is created in the magnitude response. This notch increases the attenuation near the cut-off frequency, but results in peaks in the pass-band.

The low-pass filter in the proposed design is selected as Butterwoth type to reduce the group delay variations. The cut-off frequency is selected as 264 MHz in order to achieve maximum attenuation of out-of band interferers without attenuating the desired channel. Since the VGA and the notch filter have finite bandwidths, they will also attenuate the out-of band interferers. Although finite bandwidth relaxes the low-pass filter order, the cut-off frequency will be lowered. By selecting the bandwidths of notch filter and VGA properly, the degradation on overall cut-off frequency

Table VIII. Attenuation at 802.11a Interference.

Filter Order	Attenuation of 802.11a	Power Level at the output	Attenuation of Microwave oven	Power Level at output
1	10.11 dB	−25.11 dBm	11.65 dB	−26.65 dBm
2	19.37 dB	−34.37 dBm	22.7 dB	−37.7 dBm
3	29 dB	−44 dBm	34.02 dB	−49.02 dBm
4	38.65 dB	−53.65 dBm	45.36 dB	−60.36 dBm
5	48.31 dB	−63.31 dBm	56.7 dB	−71.7 dBm
6	58 dB	−73 dBm	68.03 dB	−83.03 dBm
7	67.64 dB	−82.64 dBm	79.37 dB	−94.37 dBm

is minimized. The attenuation at the 802.11a interference determines the filter order, since it is closer than microwave and 802.11b operating frequencies. If 802.11a interference power is equal to noise level and there is extra 20 dB attenuation due to notch filter and VGA, a 6th order low-pass filter will be adequate according to the Table. VIII. Increasing filter order further requires more area, and also degrades noise performance.

4. Linearity

Linearity determines the upper limit for maximum RF signal that the receiver can process with adequate output SNR. It is usually characterized using two-tone test, which is used to determine second and third order intermodulation products. These unwanted tones are due to nonlinear elements in the receive chain. The nonlinearity has two effects for MB-OFDM receiver. The third order intermodulation product of adjacent and second adjacent channel is on the desired band and degrades the

signal-to-noise ratio. The out-of band blockers are removed by low-pass filter after the downconversion. Therefore, LNA and mixer must handle them without saturation or creating high intermodulation products. In MB-OFDM proposal, the maximum transmit power is -10.3 dBm. However, this level will be reduced due to distance between the victim receiver and aggressor. For 20 dB attenuation, the total required IIP3 is -13.11 dBVrms. For baseband blocks, the signal itself creates intermodulation products. Since OFDM is a multi-tone signal, the intermodulation products due to second, third and higher order products create the noise floor. The lower limit of linearity is also verified by system simulations. The IIP2 and IIP3 points of the receiver are swept and degradation on the packet-error-rate is determined. Simulation results shown in Figs. 42 and 43 indicate that IIP2 and IIP3 should be greater than -15 dBVrms in order to have reliable communication. With 10 dB margin, overall system input referred third order intercept point is selected as -5 dBVrms. Since the receiver is fully differential, the second order intercept point is selected as 15 dBVrms.

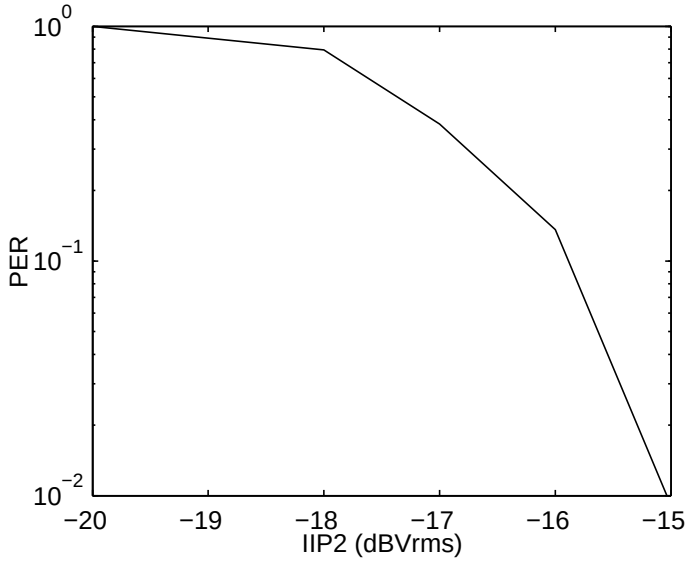

Fig. 42. IIP2 (dBVrms).

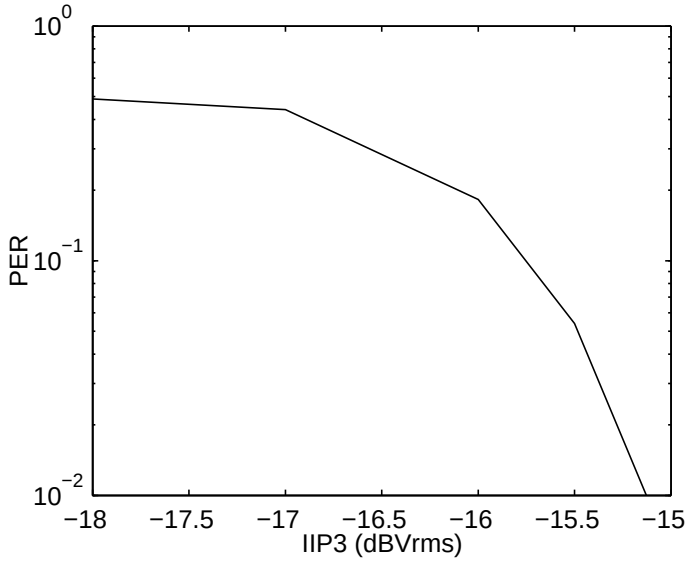

Fig. 43. IIP3 (dBVrms).

5. IQ Imbalance and DC offset

IQ imbalance can be separated as gain and phase imbalance. Gain imbalance causes reduction in the desired signal power. Phase imbalance creates crosstalk interference between in-phase and quadrature components. Since in-phase and quadrature components' average powers are similar, a small phase error causes a large degradation in performance. The gain and phase imbalance specifications are extracted using system level simulations. During the gain imbalance simulations, phase imbalance is selected as 0°. The simulation result depicted in Fig. 44 indicates that the gain imbalance should be less than 2 dB. During the phase imbalance simulations the gain imbalance is selected as 0 dB. The phase imbalance shown in Fig. 45 indicates that the phase imbalance should be below 10°. With a margin the overall gain and phase imbalance should be less than 1 dB and 5°, respectively.

The input level of analog-to-digital converter is optimized for maximum signal-

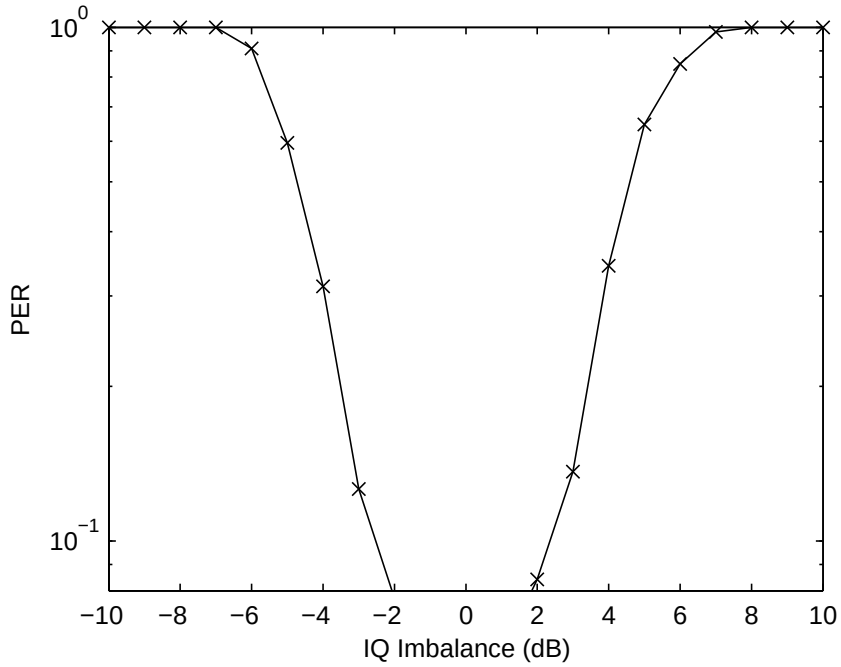

Fig. 44. IQ Gain Imbalance (dB).

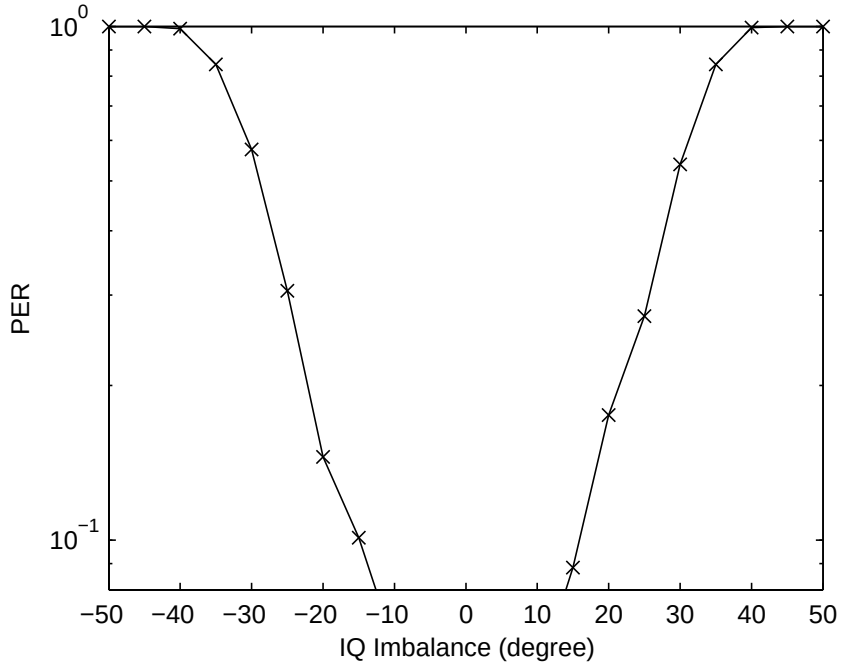

Fig. 45. IQ Phase Imbalance (deg).

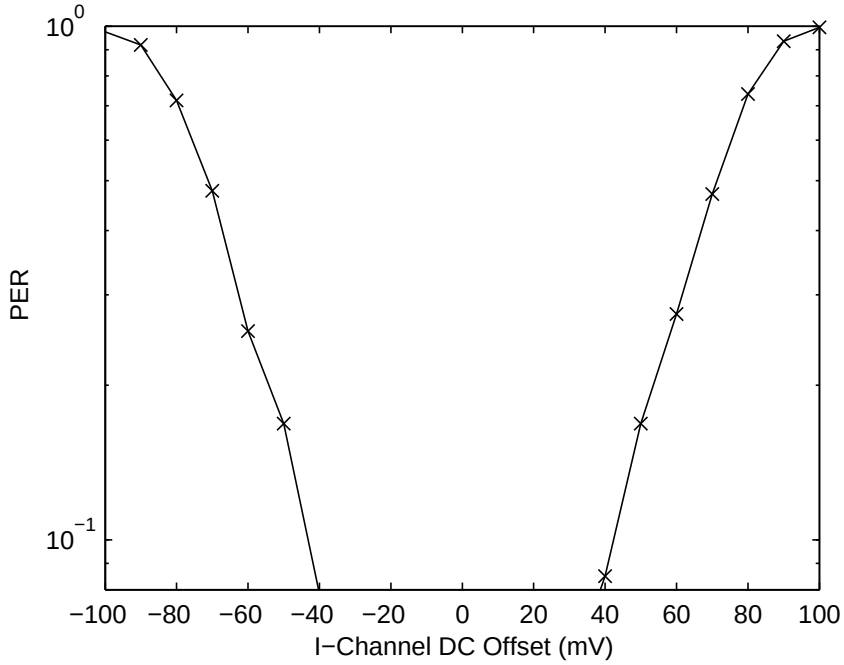

Fig. 46. DC Offset on the I Channel (mV).

to-quantization noise. If there is a DC offset on I or Q channel, the signal will be clipped and quantization noise increases due to the overdrive of the converter. The DC offset on the I and Q channels should be limited for optimum performance. The maximum tolerable DC offset levels are determined by simulation. According to the results depicted in Figs. 46 and 47 the DC offset should be below ±40 mV. To guarantee proper operation the offset is limited to ±20 mV.

6. Frequency Response

The frequency response of individual blocks affects the overall frequency response of the receiver. Usually it is desired that the low-pass filter determines the overall frequency response of the receiver. With proper tuning algorithms or circuit techniques, the 3-dB bandwidth of the filter is well-controlled. Therefore, attenuation at the cut-off frequency of low-pass filter should be minimal for the rest of the chain.

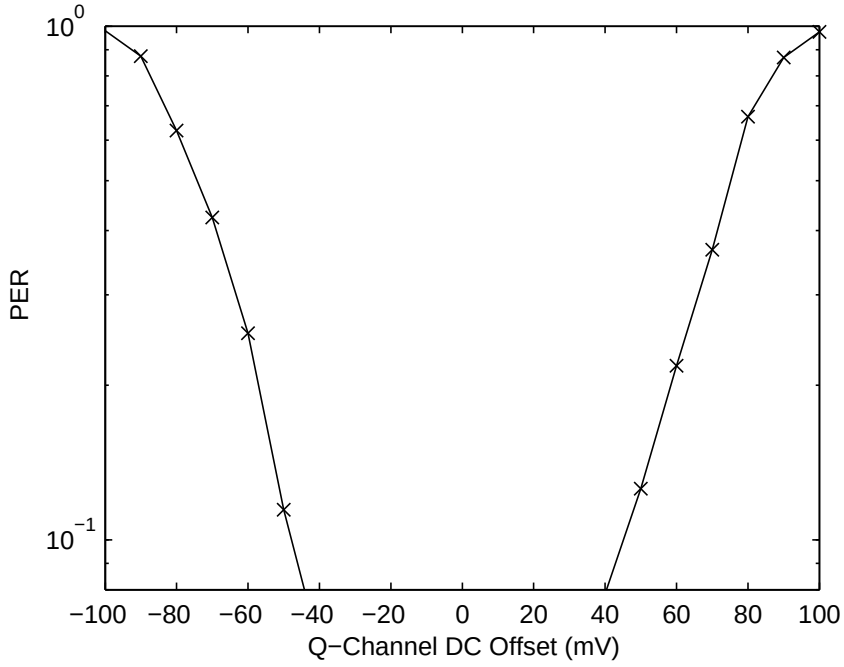

Fig. 47. DC Offset on the Q Channel (mV).

The cut-off frequency of the low-pass filter is selected as 264 MHz. Since the last two subcarriers are used to relax the filter requirements, the overall cut-off frequency should be above 255.75 MHz. However, the overall cut-off frequency reduces due to the finite bandwidth of other blocks. Their bandwidth is selected as 420 MHz. The total frequency response is shown in Fig. 48. The overall 3-dB frequency is 261 MHz. The attenuation at 255.75 MHz is −2.5 dB.

The total group delay variation as depicted in Fig. 49 is 2.27 ns. The low-pass filter creates maximum variation because it has the minimum cut-off frequency and highest order. The variation due to the LPF is 1.58 ns.

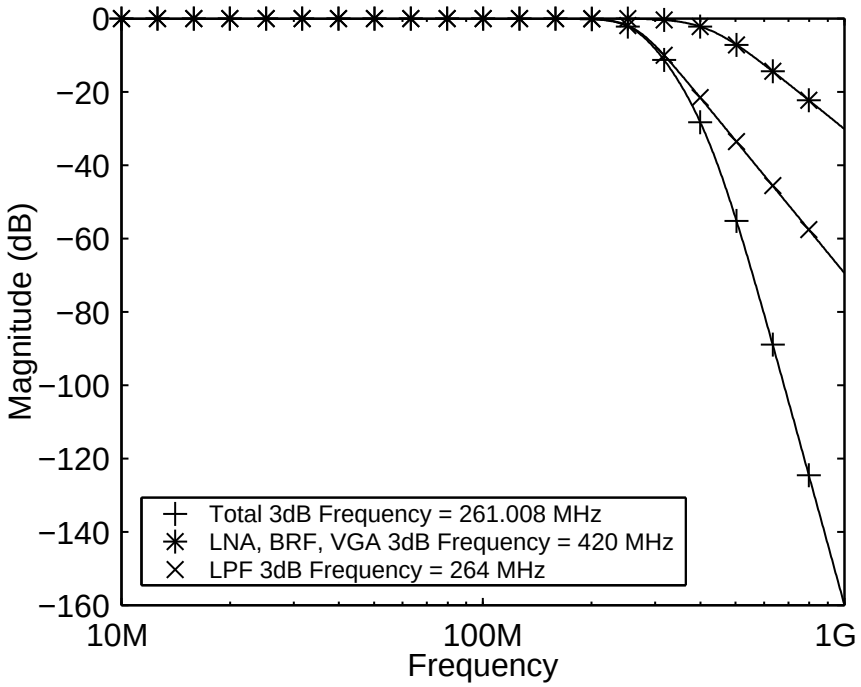

Fig. 48. Receiver Frequency Response.

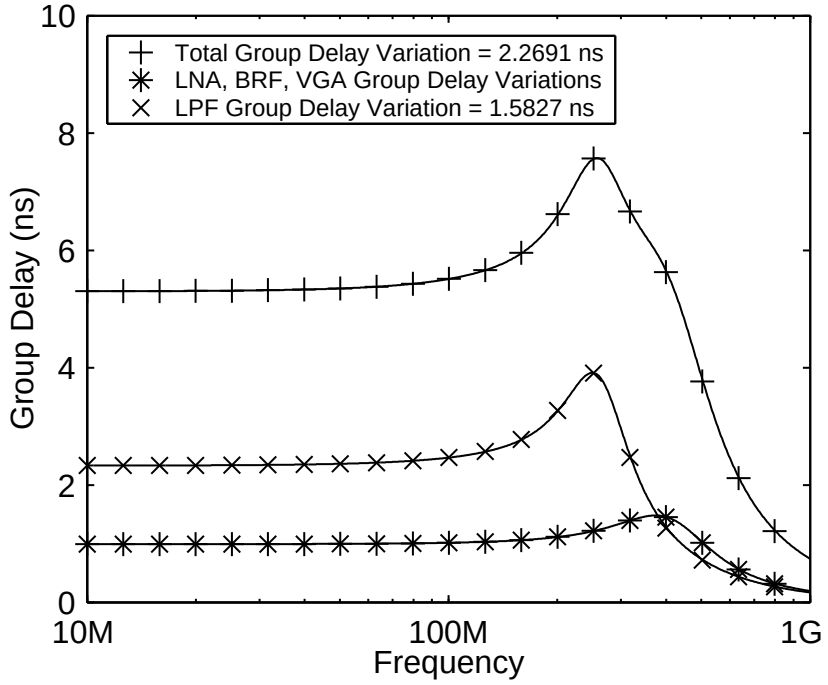

Fig. 49. Receiver Group Delay.

7. Phase Noise

Phase noise specification is more relaxed in UWB systems compared to narrowband systems, since there is no interferer close to the oscillator frequency. Phase noise causes downconversion of adjacent tones at the same frequency and reduces signal-to-noise ratio. The phase noise specification for the proposed system is extracted for maximum mandatory data rate. The simulation result shown in Fig. 50 indicates that the degradation is negligible if the phase noise is below -85 dBc/Hz at 100 KHz. Therefore, the phase noise specification is selected as -90 dBc/Hz with 5 dB margin. Since the phase noise model assumes $1/f^2$ characteristics, a phase noise mask, shown in Table. IX, is defined to guarantee synthesizer's phase noise performance.

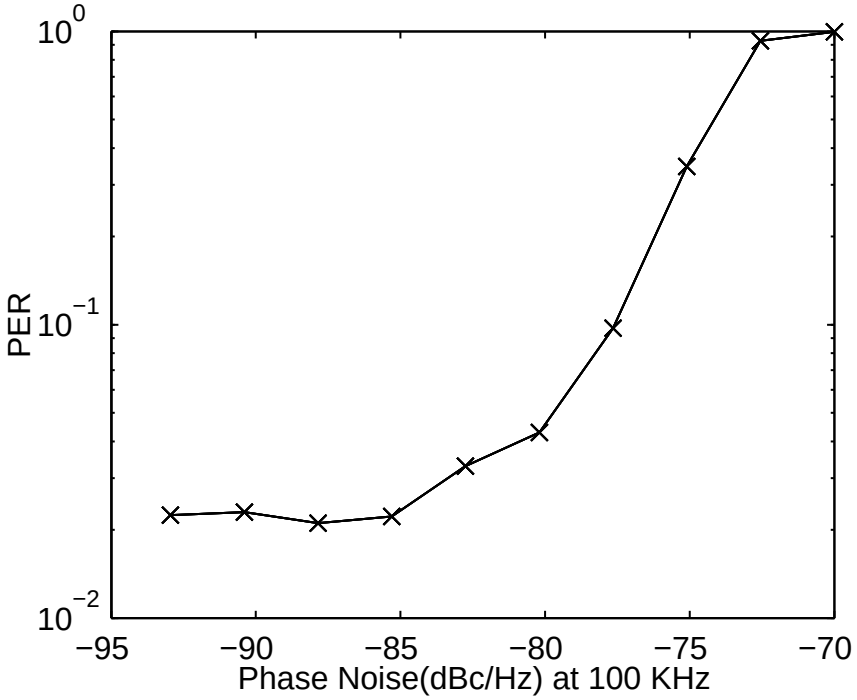

Fig. 50. Phase Noise Performance (Eb/No=4.7 dB).

Table IX. Phase Noise Mask.

Offset Frequency	Phase Noise
1 KHz	−50 dBc/Hz
10 KHz	−70 dBc/Hz
100 KHz	−90 dBc/Hz
1 MHz	−110 dBc/Hz
10 MHz	−130 dBc/Hz

8. Analog-to-Digital Converter

A typical receiver has an automatic gain control (AGC) loop, which is used to set the overall receiver gain to maintain the output signal at a constant level. This level is determined by the signal characteristics and ADC input range. If the received signal also has an unwanted interference component, the AGC loop can not distinguish this unwanted signal from the desired one and will set the gain according to the sum of both signals. This unwanted interference also changes the peak-to-average ratio (PAR) of the received signal. If the PAR of the original signal is less than the PAR of the interference, clipping will occur at the ADC. For signals with PAR level higher than interference's PAR, the data signal to quantization noise ratio (S_dQNR) degrades, since AGC is locked to the interference and the data signal is not amplified properly to cover the entire ADC input range.

According to the FCC, the UWB signal should have flat spectrum. Therefore, the MB-OFDM proposal divides the OFDM symbol to 128 tones with equal amplitudes. The information data is coded on the phases of the tones. Since the information is random, the OFDM tones show a stochastic distribution. The conversion from

frequency to time domain is performed using IFFT, which multiplies each tone with a different constant and adds the results. Although the distribution of the signal in the frequency domain is not known, the resulting time domain waveform shows Gaussian distribution due the central limit theorem. The Gaussian signal's peak values are much higher than their average value. However, the probability of a high peak is low; therefore, PAR is fixed for practical systems. In the MB-OFDM proposal, the PAR is selected as 9 dB.

The quantization noise of ADC for Gaussian distributed signals is slightly different from the conventional single carrier systems [31]. The quantization noise is determined numerically by evaluating the following integral

$$\begin{aligned} P_q &= 4\sum_{i=0}^{2^{b-1}-2}\int_{i\Delta}^{(i+1)\Delta}(z-(i+1/2)\Delta)^2\,p(z)dz \\ &\quad +4\int_{1-\Delta/2}^{\infty}(z-1)^2\,p(z)dz \end{aligned} \tag{5.12}$$

where $p(z)$ is the probability density function (pdf) of the received signal, b is the ADC number of bits, and Δ is the quantization step size. For a given number of bits and Gaussian distributed signal, the ADC has an optimum PAR, which maximizes the signal-to-quantization noise ratio (SQNR). If the ADC operates with less than its optimum PAR, the peaks of the signal overload the ADC. This results in an increase of quantization noise due to the clipping. Above the optimum PAR, the signal level decreases, because the ADCs full scale must cover higher peak levels. The SQNR vs. PAR for 4-6 bit ADCs is depicted in Fig. 51. A more generalized picture is shown in Fig. 52. When PAR is fixed, SQNR saturates after a certain number of bits. In Table X, the maximum SQNR, optimum PAR and SQNR for 9 dB PAR is listed for different number of bits. For example, increasing ADC number of bits from 7 to 8 improves SQNR only 0.6 dB, when PAR is 9 dB.

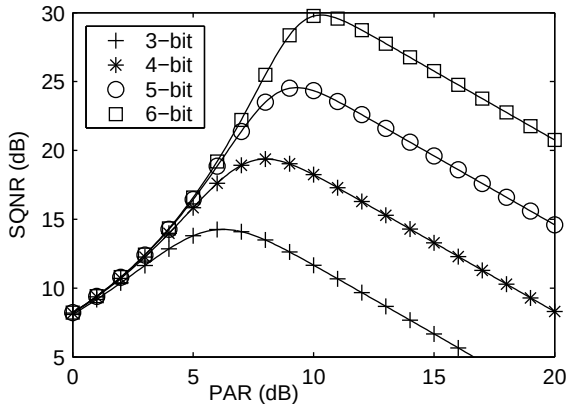

Fig. 51. Signal to Quantization Noise vs. Peak to Average Ratio of the Received Signal.

Table X. SQNR and PAR for Different Number of Bits.

ADC Number of Bits	Maximum SQNR (dB)	Optimum PAR (dB)	SQNR (dB) for 9 dB PAR
2	9.25015	3.48428	5.29174
3	14.26668	6.23960	12.62738
4	19.37686	8.00732	19.02849
5	24.56527	9.29620	24.51496
6	29.82948	10.31214	28.36301
7	35.16651	11.15278	30.18963
8	40.57069	11.87060	30.78611
9	46.03469	12.49696	30.94746
10	51.55088	13.05221	30.98856

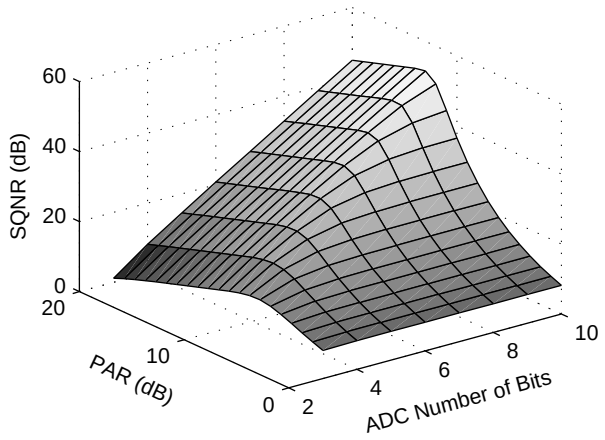

Fig. 52. Signal to Quantization Noise vs. PAR and ADC Number of Bits.

9. Block Level Specifications

The main purpose of the receiver is to deliver the RF signal to digital domain with maximum signal quality. Link budget analysis is required to determine the parameters of individual blocks on the receive chain. Their gain, noise and linearity determine the overall system performance. Therefore, system's dynamic range, noise and nonlinearity requirements, which are presented in the previous sections, are evaluated using the approach discussed in Chapter IV. To check different scenarios and evaluate quickly all noise and nonlinearity formulas, a spreadsheet program is used.

To reduce the overall noise, the received signal should be amplified as high as possible without adding noise, when it enters the receiver. On the other hand, nonlinearity requirement dictates as small signal swing as possible to reduce unwanted nonlinearity products. These two requirements are contradictory, and an optimization is required. However, this optimization does not only depend on noise and nonlinearity, but also depend on power consumption, area and overall circuit behavior. Therefore, this optimization procedure is an iterative process.

Low noise amplifier is the first block in the chip, and amplifies the desired signal

with minimal noise. Its gain should be high to attenuate the noise contribution of the following stages. However, it should also handle high power signals as well as low level signals. It is not possible to achieve these two requirements at the same time with only one gain level. If the gain is reduced to handle large swing, the following stages should be low noise in order to handle signals at the sensitivity level. If the gain is kept high, LNA should handle large swing signals. Since the supply voltage is limited, the maximum signal at the output of LNA is less than the supply. Therefore, LNA should have different gain levels to handle both situations. To reduce the design complexity of LNA, it is designed to have two gain levels. Implementing more than two gain levels at high frequencies requires multi input stages, where each stage should match 50 Ohm input. However, the power consumption of each stage increases total consumption. LNA is followed by a mixer, which generates I and Q channels. Mixer input is also at high frequency and for maximum power transfer the mixer input impedance and LNA output impedance should be complex conjugate. Therefore, the termination at LNA output will determine overall performance of LNA and mixer. Since both circuits are in the same chip and does not require driving external load, the output impedance of LNA does not need to be 50 Ohm. This requires the LNA and mixer be designed together and specified as a whole block. The combined specifications of LNA and Mixer is summarized in Table. XI.

Low-pass filter is used to suppress out-of band interference, where its approximation and order are discussed in section V.3. Since LPF is also on the receive chain, it adds noise to the desired signal and create nonlinearity. Therefore, its noise and linearity performance must be taken into account during link budget calculations. Since it operates after LNA, its noise contribution will be attenuated by LNA. Therefore, its noise can be higher than LNA's noise. However, it must handle strong out-of-band blockers, which is already amplified by LNA and mixer. This dictates higher

Table XI. Low-Noise Amplifier and Mixer Specification.

	Min	Typ	Max
Gain (high)		33 dB	
Gain (low)		7 dB	
Input Impedance		50 Ω(single)	
Output Load		0.5 pF	
Cut-Off Frequency (low)			3.012 GHz
Cut-Off Frequency (high)	4.908 GHz		
S11			−10 dB
Input Referred Noise density			0.95 nV/$\sqrt{\text{Hz}}$
Noise Figure			3.2 dB
IIP3	0dBVrms		
Temperature	0°C	27°C	125°C

Table XII. Low-Pass Filter Specification.

	Min	Typ	Max
Gain		0 dB	
Gain Flatness	−0.5 dB		0.5 dB
Cut-Off Frequency	264 MHz		
Input Capacitance		0.2 pF	
Output Load		0.5 pF	
Input Referred Noise density			10 nV/$\sqrt{\text{Hz}}$
IIP3	6 dBVrms		
MTPR	25 dB		
Temperature	0°C	27°C	125°C

linearity requirements. Its parameters are summarized in Table. XII. Although IIP3 is a figure of merit for linearity, it is not adequate for multi-band signals. Therefore missing tone power ratio (MTPR) specification is also given to guarantee harmonics and intermodulation products of higher order to be within the specifications. The MTPR test is evaluated for 1 Vpp multi-tone signal, which occupies the whole base-band. Low-pass filter's maximum input capacitance is limited to 0.2 pF. Since mixer can drive max 0.5 pF, there is a 0.3 pF margin for interconnect capacitances.

To suppress in-band interference, a notch filter is also added. It also adds noise and creates nonlinearity. Therefore, its noise and nonlinearity is also specified. Since out-of band interference is attenuated by LPF, it does not require strong out-of blockers. However, it should handle in-band interference. Therefore, it is assumed that notch filter should be as linear as LPF. It has also relaxed noise specification, since its noise is suppressed by LNA. Parameters of the notch filter are summarized in

Table XIII. Notch Filter Specification.

	Min	Typ	Max
Gain		0 dB	
Gain Flatness	−0.5 dB		0.5 dB
Cut-Off Frequency	420 MHz		
Input Capacitance		0.2 pF	
Output Load		0.5 pF	
Input Referred Noise density			10 nV/$\sqrt{\text{Hz}}$
IIP3	6 dBVrms		
MTPR	25 dB		
Temperature	0°C	27°C	125°C

Table. XIII. The input capacitance of notch filter is limited to 0.2 pF. It should drive 0.5 pF load capacitance of following the stage, including interconnect capacitance. Designing the filter drive capability higher than 0.5 pF increases overall power consumption.

Variable-Gain Amplifier is located before the ADC at the receive chain and amplifies the received signal to utilize maximum dynamic range from ADC. Since it is at the last stage of receive chain, its noise is not significant. However, it should handle high swing signals regardless of the received RF input signal power. Therefore, its linearity specifications are determined by not blockers or interferers, but the desired signal swing. Its parameters are summarized in Table. XIV. To capture any high order nonlinearity, its linearity is also defined by MTPR test.

Analog-to-digital converter is at the border between analog and digital domains and converts analog signals to digital. Since the upper cut-off frequency of baseband

Table XIV. Variable-Gain Amplifier Specification.

	Min	Typ	Max
Gain	0 dB		47 dB
Gain steps		1 dB	
Gain Flatness	−0.5 dB		0.5 dB
Cut-Off Frequency	420 MHz		
Input Capacitance		0.2 pF	
Output Load		0.5 pF	
Input Referred Noise density			10 nV/$\sqrt{\text{Hz}}$
IIP3	6 dBVrms		
MTPR	25 dB		
Temperature	0°C	27°C	125°C

is 264 MHz, the sampling frequency should be minimum 528 MHz due to Nyquist theorem. Required number of bits is discussed in section V.8. ADC's linearity is also defined using MTPR test to guarantee performance in the presence of high order nonlinearity. Its input capacitance is limited to 0.5 pF. The first stage of ADC is a sample-and-hold and its noise is limited by kT/C noise. For 0.1 pF, the kT/C noise is 203.47 μV and is lower than quantization noise. Therefore, 0.5 pF limit is adequate from noise perspective. ADC SNR is also degraded by the clock jitter. The relationship between clock jitter and ADC SNR is given as

$$SNR = -20\log\left(2\pi f_{max} \cdot \tau_{Jitter,RMS}\right) \tag{5.13}$$

where f_{max} is the maximum input frequency. The degradation due to jitter is negligible, provided that the effective number of bits of ADC due to jitter is set 2 bits

Table XV. Analog-to-Digital Converter Specification.

	Min	Typ	Max
Gain		0 dB	
MTPR	25 dB		
Input Capacitance			0.5 pF
Input Peak-to-Peak Voltage			1 V
Clock Frequency		528 MHz	
Clock Jitter		7.7 ps	
Temperature	0°C	27°C	125°C

higher than actual number of bits. Therefore, the clock jitter is limited to 7.7 ps.

The frequency synthesizer generates the ADC clock and the local oscillator clock for down conversion. Since MB-OFDM is a frequency hopping system, synthesizer should change its output frequency every 312.5 ns. Phase noise requirement of the synthesizer is derived in section V.7. The overall IQ imbalance requirement for the whole system is evaluated in section V.5. IQ phase imbalance is dictated by synthesizer, since I and Q chains in baseband have good phase match. On the other hand, gain mismatch is caused by the synthesizer and the mismatch between I and Q baseband blocks. Therefore, synthesizer gain mismatch is limited to 1 dB. Since the limit for whole system is 2 dB, the maximum mismatch between baseband blocks is 1 dB. Phase mismatch is limited to 5 degrees to have also 5-degree margin. ADC clock jitter requirements are derived according to ADC clock requirements. Switching time is dictated by MB-OFDM proposal. The synthesizer parameters are summarized in Table. XVI.

The effect of individual blocks is evaluated for overall system performance using

Table XVI. Frequency Synthesizer Specification.

	Min	Typ	Max
Output Frequencies		3.432 MHZ	
		3.960 MHZ	
		4.488 MHZ	
Frequency Hopping Period		312.5 ns	
ADC Clock		528 MHz	
ADC Clock Jitter			7.7 ps
Switching Time			5 ns
Phase Noise at 1 KHz			−50 dBc/Hz
Phase Noise at 100 KHz			−90 dBc/Hz
Phase Noise at 10 MHz			−130 dBc/Hz
IQ Gain Mismatch			1 dB
IQ Phase Mismatch			5 deg
Temperature	0°C	27°C	125°C

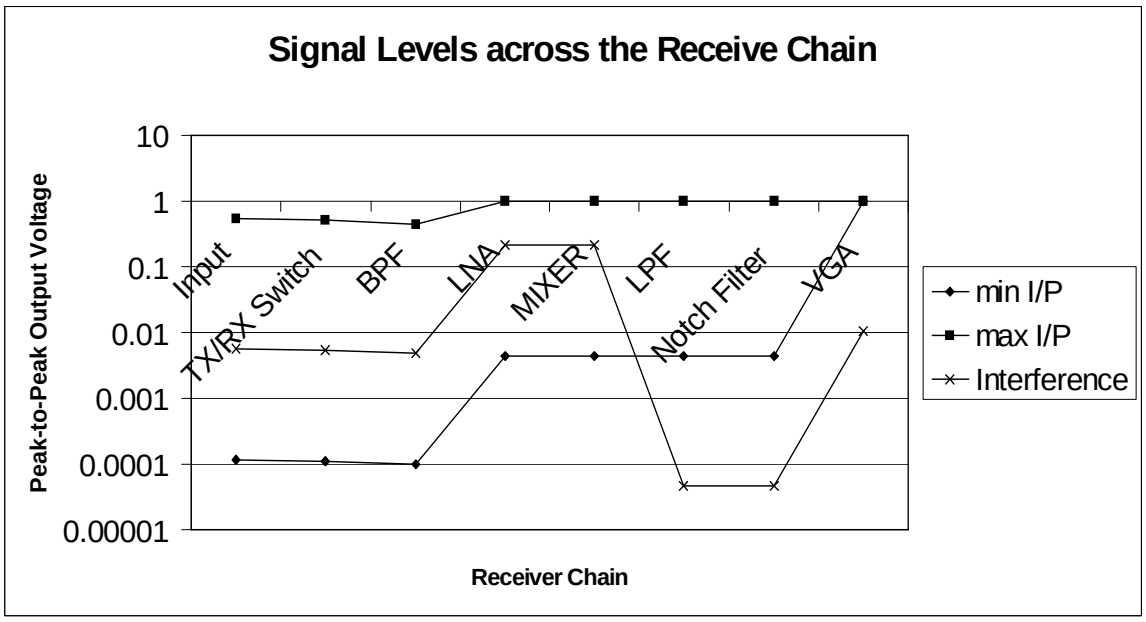

Fig. 53. Signal Levels for High and Low Gain.

spreadsheet. The advantage of spreadsheet is to verify the effects of first order parameters, such as noise, gain and nonlinearity, using formula-based approach. The formulas explained in chapter IV is used to construct the spreadsheet. First, signal levels in the receive chain for sensitivity, maximum signal level and in presence of out-of-band blocker is evaluated. Since the maximum peak-to-peak signal swing is limited to 1 V, the signal swing should not be above 1 Vpp at any stage. The signal levels across the receive chain are shown in Fig. 53. For the maximum and the minimum signal levels, the signal swing at the VGA output is 1 Vpp. Since the blocker is attenuated by LPF, LNA and mixer must handle increased signal swing due to the blocker.

Once the signal swings are determined, overall noise performance for all possible input power levels is evaluated. Quantization noise of ADC limits maximum SNR. To determine the effect of VGA gain step, overall noise and signal level is also swept

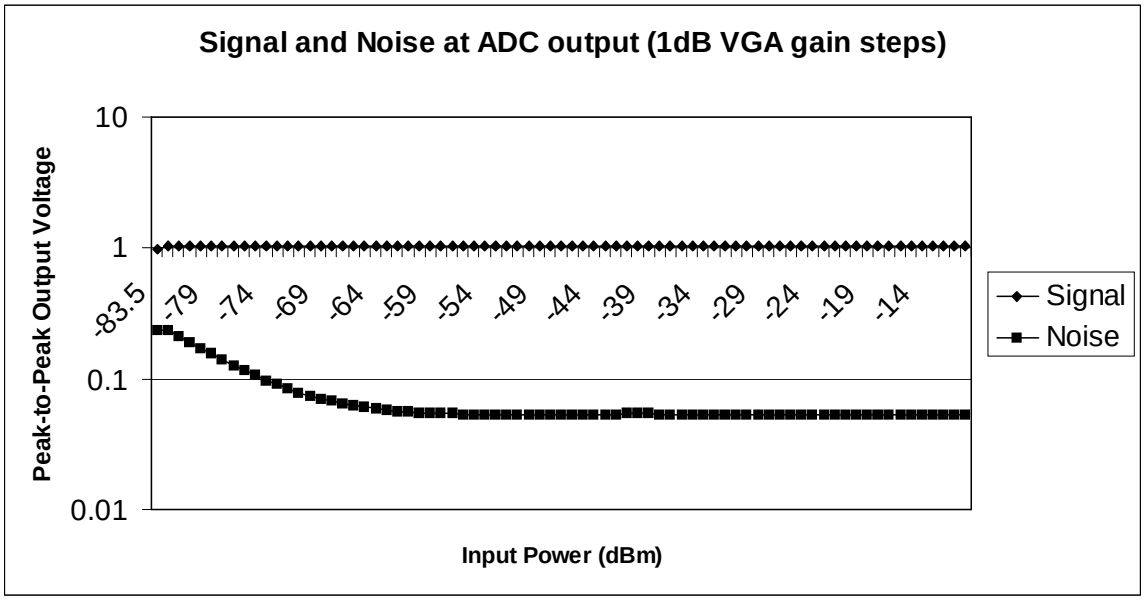

Fig. 54. Signal and Noise Levels vs Input power (1 dB Steps).

for 1 dB and 5 dB gain steps as shown in Figs. 54 and 55, respectively.

The SNR for high input levels is limited due to ADC's quantization noise. SNR at the ADC output and input vs. input signal power are shown in Figs. 56 and 57, respectively. SNR degradation due to LNA gain switching is negligible, because at the input power level where LNA switches to low gain, ADC quantization noise is the dominant noise source.

The noise distribution in percentage for the sensitivity and the maximum signal levels are shown in Figs. 58 and 59. At the sensitivity, 60% of total noise is generated by LNA and mixer. At high input levels, almost 100% of noise is ADC's quantization noise.

The performance in the presence of blocker is evaluated when the desired signal is 6 dB above sensitivity. Interference power vs. SNR at the output of ADC is shown in Fig. 60. Since AGC can not distinguish blocker from the desired signal, AGC switches LNA to low gain in order not to saturate it. However, at low LNA gain the

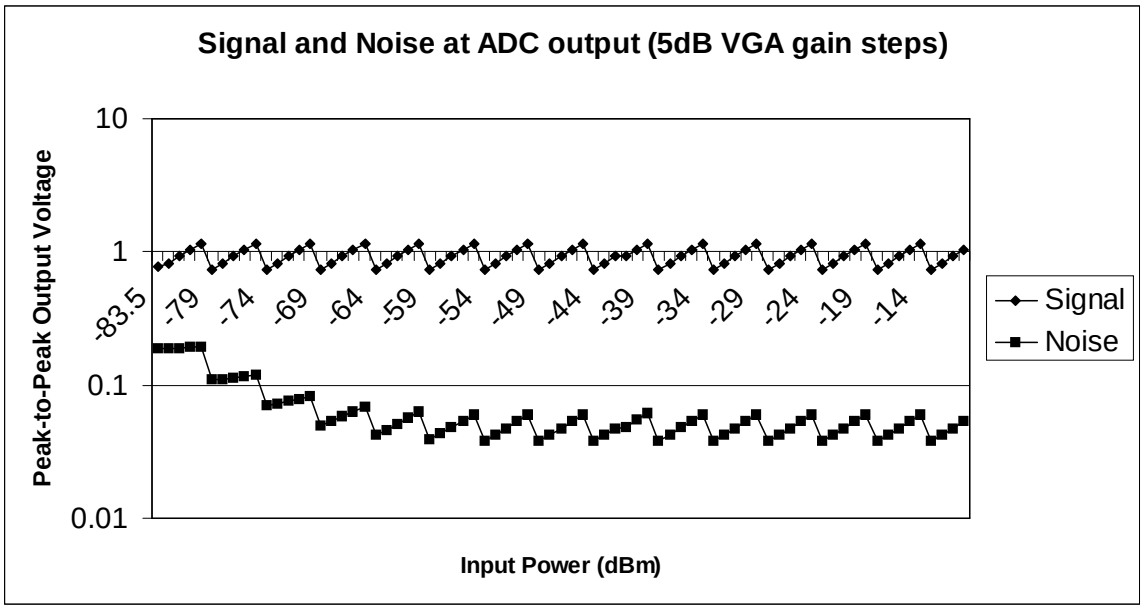

Fig. 55. Signal and Noise Levels vs. Input power (5 dB Steps).

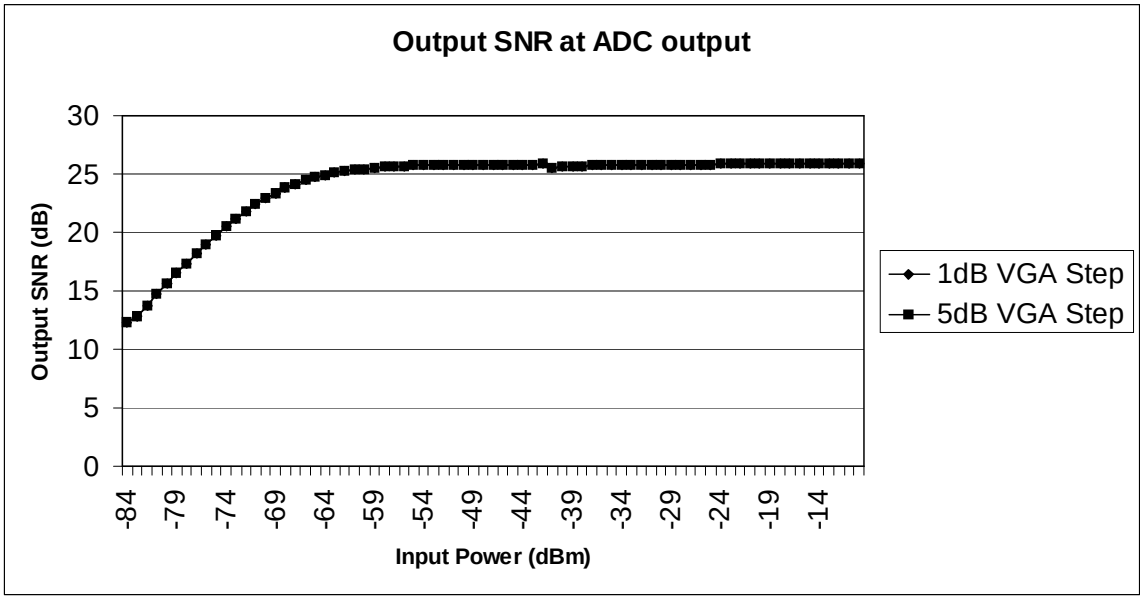

Fig. 56. Signal-to-Noise Ratio vs. Input power with ADC.

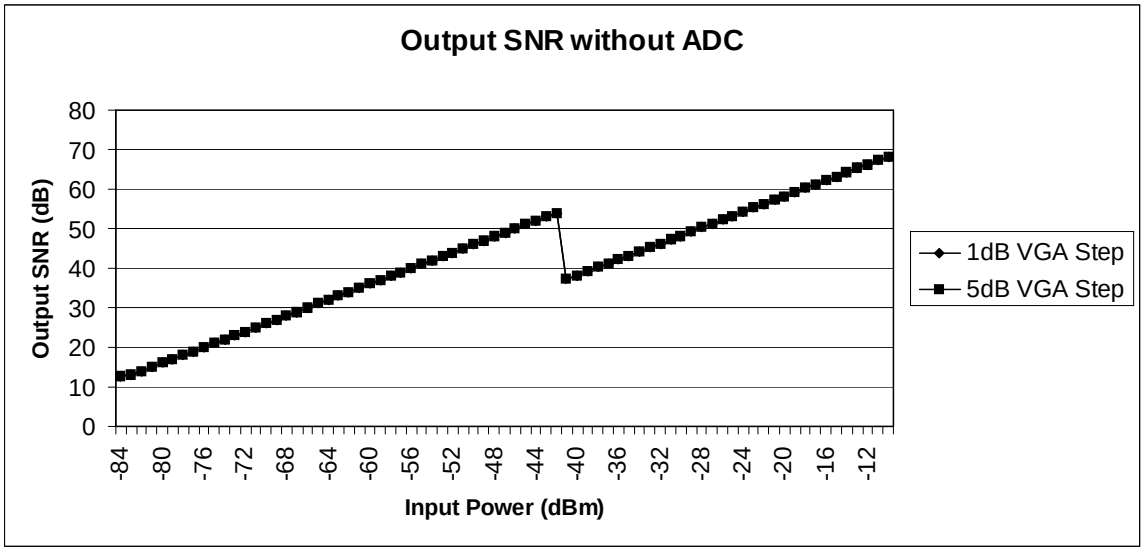

Fig. 57. Signal-to-Noise Ratio vs. Input power without ADC.

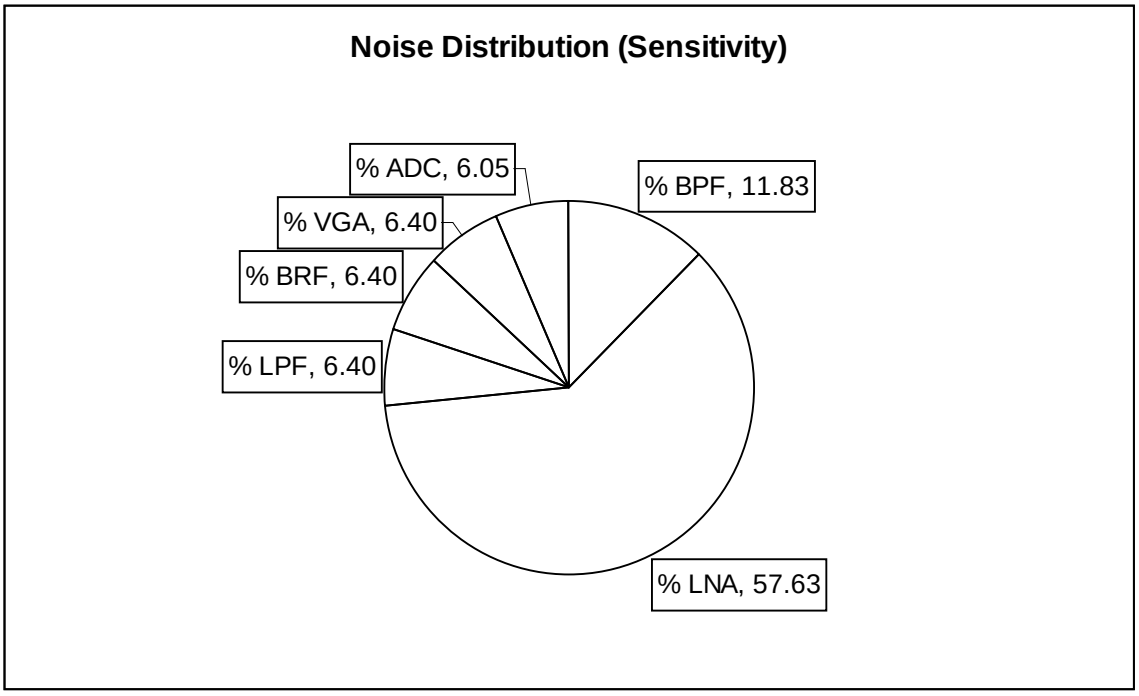

Fig. 58. Noise Distribution at Sensitivity.

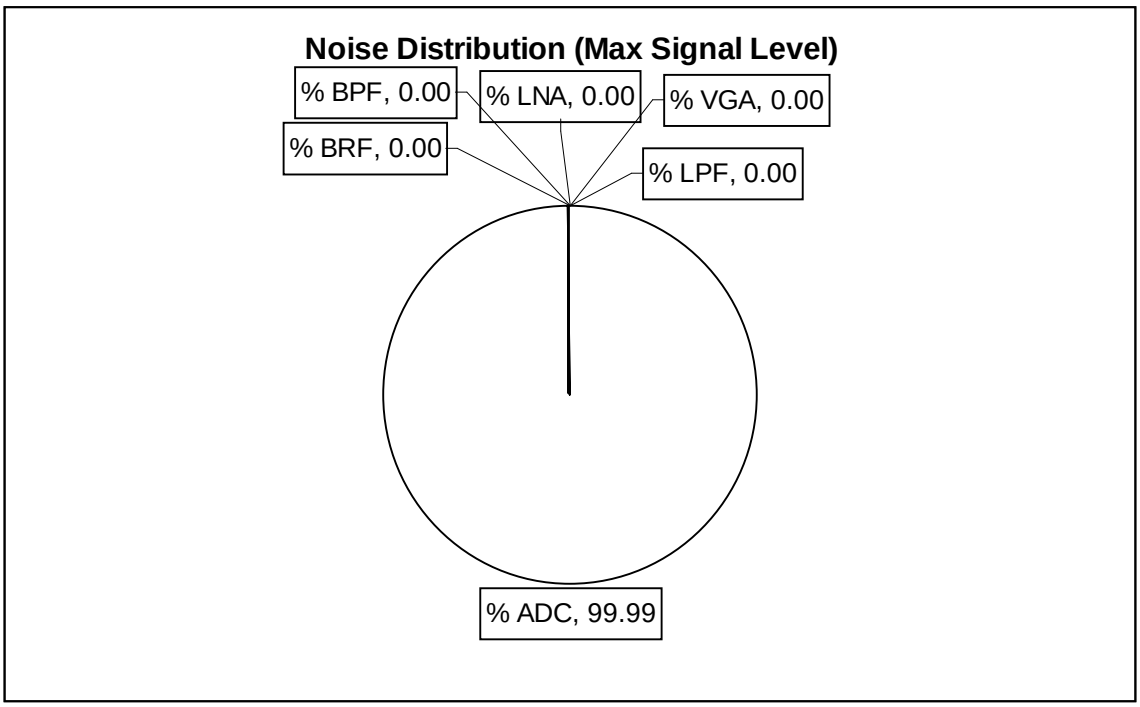

Fig. 59. Noise Distribution at Maximum Input Signal.

noise contribution of the following stages increases and overall noise figure degrades. If LNA does not switch to low gain, it saturates and degrades overall performance.

The gain from antenna input to VGA output is calculated as 78.3 dB. System's noise figure is evaluated for maximum gain, since AGC sets the gain to maximum for the input signal levels at sensitivity. The calculated noise figure of the system is 5.6 dB. The input referred second and third harmonic is evaluated for minimum gain. When the received signal is at its maximum value, AGC sets the total gain to minimum to reduce the voltage swing. The calculated IIP2 is 16 dBVrms, and IIP3 is -2.4 dBVrms.

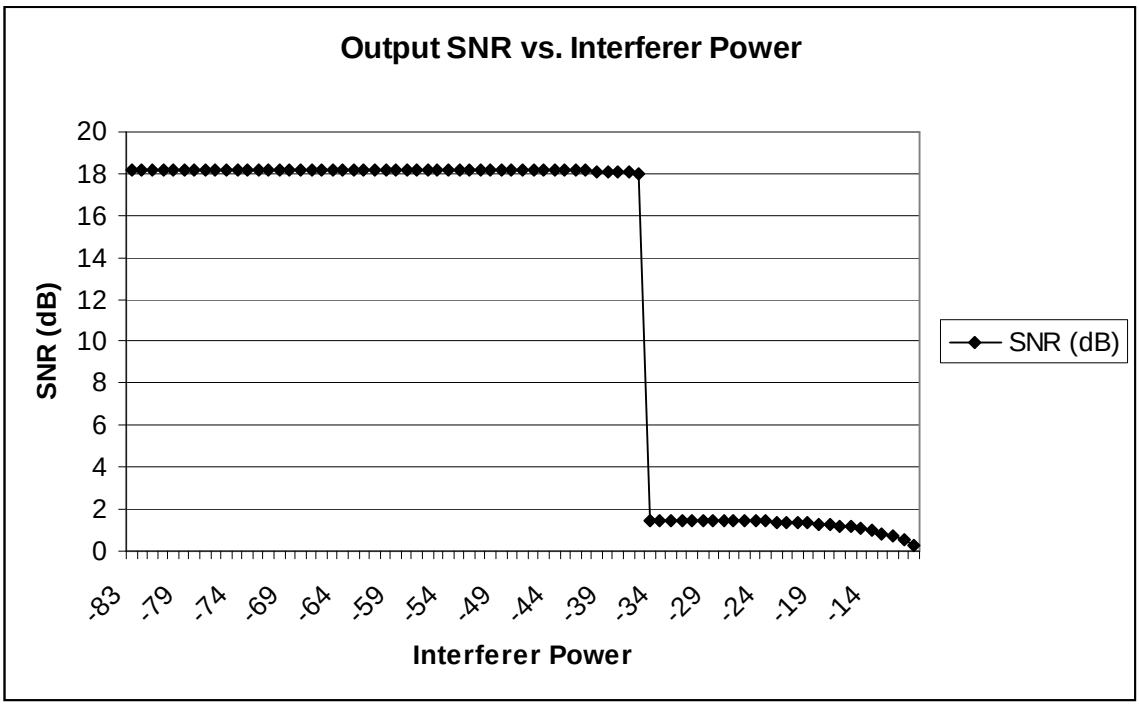

Fig. 60. Output SNR vs. Interferer Power.

10. Automatic Gain Control

The automatic gain control circuit is a closed-loop system that maintains the input level at the analog-to-digital converter at a constant level, even though the input at the receiver may vary substantially. AGC can be implemented in analog or digital domain, or in both. The analog domain approach requires a power detector and a loop to set the gain levels. The digital approach requires a high resolution analog-to-digital converter to achieve high dynamic range. On the other hand, a mixed-mode approach results in minimum analog complexity and relaxed ADC requirements.

In mixed-mode AGC, the amplifiers' gains are set digitally. This results in discretization of the overall gain. If the optimum gain is between two gain steps, ADC will not operate at the optimum signal-to-quantization ratio. However, this degradation can be reduced by increasing the number of gain settings.

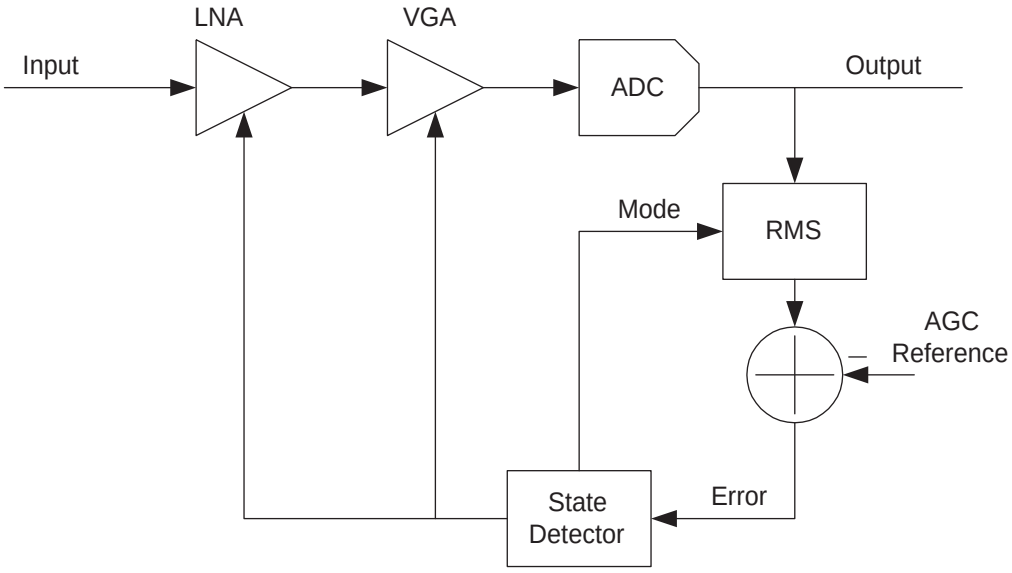

Fig. 61. Automatic Gain Control Block Schematic.

The overall AGC block diagram is depicted in Fig. 61. The AGC has two different modes. In both modes the root-mean square (RMS) of samples is calculated according to

$$RMS = \sqrt{\frac{1}{N}\sum_{N} x_n^2} \tag{5.14}$$

where x_n is the incoming samples and N is the number of samples. The computed RMS is then compared to a reference level, which maximizes the signal-to-quantization ratio at the input of ADC. Since the PAR of the MB-OFDM signal is 9 dB and the maximum amplitude of ADC input is 0.5 V, the reference level is 0.177 V. The AGC loop error signal is computed by subtracting the reference level from computed RMS. The loop tries to minimize this error signal.

Theoretically, the number of samples should be infinite to calculate the RMS. However, in practice the number of samples in one symbol is 165. If the loop needs several iterations to settle down, the first symbols will be unreliable. To settle down the loop fast, initially 5 samples are used to compute the error signal. When the

signal settles within 6 dB of the final value, 25 samples are used to compute the error signal. When the error is less than 2 dB, the loop stabilizes the gain. Any change less than 2 dB is ignored in order not to create steps at the receiver chain. If the error is greater than 6 dB, the AGC switches to fast mode until the error is less than 6 dB.

B. In-Band Interference Suppression

UWB systems must coexist with existing systems. Therefore, its transmit power is low in order not to interfere them. Moreover, it must operate even in the presence of unintentional radiation of FCC Class-B compatible devices. This unwanted disturbance may appear as in-band interference and can degrade the performance of the UWB link.

1. Narrow-Band Interference Sources

FCC part 15 sets the maximum unintentional radiation level in the 2-15 GHz bandwidth at -41.3 dBm/MHz for any class-B compatible device. Since most communication systems radiate at higher power levels, interference from unintentional radiation is not a serious problem for current narrowband communications. However, UWB systems were developed to coexist with current narrowband systems. This requirement puts a limit on the maximum transmit power density, which is -41.3 dBm/MHz. Therefore, the unintentional radiation of electronic devices may exist within the UWB band and jam UWB communication. The sources of the radiation range from computer components [32, 4, 5] to common household devices such as electric shavers and hair dryers [5].

Every electronic equipment producer must submit a report to FCC to validate their Class-B compatibility. This report usually includes the spectrum up to few giga-

hertz and may be used to examine the power and frequency of interference an UWB receiver should handle. As an example, the report of a local area network interface card indicates −49.8 dBm interference power at 3.75 GHz [32]. In another report a motherboard is examined and a tone due to microprocessor clock is present around 1.9 GHz with a peak power of −36.7 dBm, and an average power of −42.7 dBm. Although this tone is not in the UWB band, the processors are faster today. Currently, even the main clock frequency is in the UWB band. Moreover, during emission measurements, the device under test is inside a PC chassis, which forms a electromagnetic shield and attenuates the emissions more than 25 dB [33]. Therefore, the power levels inside the chassis could exceed −16.3 dBm/MHz. If the UWB transceiver is located in the PC, these signal levels can easily jam UWB communication.

The IEEE 802.15.3a physical selection criteria states the performance requirements of the UWB receiver [14]. The interference test is performed when the received UWB signal is 6 dB higher than the proposed sensitivity level. The system should satisfy a packet error rate less than 8% for 1024 byte packets in the presence of interference with power level at least 3 dB higher than the desired signal. The sensitivity level of 53.3 Mb/s data rate is −83.6 dBm [3]. Therefore, an interference level with −74.6 dBm at the receiver input should be tolerated.

Although some electronic devices radiate within the UWB bandwidth, and the power levels are near the FCC limit, the interference power will be attenuated due to the path loss. The IEEE 802.15 channel committee has provided the following path loss model

$$P_L(f_g, d) = 20 \log_{10} \left(\frac{4\pi f_g d}{c} \right) \tag{5.15}$$

where P_L is the path loss in dB, d is the distance from the source in meters, $c = 3 \times 10^8 m/s$ is the speed of the light, and f_g is the geometric average of the lower

and upper corner frequencies [34]. The smallest path loss will occur at UWB sub-band 1, which is located at the lowest frequency of the UWB band. Consider the case where an interference source occupies a 1 MHz bandwidth and is radiating in UWB sub-band 1 with an unintentional radiation power limit of −41.3 dBm. To satisfy the criteria for 53.3 Mb/s data rate, the distance between the UWB receiver and interference source should be at least 32 cm. If the interference is attenuated an extra 14 dB by a notch filter, the distance can be as close as 6 cm.

2. Quantization Noise in the Presence of Interference

When in-band interference is present, the PAR of the received signal is lower than 9 dB. In the presence of sinusoidal interference with higher power level than data signal, the PAR of the received signal approaches 3 dB. Data signal to quantization noise (S_dQNR) vs. signal to interference ratio (SIR) is shown in Fig. 62. S_dQNR decreases for low SIR levels, because the AGC loop locks to the interference, and the desired signal is not properly amplified.

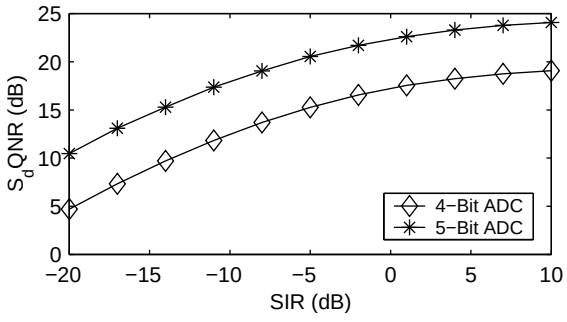

Fig. 62. Data Signal to Quantization Noise vs. Signal to Interference Ratio.

3. NBI Detection

Although the frequency of narrow-band interference is not exactly known, its location can be found by examining the spectrum of the received signal. The FFT processor, which is included in MB-OFDM, is used to obtain the spectrum. In additive white Gaussian noise (AWGN) channels, the spectral characteristic of the transmitted signal is not changed. Therefore, the interference can be easily determined, even if its power is only few decibels higher than the spectral density of the UWB signal. For example, the spectrum is depicted in Fig. 63 for one interference with a power level equal to the signal power.

The IEEE 802.15.4a channel modeling group released a report about multi-path characteristic of the UWB channel [35]. Due to the different path delays, the spectrum of the received signal has peaks. Some of the realizations have peaks with 15 dB higher than average power density. On the other hand, the difference between peaks is less than 5 dB. Therefore, the interference can be detected by comparing it with the next highest peak and the average power density. A typical spectrum of received signal in multi-path channel is depicted in Fig. 64. The difference between the interference and highest peak is 11 dB for 0 dB SIR.

If there is only one interference, which occupies only one tone, the signal spectral density to interference spectral density ratio (S_sIR) is found by the following equation

$$S_sIR = SIR - 10 \cdot \log(N_{tone}) \tag{5.16}$$

where N_{tone} is the number of tones, which is 128 for MB-OFDM systems. If the SIR is 0 dB, interference spectral density is 21 dB higher than the signal spectral density. Therefore, if SIR is below 0 dB, the interference can be easily detected by comparing threshold even in multi-path channels.

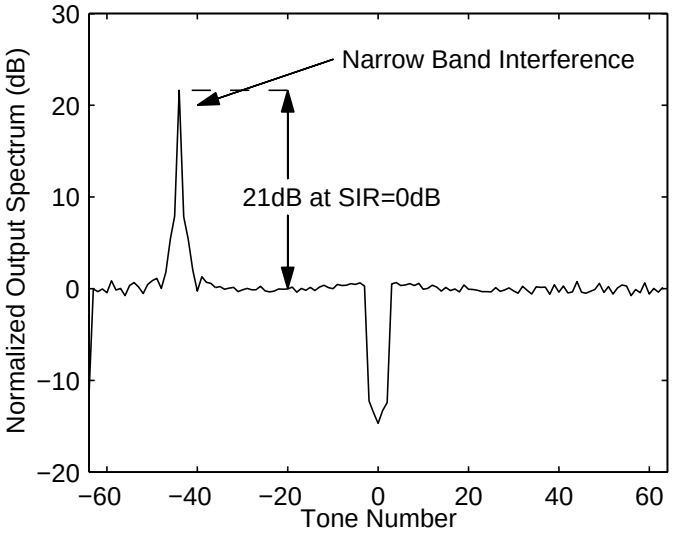

Fig. 63. Spectrum in AWGN Channel.

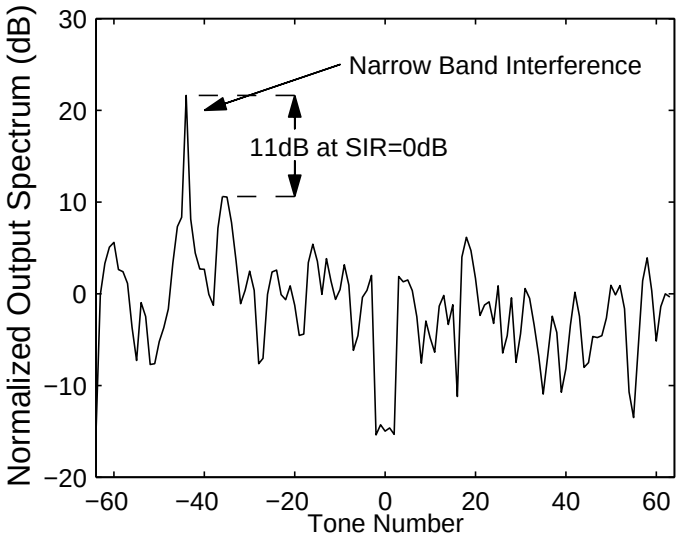

Fig. 64. Spectrum in Frequency Selective Channel.

In the presence of more than one interference, the detection is performed easily for AWGN channels due to its flat spectrum. However, for multi-path channels, unless the levels of the interferences are 15 dB higher than average density or at least 5 dB higher than the rest of the peaks, it is not possible to detect interferences. On the other hand, the interferences are stationary most of the time, since they are due to the unintentional radiation of electronic devices. Furthermore, the UWB communication link is active for a small amount of time compared the operating time of the electronic devices. Therefore, the exact frequencies and power levels of the existing interferences can be detected by listening to the channel, when there is no communication.

4. Adaptive NBI Suppression

Since the frequency of narrowband interference is unknown, the suppression should be done adaptively. The suppression has two phases, detection and tuning. The detection is performed using FFT processor in the digital domain. Due to the discrete time nature of FFT, the interference frequency is quantized to nearest tone frequency. If the interference is between tones, the interference power is spread out to the nearest tones. Therefore, the notch filter's frequency step needs to be smaller than the frequency resolution of the FFT. To cover whole band, the notch frequency should be discretely tunable between DC and 264 MHz. Each sub-band in MB-OFDM has 128 tones, therefore, to guarantee suppression for interferences between tones, the number of frequency steps is selected 256.

a. Interference Suppression

MB-OFDM based UWB system is a frequency hopping system and at every 312.5 ns the down-converted band is changed. If the interference affects only one sub-band, the interference periodically appears only for 312.5 ns in the baseband. During the

other times it is out-of band interference and will be attenuated by the low-pass filter. Since the overall receiver gain is not changed between sub-bands, interference causes a step in time domain. This step is not a problem for low-pass filter and VGA, since their bandwidth is high enough to settle fast. However, the settling time of the notch filter is inversely proportional to the notch bandwidth, which is selected low in order not the attenuate adjacent tones. When there is a sharp change in the signal level, the notch filter starts ringing with exponentially decaying envelope. This creates problems for two sub-bands. One is the sub-band with interference and the other is the band which is down-converted after that band. If the notch filter is turned on only for the sub-band affected by the interference, the undesired effect on the adjacent sub-band can be eliminated, . Another drawback of turning on the notch filter all the time is that it attenuates the data signals at the notch frequency for the sub-bands, which are not affected by NBI. However, turning on and off the filter requires extra circuitry and control, which themselves should also settle fast enough.

b. Filter Types

The settling time of the filter is a function of filter approximation, notch bandwidth and filter order. For a second order system the 2% settling time is calculated using simple analytical expression. However, for higher order and different realizations, there is no simple equation. The upper bound of the settling time can be determined by realizing the filter transfer function using cascade biquads. The biquad with minimum bandwidth gives the upper bound. To obtain accurate settling time, the transfer function should be evaluated numerically. The evaluation for four different realization is shown in Tables XVII and XVIII for 4 Mhz and 40 MHz notch bandwidth, respectively. The notch frequency is selected as 100 MHz. The first three realizations are magnitude based approximations [36]. The settling time degrades with increasing

Table XVII. Different Filter Approximations for 4 MHz Notch Bandwidth.

Filter Type	Settling Time		20 dB Bandwidth	
	4th order	6th order	4th order	6th order
Butterworth	418 ns	543 ns	1.27 MHz	1.86 MHz
Chebyshev	393 ns	528 ns	1.45 MHz	2.27 MHz
Elliptic	393 ns	708 ns	1.51 Mhz	2.49 MHz
Bessel	473 ns	433 ns	1.02 MHz	1.38 MHz

filter order except Bessel approximation. Although 6^{th} order Bessel filter gives better settling time than 4^{th} order, the required bandwith of biquads is decreased for higher orders. This requirement results in higher power consumption due to increasing of filter's quality factor. The 20-dB bandwidth, which is an indication of the attenuation at adjacent tones, increases with increasing notch bandwidth and filter order, as expected. The filter approximation also changes the bandwidth significantly. Elliptic filters give highest 20 dB bandwidth because of their sharp transition between the passband and stopband. Bessel filters give the smallest 20 dB bandwidth due to their smooth attenuation in the stopband. The settling time of the notch filter is decreased by reducing filter order. Therefore, the minimum settling time is achieved when a second order filter is used.

Table XVIII. Different Filter Approximations for 40 MHz Notch Bandwidth.

Filter Type	Settling Time		20 dB Bandwidth	
	4th order	6th order	4th order	6th order
Butterworth	44.8 ns	59.1 ns	12.7 MHz	18.6 MHz
Chebyshev	48.4 ns	74.3 ns	14.5 MHz	22.7 MHz
Elliptic	53.8 ns	74.6 ns	15.1 Mhz	24.9 MHz
Bessel	49.2 ns	44.5 ns	10.2 MHz	13.8 MHz

c. 2^{nd} order Notch Filter

The attenuation at the notch frequency is ideally infinite. However, in practical circuits the attenuation is finite. Therefore, the filter is modeled by the following transfer function.

$$H(s) = \frac{s^2 + \omega_{BW} \cdot A_N \cdot s + \omega_o^2}{s^2 + \omega_{BW} \cdot s + \omega_o^2} \tag{5.17}$$

where A_N is the attenuation at the notch frequency, ω_{BW} is the notch bandwidth and ω_0 is the notch frequency in rad/s. The step response is

$$t_s = 1 + 2\frac{\omega_{BW}(A_N - 1)\, e^{-\frac{t\cdot\omega_{BW}}{2}} \sin\left(\frac{t\sqrt{4\cdot\omega_0^2 - \omega_{BW}^2}}{2}\right)}{\sqrt{4\cdot\omega_0^2 - \omega_{BW}^2}} \tag{5.18}$$

The step response decays exponentially and the settling time is only a function of notch bandwidth. The 2% settling time is written as follows,

$$t_s = \frac{-2\cdot\ln(0.02)}{2\cdot\pi\cdot f_{BW}} \tag{5.19}$$

where f_{BW} is the 3 dB notch bandwidth in Hz. For 4 MHz and 40 MHz bandwidth the settling time is 311 ns and 31 ns, respectively. If there is more than one notch frequency, the settling time of the multi-notch is not a simple equation. The upper bound of settling time is the settling time of the biquad, which has lowest bandwidth.

If the notch frequency is much higher than the bandwidth and the attenuation at the notch frequency is much greater than 20 dB, the 20 dB bandwidth of the notch filter is approximated as

$$f_{bw20dB} \approx \frac{f_{bw}}{\sqrt{99}} \tag{5.20}$$

For 4 MHz and 40 MHz bandwidth, the evaluation of the (5.20) gives approximately 402 KHz and 4 MHz, respectively. The second order filter shows the lowest settling time and it also gives the smallest 20 dB bandwidth.

d. Optimum Bandwidth

At the output of notch filter, interference has two components one is steady state and the other is transient as indicated in (5.18). The steady state power level is determined only by the attenuation at the notch frequency. However, the total interference power at the output of the notch filter is also a function of the notch bandwidth and frequency hopping period due to the frequency hopping property of the MB-OFDM signal.

To simplify the analysis the interference is assumed sinusoidal without any modulation and there is only one interference. Using the assumptions $\omega_{BW} \gg \omega_0$ and $A_N \gg 1$, the interference power is approximated as

$$P_{i,o} = P_{i,i}\left(A_N^2 + \frac{4A_N + 1 - 4A_N e^{-\frac{T\omega_{BW}}{2}} - e^{-T\omega_{BW}}}{\omega_{BW}T}\right) \tag{5.21}$$

where $P_{i,i}$ and $P_{i,o}$ are the interference power at the input and output of the notch filter. T is the frequency hopping period of MB-OFDM. The notch filter does not attenuate the interference but it also attenuates the desired signal due to its bandwidth. The total signal power at the output of the notch filter is approximated using

the same assumptions as used in the (5.21).

$$P_{s,o} \approx P_{s,i} \frac{1}{1 + \frac{\omega_{BW}}{\omega_0}} \tag{5.22}$$

where $P_{s,i}$ and $P_{s,o}$ are the signal power at the input and output of the notch filter.

The signal-to-noise power at the output of notch filter is

$$SNR = \frac{P_{s,o}}{P_{i,o} + P_N} \tag{5.23}$$

where P_N is the sum of thermal and quantization noise. Inserting (5.21) and (5.22) into (5.23) gives

$$SNR = \frac{P_{s,i} \frac{1}{1 + \frac{\omega_{BW}}{\omega_0}}}{P_{i,i} \left(A_N^2 + \frac{4A_N + 1 - 4A_N e^{-\frac{T\omega_{BW}}{2}} - e^{-T\omega_{BW}}}{\omega_{BW} T} \right) + P_N} \tag{5.24}$$

Optimum bandwidth is obtained by differentiating (5.24) with respect to ω_{BW} and equating to zero. However, an analytical solution is not present and the optimum bandwidth is calculated numerically. The optimum bandwidth vs. SNR for different SIR is depicted in Fig. 65. At high SIR levels, the ringing is not a serious problem because the difference between the signal and the interference is low. Therefore, attenuating interference without degrading SNR of neighbor tones maximizes overall SNR. At low SIR levels, ringing is dominant. Therefore, to reducing ringing maximizes overall SNR. Optimum bandwidth is not only function of SIR, but also SNR. For high SNR levels, noise term in (5.24) is low and reducing the term due to ringing improves the performance. When SNR is low, the noise term in (5.24) is dominant and not attenuating neighbor tones maximizes overall performance.

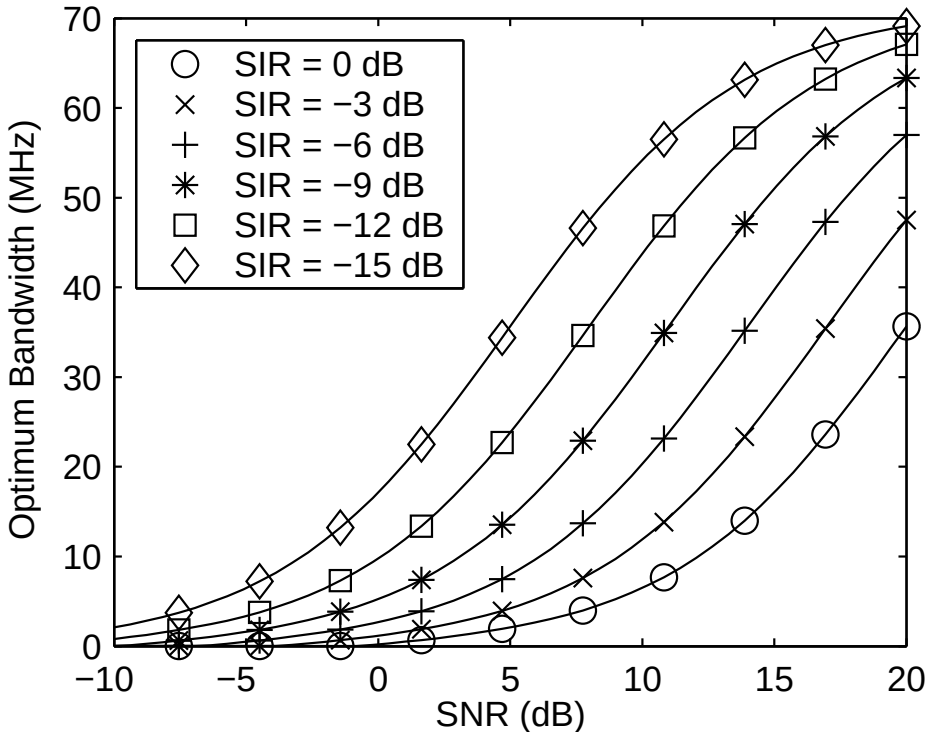

Fig. 65. Optimum Bandwidth vs. SNR.

CHAPTER VI

MODELING AND CIRCUIT IMPLEMENTATIONS

The effect of package parasitics determines overall high frequency performance of the receiver. Therefore, accurate modeling of package is important to meet specifications. In this chapter, first package modeling approach is explained. The design of digital control block is explained in the following section. Current and voltage reference design is discussed in the last section.

A. Package

Connections to the printed circuit board (PCB) are done through the package. The die is located in the package cavity, where the chip's pads and package lead are connected using bond wires, usually made of gold. The package lead is connected to the package pin, which is connected to the PCB trace. The ideal bond wire has zero inductance and zero capacitance. In practice, each bond wire has finite parasitic inductance and capacitance, which is going to affect the circuit performance.

The overall parasitic between the chip pad and the PCB is divided into two parts: the package and bond wire. The package parasitics depend on the package size and type. However, bond wire parasitics depend on the bond type and the distance between the bond pad and package pad. The bond wire configurations are categorized as ball or wedge type based on the connection technique to the pad. Currently, majority of the industry uses ball type wire bonding, because it can be applied to smaller pad than wedge type. However, the ball type bonding requires slightly longer wire. Although this results in higher inductance, the difference is negligible for most applications. Since ball type bonding is widely used in production, the bond wire models are generated for ball type bonding.

1. Bond Wire Modeling

The bond wire is modeled using the EIA/JEDEC bond wire modeling standard [37]. It provides two models of bond wire. One requires five parameters, whereas the other one requires only three. The simplified model with three parameters is depicted in Fig. 66. The required parameters are the total distance the wire covers in the horizontal plane (d), the height between the bond pad and the top of the loop (h_1), and the height between the bond pad and the lead (h_2). Using the three parameters model, the bond wire parasitics is calculated using a three dimensional field solver.

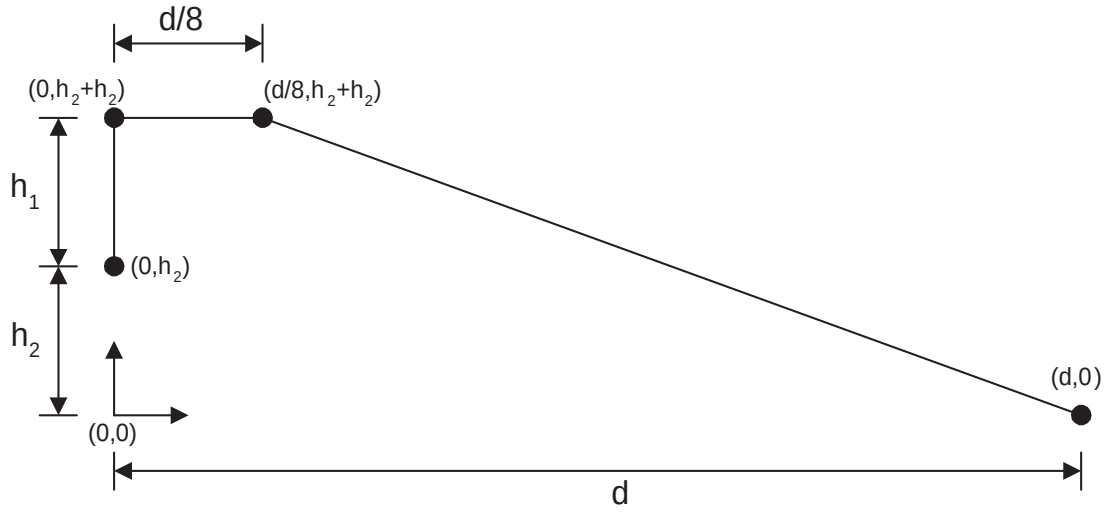

Fig. 66. Bond Wire Geometry.

The bond wire modeling standard also provides an approximate parasitic inductance calculation method. Once the bond wire parameters have been defined and the coordinates are calculated, the overall length of the bond wire is calculated using the following formula

$$l = h_1 + d/8 + \sqrt{(d - d/8)^2 + (h_1 + h_2)^2} \tag{6.1}$$

If the length of bond wire is longer than its diameter, the self inductance is calculated

as

$$L_s = 2 \cdot l \left[\ln \left(\frac{2l}{r} \right) - 1.0 \right] \tag{6.2}$$

where r is the bond wire diameter, which is typically 1 mil. The inductance is obtained in nH if all dimensions are in cm. The mutual inductance between bond wires is calculated as

$$M = 2 \cdot l \left[\ln \left(\frac{2l}{d} \right) - 1 + \frac{d}{l} \right] \tag{6.3}$$

where d is the distance between two bond wires. The mutual coupling between bond wires is calculated as

$$K_{1-2} = \frac{M_{1-2}}{\sqrt{L_1 \cdot L_2}} \tag{6.4}$$

Equations (6.2) and (6.3) are first order approximations. Especially, the calculation of the mutual inductance between the unparallel lines is long and inefficient for hand calculations. Therefore, the bond wire parasitics are calculated using a three-dimensional inductance extraction tool, FastHenry. It can compute the frequency dependent self and mutual inductances and resistances between conductors and complex shapes. Its input file contains the description of conductor geometries. This geometry description file is generated using a Matlab code, which is added in Appendix D. The extractor output is converted to Spice file and included in the simulations. The three-dimensional geometry of the bond wires is depicted in Fig. 69. The maximum and minimum values of self and mutual inductances and resistors are given in Table. XX.

Quad Flat No-lead (QFN) package, shown in Fig. 67 is a plastic encapsulated leadframe with lead pad on the bottom of the package to provide electrical interconnection with the PCB. This package offers small form factor with 60% size reduction compared to conventional QFP package. It provides good electrical performance due to the short electrical path in the inner leads and wires. Therefore, QFN is chosen

Table XIX. QFN Package Parasitics.

	Max	Min
Self Inductance	0.02 nH	0.01 nH
Mutual Inductance	0.003	0.002
Resistance	0.6 mΩ	0.5 mΩ
Self Capacitance	137 fF	124 fF
Mutual Capacitance	22 fF	18 fF

for the proposed MB-OFDM system implementation.

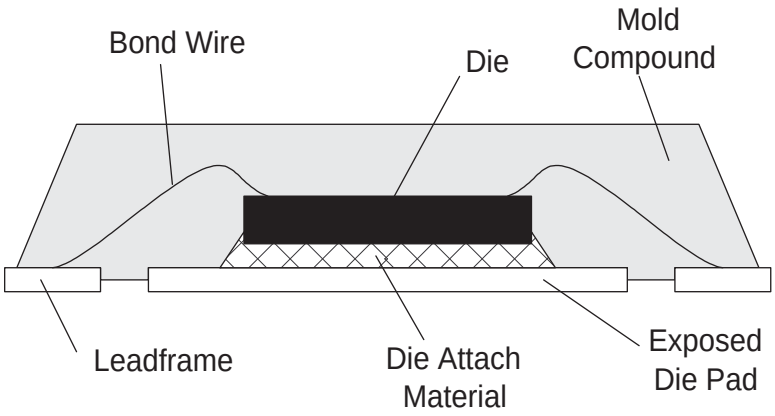

Fig. 67. Quad Flat No-Lead Package Cross Section.

The package and bond-wire parasitics are modeled as lumped elements, as shown in Fig. 68. Package parasitics do not depend on the die location and size, and are summarized in Table. XIX.

The die is placed in the middle of the package to obtain fully symmetric parasitics. Although the inductance at the LNA input is slightly increased, this can be compensated in design. Three-dimensional plot of the bond wires is shown in Fig. 69. The computed bond wire parasitics are summarized in Table. XX. This model is then

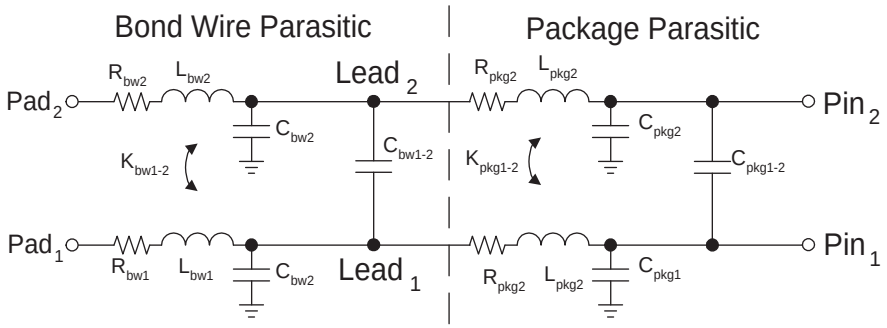

Fig. 68. Equivalent Parasitic Schematic.

Table XX. Calculated Bond Wire Parasitics.

	Max	Min
Self Inductance	3.75 nH	3.02 nH
Mutual Inductance	1.45 nH	0.4 pH
Resistance	120 mΩ	106 mΩ

used to optimize the pin locations for minimum coupling and maximum performance.

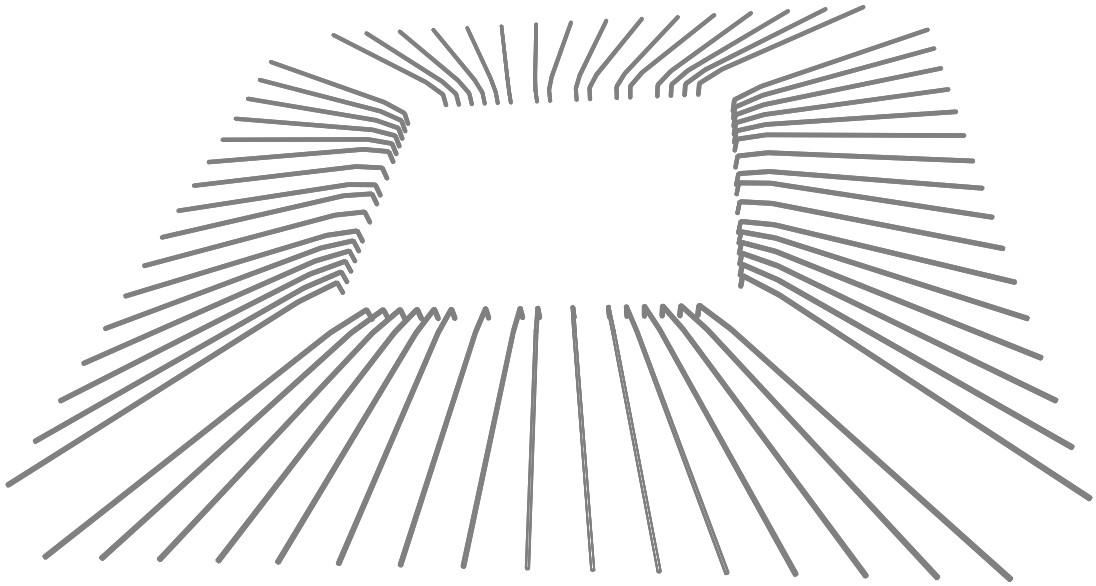

Fig. 69. QFN 64 Three Dimensional Bond Wire Setup.

B. Digital Control

Observability and controllability requires access to internal nodes of the individual blocks. The simplest method is to add a pin for the desired signals or controls. Since every block has many stages that require control, it is not practical to bring every control node to output. For example, if every block requires extra 10 control signals, the total increase of number of pins is 100. Therefore, a bigger package is required to accommodate so many pins. The main problem of bigger package is that the package size and die size differ more. This increases the bond wire length and so the bonding inductance is increased. To reduce the number of pins without degrading controllability a digital control block is designed.

The digital control block consists of 32 8-bit registers, where each register is accessed independently. The communication between the block and external world is performed serially through two pins. The communication standard is a reduced version of I2C, which is a serial communication standard widely used by industry.

The external signals are clock input SCL, and data input SDA. In normal operation, data is applied to the SDA input, and SCL is needed to synchronize the data. Data can change when SCL is low, and it is sampled at the positive edge of SCL. Therefore, SDA must be stable before positive edge of SCL and when SCL is high. To prevent any undesired access to internal registers, a start signal and stop signal is also defined. When SCL is high, the negative edge of SDA is the start signal, which is shown in Fig. 70.When SCL is high, the positive edge of SDA is the start signal, which is shown in Fig. 71. After the start signal, only 5 address bits and 8 data bits are read and the rest is ignored. If stop is executed before the transmitted bit number reaches (5+8), the transmitted data is also ignored. This access procedure guarantees to prevent any unwanted access. The procedure to write data (10101010) in address (10100) is shown in Fig. 72. The communication starts with a start signal. Following the start, the least significant bit of the address is sent. After the most significant bit of address is sent, the least significant bit of data is sent. When all data bits are sent, the internal logic updates the register at the desired address.

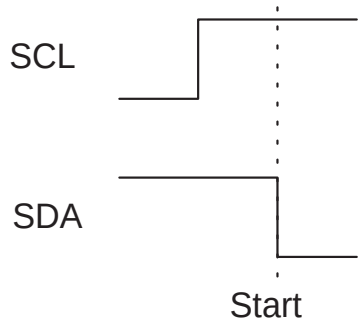

Fig. 70. I2C Start.

Digital block consumes only 0.09 mm^2. It's layout is compact and is shown in Fig. 73.

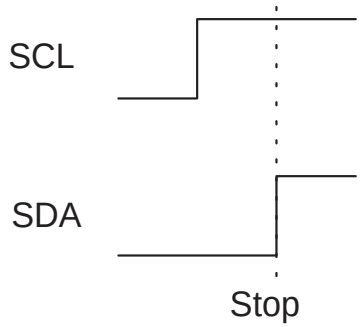

Fig. 71. I2C Stop.

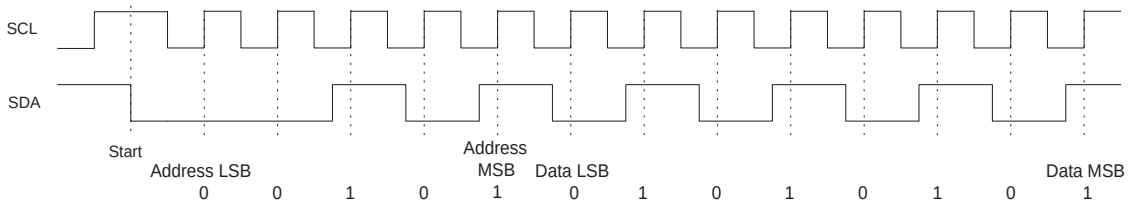

Fig. 72. I2C Operation.

C. Current Reference

Current reference circuits are widely used in analog applications, such as data converters and amplifiers. They are popular due to the simplicity and accuracy of scaling offered by current mirroring. Temperature independence is obtained by means of bandgap references, where two quantities that have opposite temperature coefficients are summed. The negative temperature coefficient can be generated with a forward biased pn junction, whereas the positive temperature coefficient can be observed as the difference between the base-emitter voltages of two bipolar transistors operating at different current densities [38]. A simple integrated circuit implementation was published in 1974 [39]. The current reference is simply generated by converting the bandgap voltage to a current using a resistor [40].

Bandgap references usually require external current sources for proper operation.

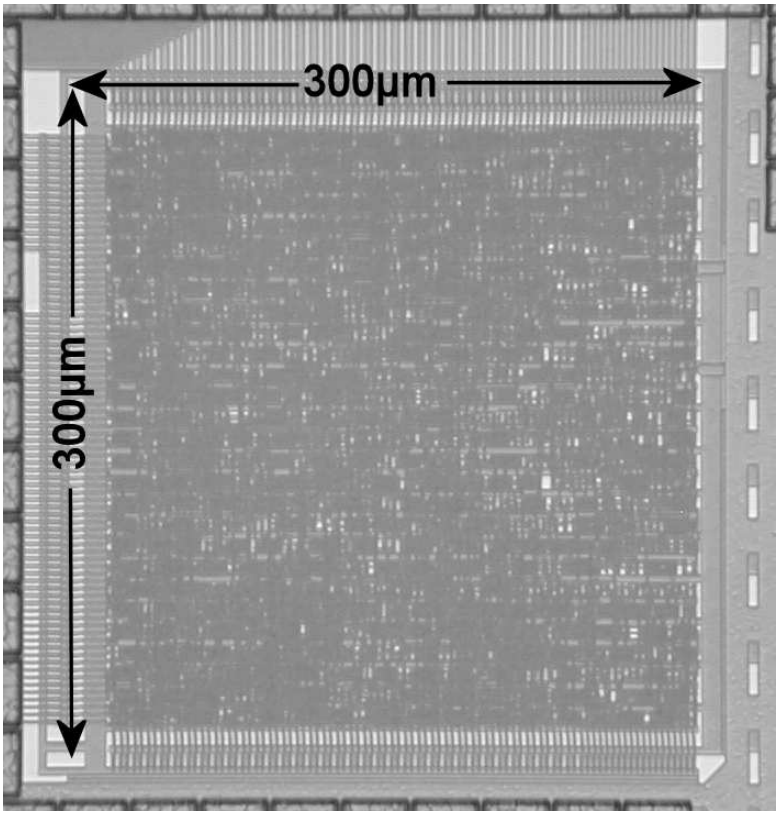

Fig. 73. Layout of Digital Control Block.

This increases not only the total pin count of the chip, but also the required printed circuit board (PCB) area. Due to increasing complexity of electronic systems and the demand for smaller devices, integrating external components into a single chip becomes necessary to reduce the size and the overall cost.

A current reference circuit with no external components is designed to generate bias currents for internal blocks. The circuit is biased using an internally generated temperature independent current source. Since this method results in two stable operating points, a startup circuit is used to guarantee proper operation. By self-biasing the bandgap reference, valuable PCB area and a package pin is saved.

1. Operation of Current Reference

Block diagram of the proposed current reference circuit is depicted in Fig. 74. The temperature independent voltage V_{ref} is generated by the bandgap reference circuit. This voltage is then converted to a current, I_{bias}, which is used to bias the bandgap reference itself. This method results in two stable operating points. One has all of the transistors in the cutoff region, where there is no current flow. The other is the normal, desired operation of the current reference. To avoid the unwanted operating point, a startup circuit is necessary.

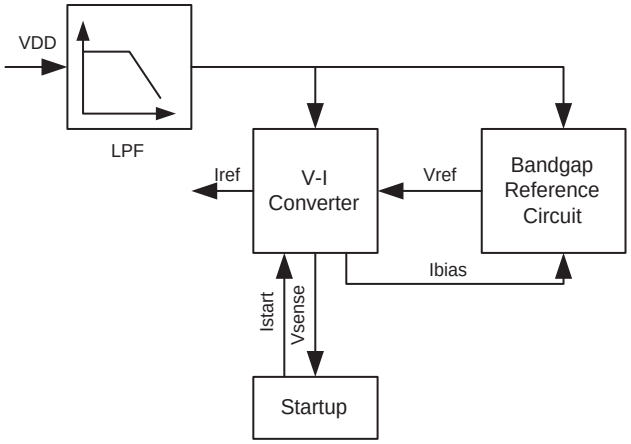

Fig. 74. Block Diagram of the Proposed Current Reference.

a. Bandgap Reference Circuit

The bandgap reference circuit is depicted in Fig. 75. The bandgap voltage (V_{ref}) is generated by Q_1, Q_2, R_1, R_2 and R_3. The operational amplifier (shown as Opamp1) forces equal currents on Q_1 and Q_2 by changing the current of M_1. The feedback guarantees high power supply rejection ratio (PSRR) at frequencies below the loop

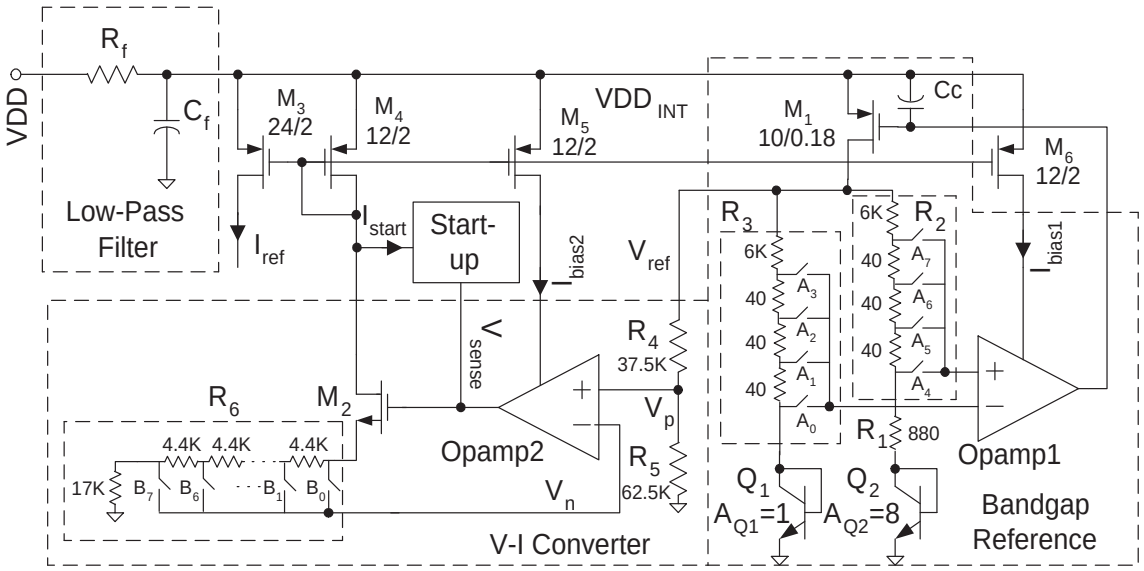

Fig. 75. Current Reference Schematic.

bandwidth, which is expressed as

$$f_{bw} = \frac{1}{2\pi(C_C + C_{g1})r_{o1}} \tag{6.5}$$

where r_{o1} is the output resistance of Opamp1, and C_{g1} is the gate capacitance of M_1. The non-dominant pole is at the drain of M_1, and is given by,

$$f_{nd} = \frac{1}{2\pi((R_3 + R_D)\|(R_1 + R_2 + R_D))C_{par}} \tag{6.6}$$

where C_{par} is the parasitic capacitance at the drain of M_1, and R_D is the small signal resistances of diode connected Q_1 and Q_2. A folded cascode architecture is selected for Opamp1 to achieve high gain and bandwidth. Gain bandwidth product (GBW) of the loop is approximated as

$$GBW = \frac{g_{m,O1}}{2\pi(C_C + C_{g1})} \tag{6.7}$$

where $g_{m,O1}$ is the transconductance of Opamp1. The phase margin of the loop is calculated as,

$$PM = 90^o - \tan^{-1}\left(\frac{GBW}{f_{nd}}\right) \tag{6.8}$$

The current of M_1 in Fig. 75 is proportional to the positive absolute temperature, and is given as

$$I_{PTAT} = 2\frac{V_T \ln(m)}{R_1} \tag{6.9}$$

and the reference voltage can be obtained as

$$V_{ref} = V_{BE1} + \left(\frac{R_2}{R_1}\right) V_T \ln \frac{R_2}{R_3} m \tag{6.10}$$

where

$$m = \frac{A_{Q2}}{A_{Q1}} = 8 \tag{6.11}$$

Since $\partial V_{BE}/\partial T \approx -1.5$ mV/K and $\partial V_T/\partial T \approx +0.087$ mV/K, the reference voltage will be independent of temperature if $(R_2/R_1)\ln(mR_2/R_3)$ equals to 17.2 [41]. However, any mismatch between R_1 and R_2 or R_2 and R_3 deviates the result from the desired value. Programming R_2 and R_3 at discrete steps reduces mismatch between them from %2 to %0.3. The temperature dependence of the switches does not effect the performance, because they are added in series with the opamp input. Since the mismatch is process dependent and does not change with temperature, it will be measured after the production. This mismatch information is then used to program the switches.

b. Voltage to Current Converter

The reference voltage is reduced by a resistor divider and converted to current using Opamp2, M_2 and R_6, as shown in Fig. 75. The feedback forces V_p to be equal to V_n.

The reference current is obtained as

$$I_{ref} = \frac{R_5}{R_4 + R_5}\frac{V_{ref}}{R_6} \tag{6.12}$$

Nominal I_{ref} was designed to be 50 μA. The output current can be varied by changing the value of R_6, which is designed discreetly variable between 17 K and 47.8 K with a nominal value of 30.2 K. Since the output current can be scaled $\pm$57%, the power consumption of the overall system can be reduced to almost half of the normal operation. The process dependency of R_6 changes the reference current.The resistance variations is measured after the production, and the process dependency of the reference current is reduced by compensating the resistance variations digitally. For example if the resistance value is 25 K, the nominal switch is set to B3 instead of B4. Since the switches are added in series with the input of Opamp2, the switch resistance variations on the reference current is negligible.

c. Low-Pass Filter

Since low frequency supply perturbations are rejected by feedback, filtering is needed to suppress the supply noise above loop bandwidth. The optimum area, power consumption and suppression is obtained when the filter's cut-off frequency is equal to the loop bandwidth, f_{bw} from (6.5). If the cut-off is selected lower than f_{bw}, the power consumption of the reference is increased to cover the frequency which is already attenuated by the low-pass filter. On the other hand, if the low-pass filter bandwidth is higher than f_{bw}, the supply rejection is degraded between the cut-off frequency of the filter and loop bandwidth. The filter is selected first order RC-type to achieve low power consumption. The cut-off frequency is

$$f_{LPF} = \frac{1}{2\pi R_f C_f} \tag{6.13}$$

Since supply current flows through R_f, the voltage drop on it limits its value. For low voltage operation the voltage drop on R_f is selected as 200 mV. To reduce the bandwidth requirement and not to increase the total area significantly, C_f area is selected twice of the rest of the circuit. Therefore, the cutoff frequency is 3.5 MHz.

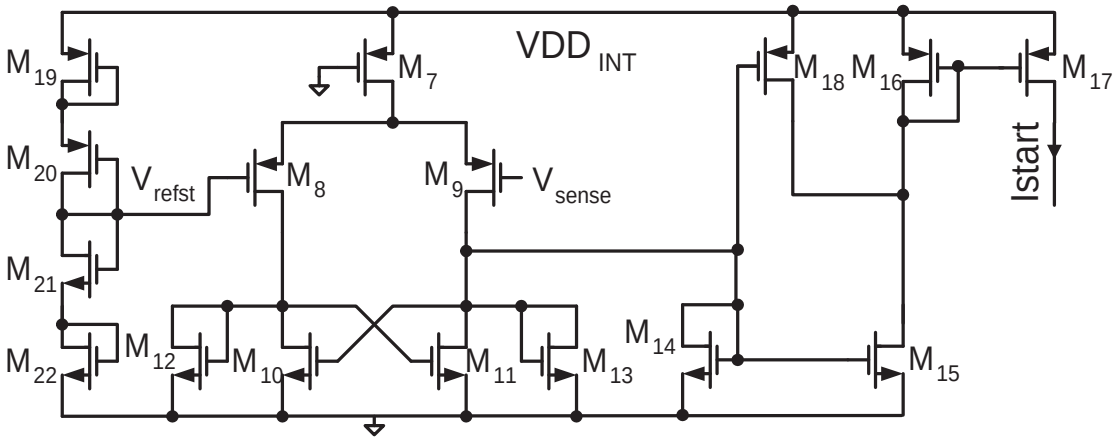

Fig. 76. Startup Circuit Schematic.

2. Startup Circuit

The undesired operating point of the current reference is avoided by a startup circuit. The unwanted stable point is where Q_1 and Q_2 are in cut-off region. The transistor M_2 in Fig. 75 is also in cut-off region, therefore, its gate voltage, V_{sense}, is zero. The startup circuit shown in Fig. 76 compares this voltage with a reference and generates a current. If V_{sense} is greater than V_{refst}, the startup current will be zero. M_{19}-M_{22} are used to generate the startup reference voltage (V_{refst}). M_8-M_{13} operate as the comparator, where M_8 and M_9 form the differential pair and M_{10}-M_{13} comprise the active load. The output current of the comparator is mirrored by M_{14}-M_{17}. If the sensed voltage is below the startup reference, most of the current of the differential pair flows through M_9. The output current of the comparator flows through the diode-

connected M_{14}, and M_{15}-M_{17} mirror this current. Therefore, the startup current has a nonzero value. When the temperature independent voltage reference starts its proper operation, the sensed voltage will be above the startup reference voltage. The current starts to flow through M_8, and the output current of the comparator becomes zero. Since M_{14} is diode connected, M_{14} and M_{15} enter cut-off region. The gate capacitance of M_{16} and M_{17} is discharged by the diode connected M_{16}. Since the transconductance of M_{16} is selected small to reduce the current consumption, the required time to discharge is increased. When M_{14} enters cut-off region, the gate voltage of M_{18} decreases to zero. The current capability of M_{18} is now greatly increased. It helps to discharge the gate source capacitance of M_{16} and M_{17} and reduces the startup time.

CHAPTER VII

EXPERIMENTAL AND SIMULATION RESULTS

The proposed UWB receiver was fabricated in TSMC 0.18μm as two chips. The first chip was designed to test each block individually. To minimize the required pin numbers, the bias currents were generated using internal current reference. To increase the controllability, bias current of each individual block could be chosen from temperature independent current, PTAT current or external current. Two pins were reserved to apply bias currents externally. Since each block had also power down control, the blocks except the measured one was set to power down, which allowed measuring each block without being affected by others. The digital control block worked without a problem, and current reference was measured and characterized across temperature.

A. Printed Circuit Board (PCB) Design

To test each block and the whole system, printed circuit board was designed. Since there were limited number of chips, every block was measured using the same board. This approach resulted in a complex PCB, as shown in Fig. 77. LNA and mixer's local oscillator inputs were applied externally. Since they are differential, on-board balun was used to convert single ended input to differential. The decoupling capacitances of LNA and mixer were placed as close as possible to their supply pins. Instead of using one capacitance, two capacitances were used to guarantee enough decoupling even at high frequencies. Since the chip supply was 1.8 V, external level shifter was used to convert external logic signals, from 3.3V and 5V. The baseband blocks require differential input and differential outputs. Therefore, on board transformers were used to convert single ended signals to differential.

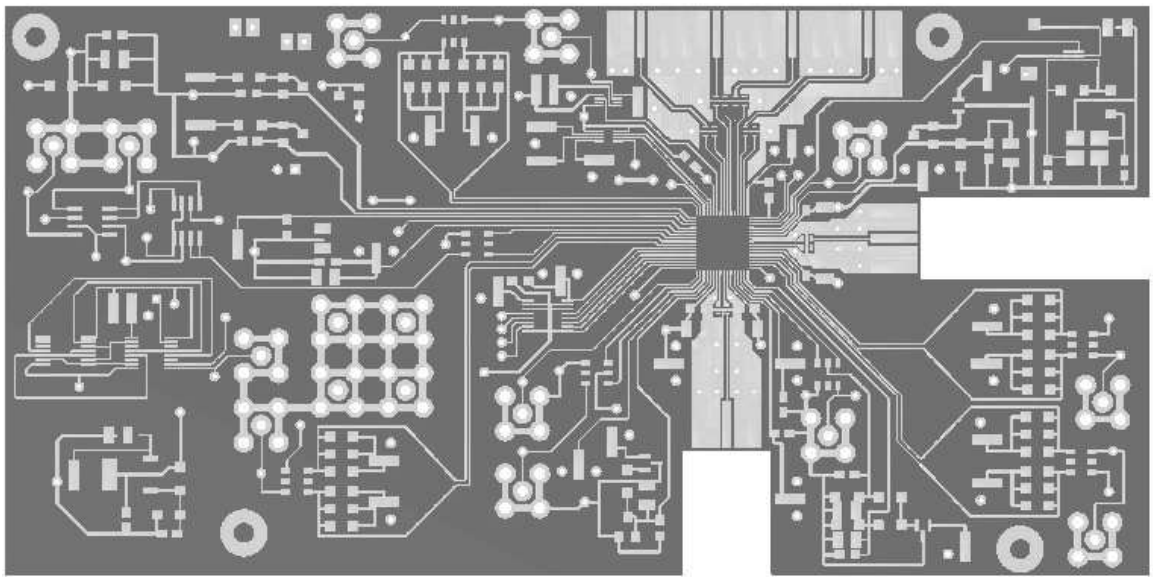

Fig. 77. Printed Circuit Board of UWB1.

B. Current Reference

The chip micrograph of the current reference is shown in Fig. 78. The capacitance, C_f, makes up nearly two thirds of the entire area. Since one terminal of R_f is connected to external supply, R_f and the current reference core are separated as far as possible to reduce supply coupling through substrate. The reference layout is surrounded with a deep n-well ring to reduce coupling between the core and the rest of the chip. The total current reference layout area is $190\mu\text{m}\times290\mu\text{m}$.

The simulations were performed with TSMC 0.18μm technology files using RC extraction for the layout parasitics. The temperature dependence of the reference current is depicted in Fig. 79 for the nominal case, where $\text{A} = \text{A}_7 \ldots \text{A}_0 = 00100010$ and $\text{B} = \text{B}_7 \ldots \text{B}_0 = 00010000$. The measurement of reference current vs. temperature for different settings of R_2 and R_3 is provided in Fig. 80. For nominal settings, the measured current is 54.1 μA and the current deviation is less than $\pm$100 nA between 22 °C and 100 °C. The measurement results depicted in Fig. 81 indicates

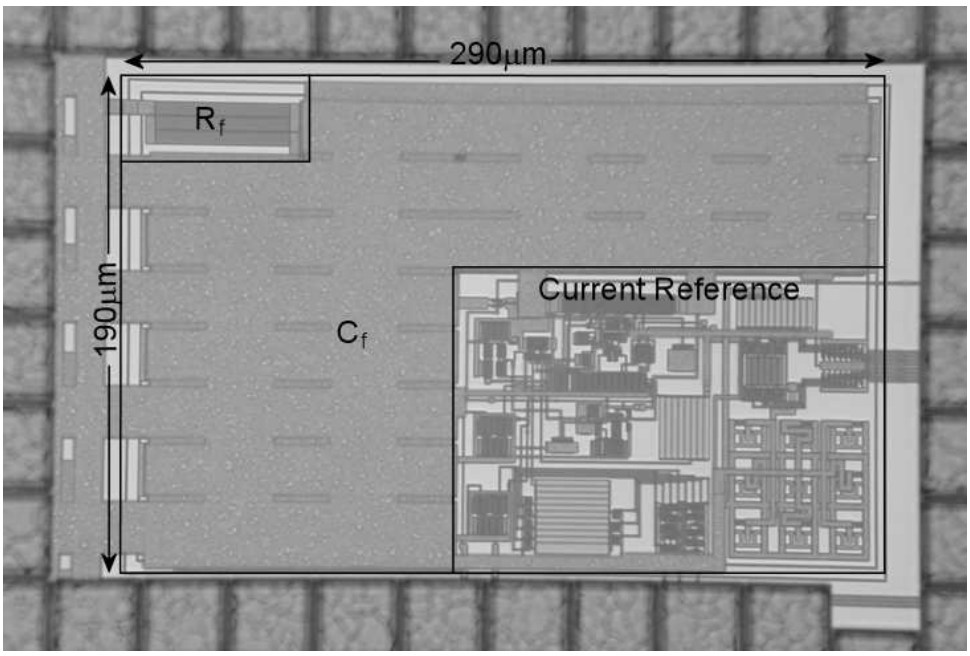

Fig. 78. Layout of the Current Reference Circuit.

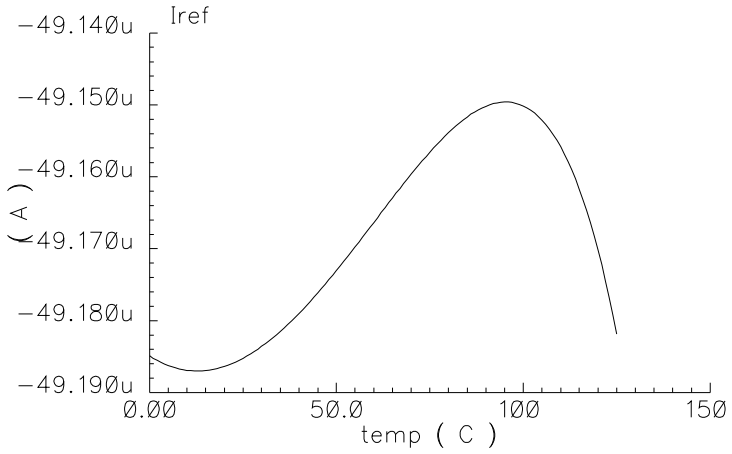

Fig. 79. Simulated Nominal Reference Current vs. Temperature (A = 0010 0010, B = 0001 0000).

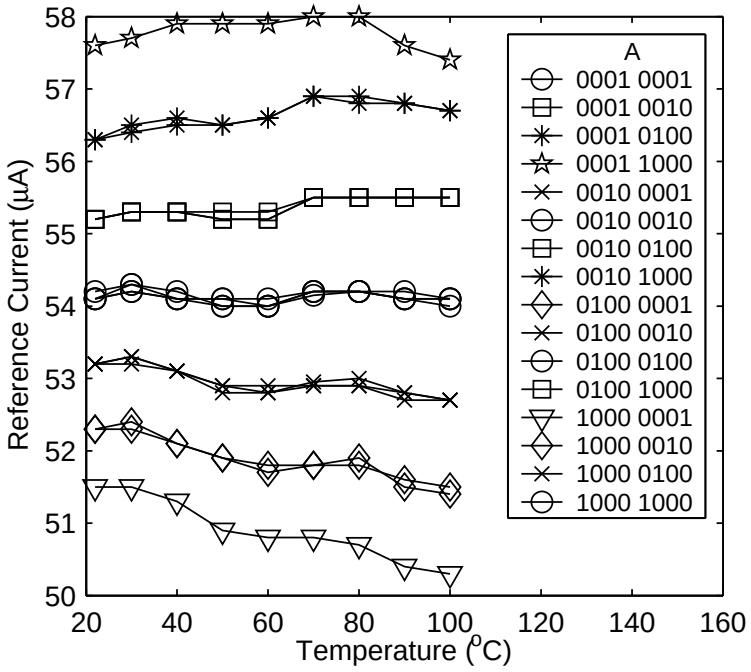

Fig. 80. Measured Reference Current vs. Temperature with B = 0001 0000.

that the current can be set close to 50 μA by programming the value of R_6. The power consumption can be scaled to between -20% and +70%, because the process variation of the resistance shifts the power scaling range. The current of M_1 shown in Fig. 75 is proportional to positive absolute temperature and its measurement for nominal settings is depicted in Fig. 82. The startup response depicted in Fig. 83 is determined by simulation, since the measurement equipment is not able to catch the startup behavior. The startup time is around 0.1 μs. The PSRR is defined as the current perturbations per supply perturbation. The simulated PSRR is shown in Fig. 84. It shows flat response at low frequencies due to finite loop gain. Above the cut-off frequency of the RC filter it reduces with 20 dB per decade. The noise density is so low that it was not possible to distinguish it from the equipment noise. Therefore, its simulation result is depicted in Fig. 85. The total measured current

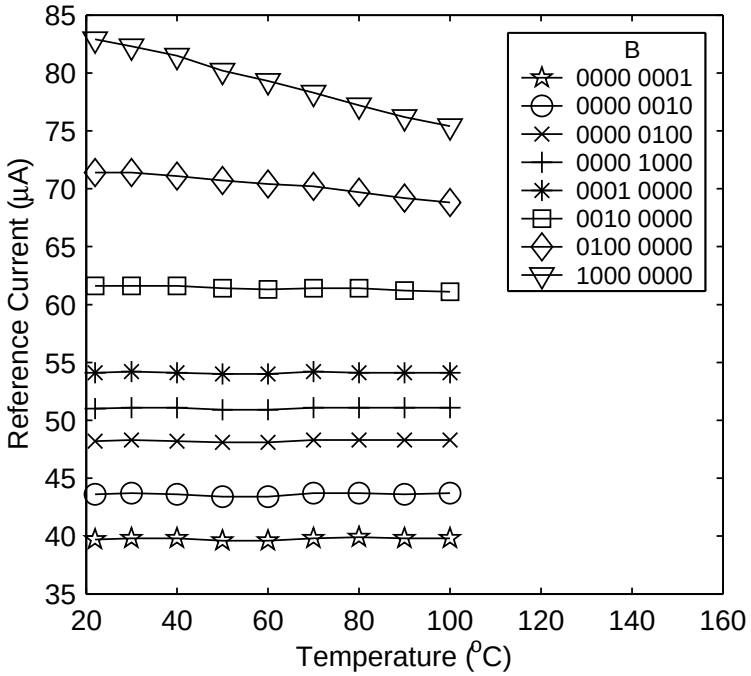

Fig. 81. Measured Reference Current vs. Temperature with A = 0010 0010.

consumption is 700 μA for a 1.8 V single supply.

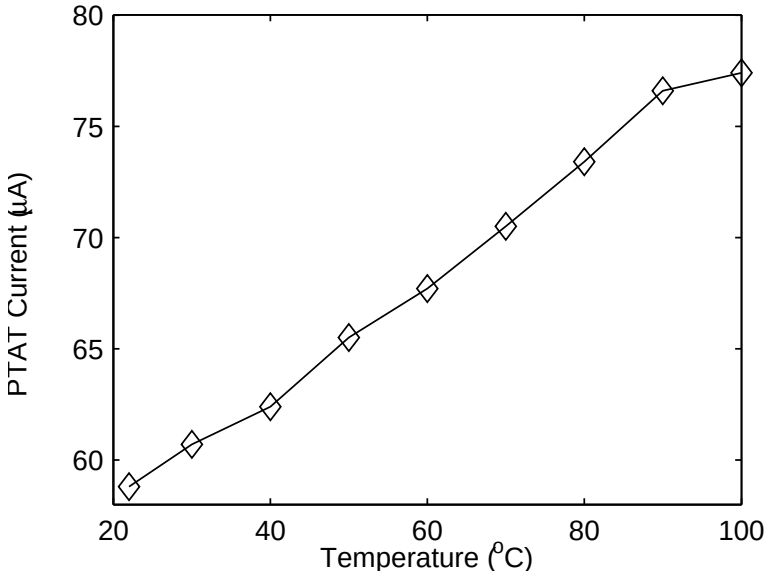

Fig. 82. Measured PTAT Current vs. Temperature.

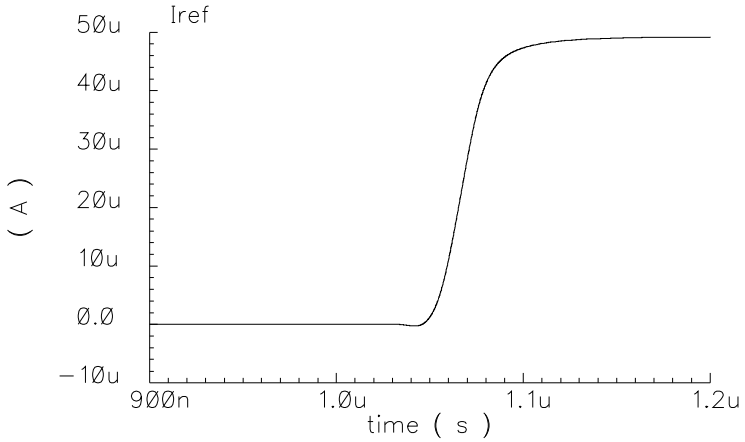

Fig. 83. Simulated Time-domain Response During Startup.

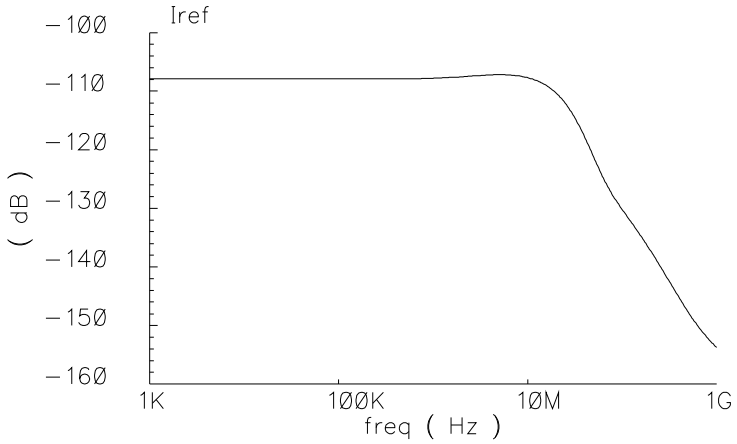

Fig. 84. Simulated Power Supply Rejection Ratio.

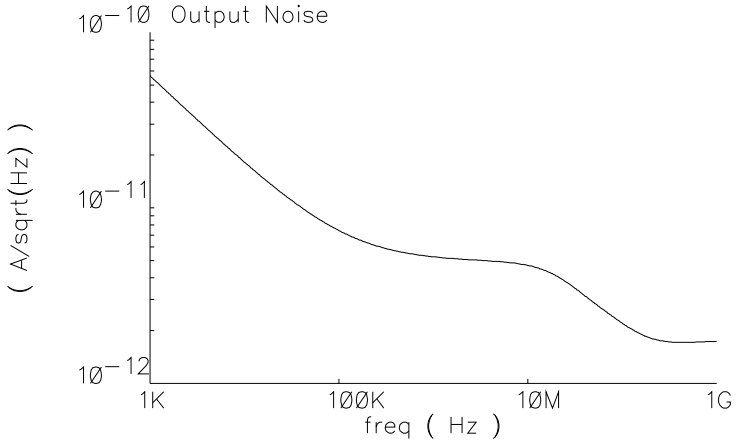

Fig. 85. Simulated Output Noise Current Density.

C. System Simulations

Although spreadsheet is very useful to evaluate first order system parameters, it is not adequate to verify the effects of all the parameters on system performance, such as the effect on nonlinearity on noise performance, or effect of finite bandwidth of individual blocks. To analyze these type of effects, a simulation-based approach is needed, where the blocks are modeled at behavioral level. However, complexity of the models slows down overall simulation. To obtain quick insight on the performance, the linearity, gain, noise and frequency response of individual blocks are modeled. Although it is not as accurate as transistor-level simulations, system-level simulation helps quickly evaluate the overall system performance.

1. Behavioral Simulations

Behavioral models are constructed with mathematical and empirical approaches. The mathematical approach is based on modeling with formulas that represent the desired response. On the other hand empirical models are based on fitting the desired response on the simulated or measured parameters. Mathematical formulas are also used during spreadsheet calculations. However, spreadsheet is not capable of solving ordinary differential equations. Therefore, it is not possible to model filters in spreadsheet. However, behavioral simulations are performed in time domain and can solve differential equations.

The behavioral model of MB-OFDM UWB's analog frontend shown in Fig. 86 is modeled in Matlab, since Matlab has an extensive library for mathematical modeling. Input signal block generates the desired UWB signal and adds channel noise. Since the transmitter and receiver is synchronized, the frequency synthesizer is located in the input signal block. Received UWB signal is first attenuated by the TX/RX

switch. Therefore, this block adds noise to the received signal. Since the switch is highly linear, its nonlinearity is not included to decrease simulation time. The bandpass filter is a SAW type filter. Therefore, its linearity does not degrade the received signal. However, it attenuates the signal and shapes its frequency. These effects are added in the band-pass filter model. Since LNA has two gain levels, its gain is applied externally. Its nonlinearity, noise performance and frequency response is added in the simulations. Mixer noise and nonlinearity are combined with the LNA noise and nonlinearity. Therefore, the mixer is implemented as a noiseless and linear block. Noise, linearity and frequency response of baseband blocks are included in their models.

First, the effect of thermal noise is evaluated using the behavioral model. Since sensitivity is limited by thermal noise, the input signal power level is set to the sensitivity level. The simulation is performed for Mode 1. Since UWB is a frequency hopping system, all three channels are present at the receiver input as shown in Fig. 87, if the signal is observed for minimum three hopping period. During the simulations, the signal is observed for twelve hopping periods. TX/RX switch and BPF attenuate the signal, while keeping the noise level constant. Therefore, the signal level at LNA input shown in Fig. 88 is 1.7 dB lower than at the antenna input, while the noise level is the same as the channel noise. Although the signal at LNA output is amplified, the noise level increases due to LNA's noise. In Fig. 89, the signal level increases 33 dB, but overall signal-to-noise is degraded. The effect of frequency response of BPF and LNA is seen at the mixer output, which is shown in Fig. 90. The noise above 264 MHz is attenuated by low pass filter shown in Fig. 91. In these simulations, the notch of band-reject filter is turned off, but its linearity, noise and frequency response due to finite bandwidth is included. Therefore, the desired signal is attenuated close to the upper edge of the band, which is shown in Fig. 92. VGA

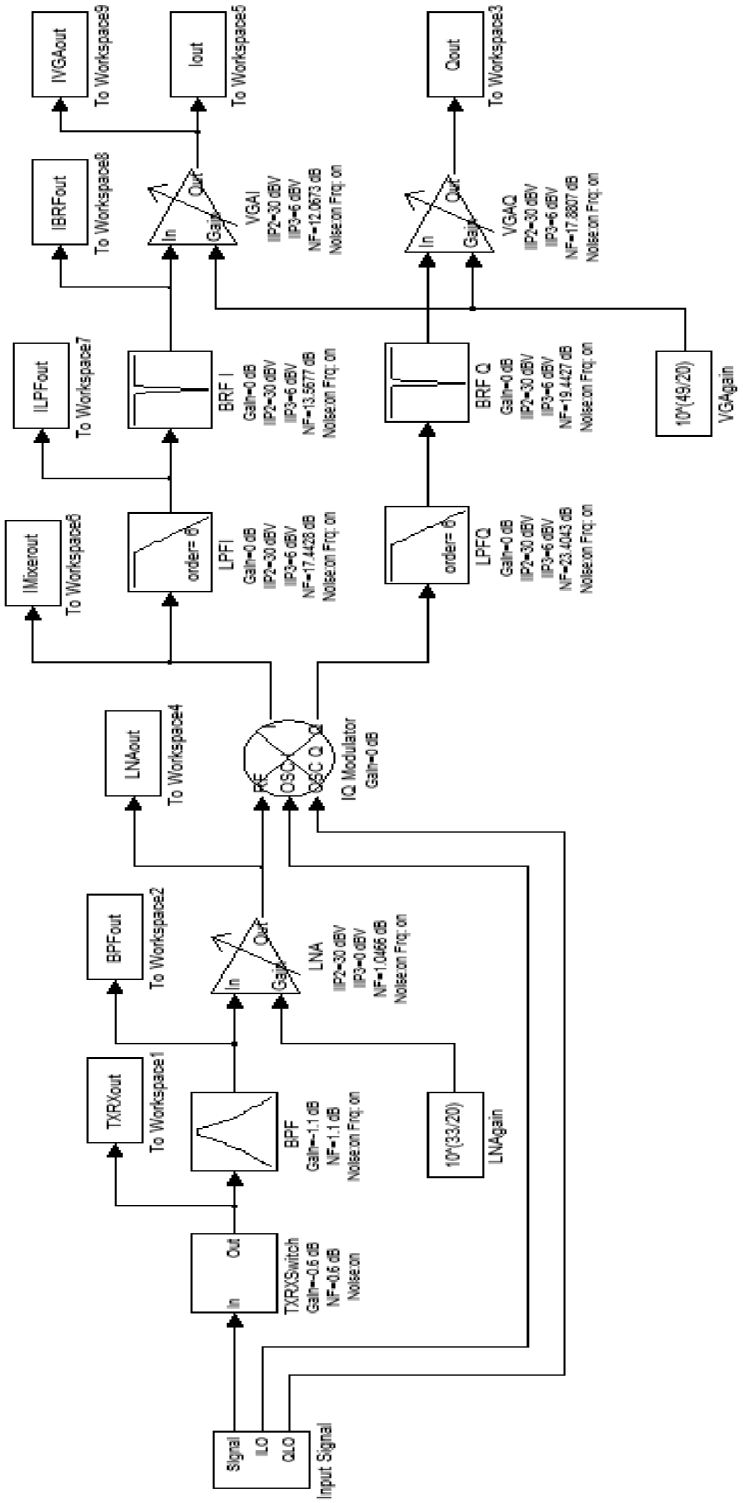

Fig. 86. UWB Analog Frontend Behavioral Model.

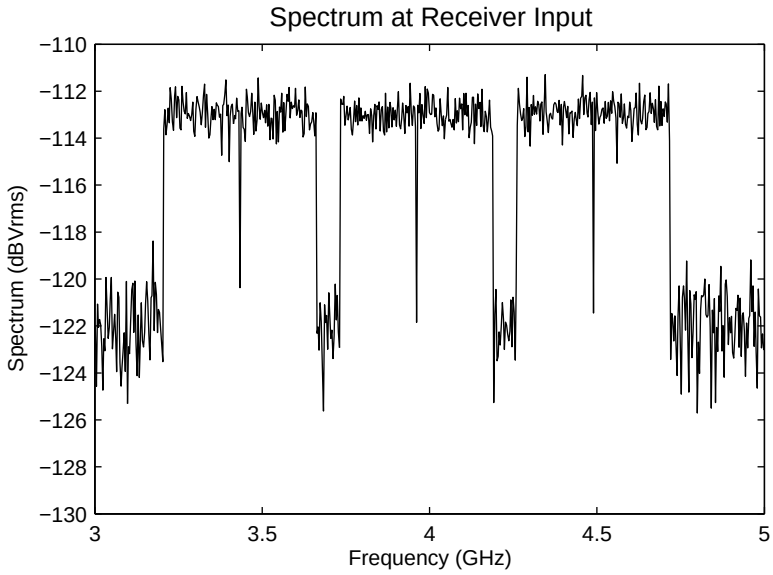

Fig. 87. Receiver Input Spectrum.

is also set to maximum gain. Therefore, the VGA output shown in Fig. 93 indicates higher signal level than rest of the blocks. Since notch filter and VGA is located after the low-pass filter, their noise contribution increases the noise floor above the channel's cut-off frequency. To calculate the overall noise figure, gain and total delay input and output waveforms are correlated. Noise figure is calculated as 5.8 dB, which is close to the value calculated in the spreadsheet. Total gain from antenna input to VGA output is 80 dB, which is close to the spreadsheet value. The total delay from antenna input to VGA output is 4.73 ns. Since the calculation of overall system delay requires evaluation of frequency responses, it is not possible to evaluate it in the spreadsheet.

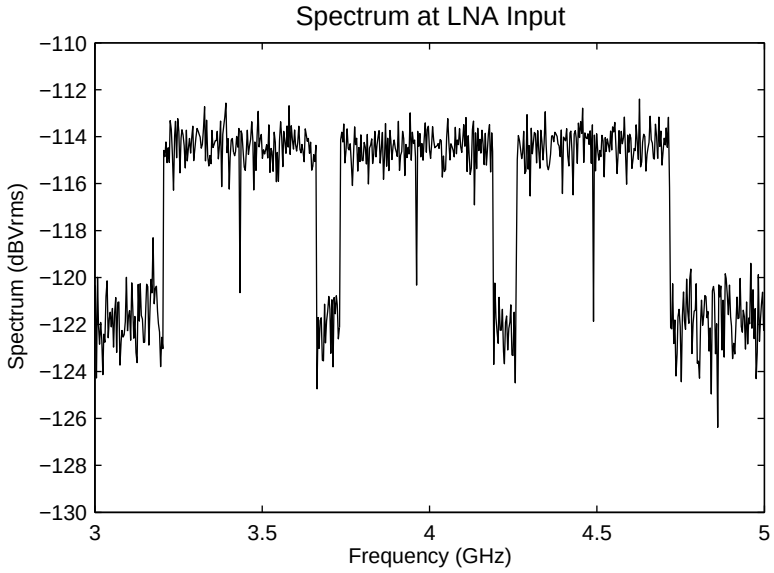

Fig. 88. LNA Input Spectrum.

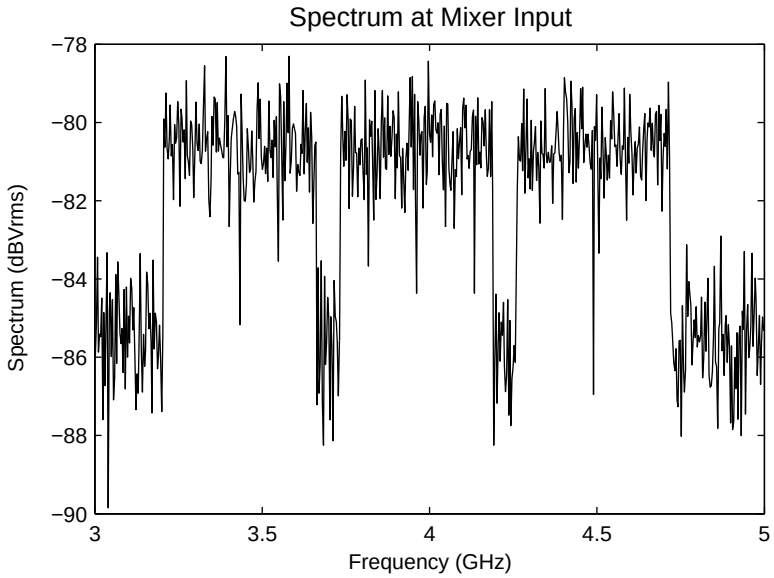

Fig. 89. Mixer Input Spectrum.

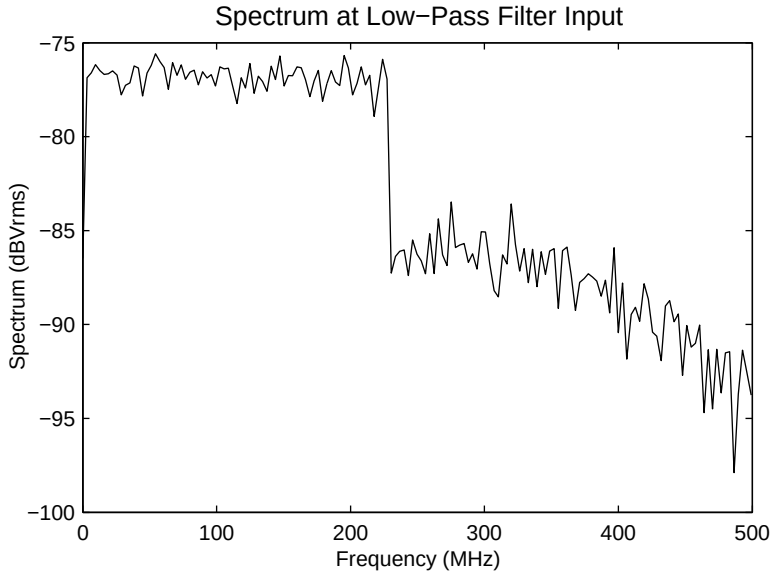

Fig. 90. Low-Pass Filter Input Spectrum.

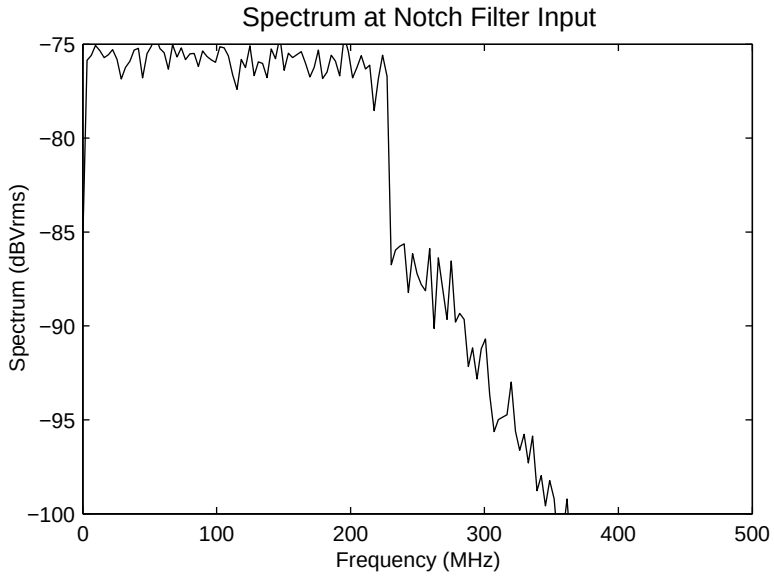

Fig. 91. Notch Filter Input Spectrum.

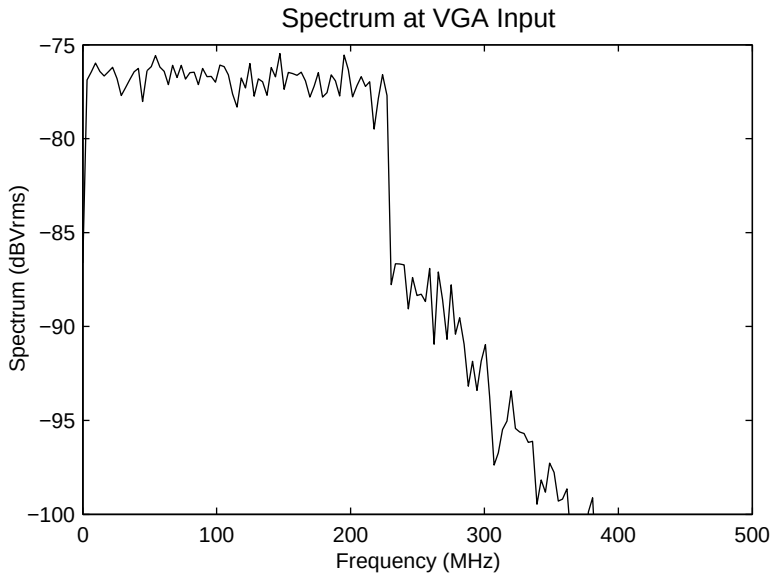

Fig. 92. Variable Gain Amplifier Input Spectrum.

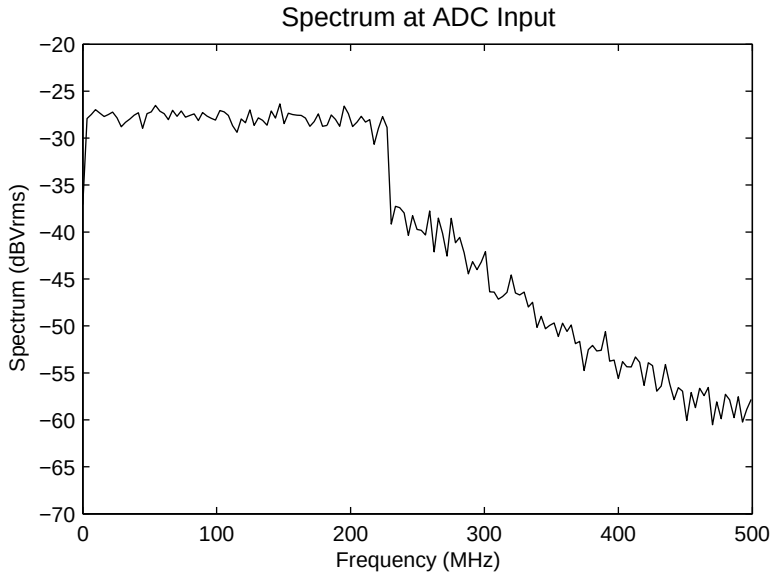

Fig. 93. Analog-to-Digital Converter Input Spectrum.

Intermodulation performance of the overall system is verified with two different methods. In the first method, the input power is swept from -80 dBVrms to -10 dBVrms and input referred second and third order intercept points are determined. The simulated IIP3 is -5 dBVrms and IIP2 is 15.15 dBVrms, as shown in Fig. 94. Spreadsheet estimates the IIP3 as -2.44 dBVrms and IIP2 as 16.02 dBVrms. Although simulation results are close to calculate values, the intercept points are lower than spreadsheet values. The second method is used to determine the overall system's missing band tone test performance. Since the analytical formulas are based on assumptions, a system level time-domain simulation estimates the performance more accurate than analytical formulas. The MTPR result is 16.41 dB as shown in Fig. 95.

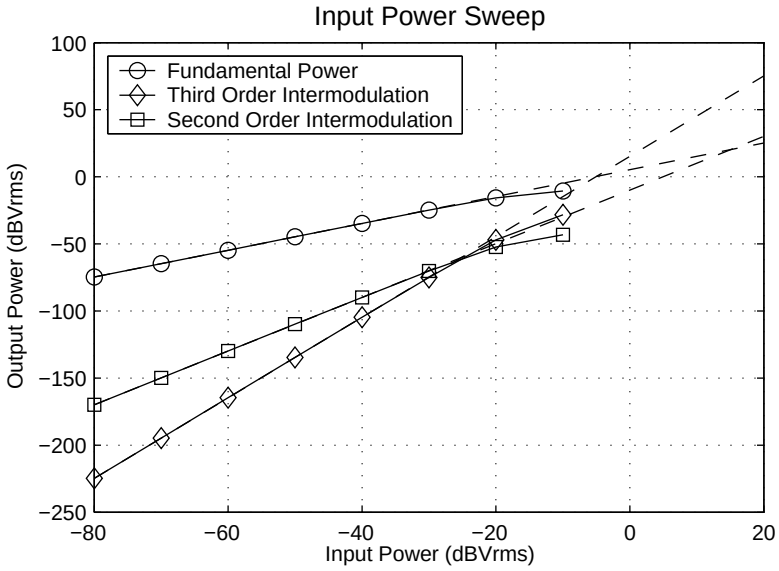

Fig. 94. Intermodulation Performance.

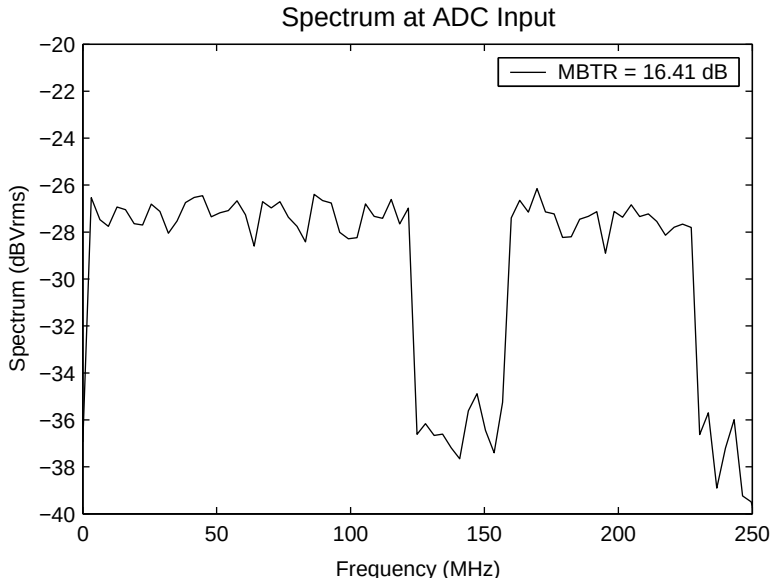

Fig. 95. Simulated MTPR at ADC Input.

2. AGC Simulations

The transient behavior of automatic gain control shows that it converges within 3 UWB symbols. AGC starts operation at the beginning of UWB communication. In the simulation the communication starts at 0.3 μs and AGC's start signal goes high. AGC enters in fast mode to reduce the time for convergence. During the fast mode shown in Fig. 96, AGC uses 5 samples to estimate the overall energy of the received signal. AGC shows second order response, so it settles with slight overshoot. At the end of 5 samples, AGC decides that LNA must be at high gain. The loop continues changing VGA gain level in order to minimize the error between estimated energy and actual energy. When the difference is less than 6 dB, AGC starts to use 25 samples to estimate the energy. Obviously, increasing number of samples gives better energy estimate of the received signal in the expense of longer settling time. Overall response of AGC is shown in Fig. 97. AGC settles to its final value at the end of the second symbol.

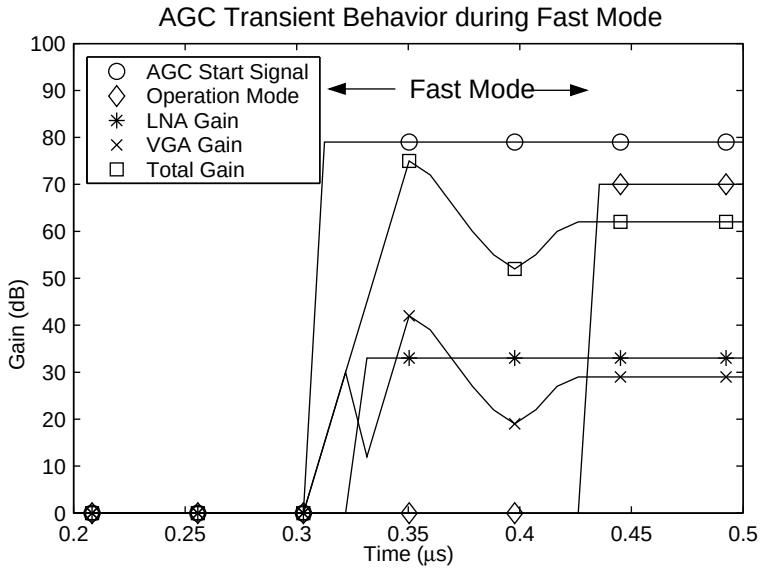

Fig. 96. AGC Transient Behavior During Fast Mode.

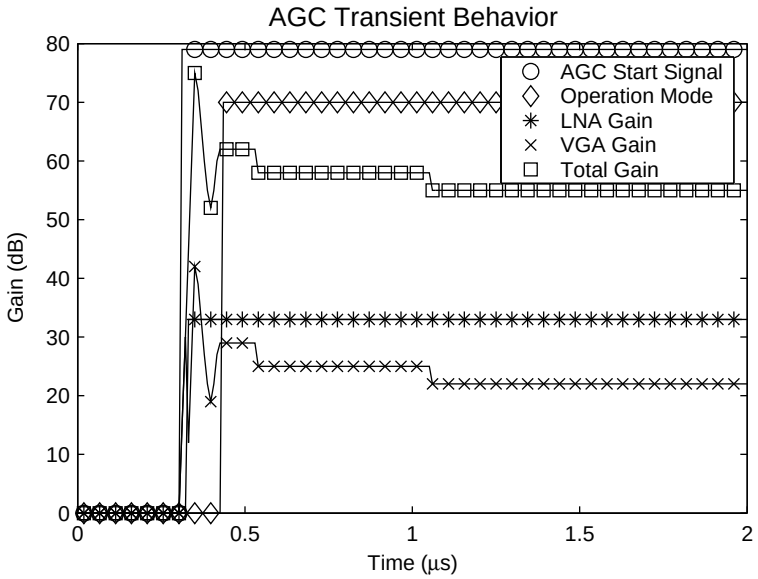

Fig. 97. AGC Transient Behavior.

3. Transistor-Level Simulations

Although behavioral simulations give good insight for overall system behavior with noise, linearity and frequency behavior, it is not feasible to model all transistor-level effects due to increase on simulation time. On the other hand, transistor-level Spice simulations are more accurate, but slower than behavioral simulations. To verify the performance at transistor-level, whole system is also simulated with package model and estimated layout parasitics. The effect of layout parasitics can be added with top level parasitic extraction. However, including every small parasitic in the system simulation creates numerical convergence problems. Estimating parasitics and adding them at the schematic level results in faster simulations than extracted ones. The speed difference between schematic level and schematic level with estimated parasitics is negligible.

The top level simulation setup is shown in Fig. 98. The input signal is converted to differential using an ideal balun, which has flat frequency response and has 50 Ohm port impedances. The external signals are connected to the chip through the package. Any effect of coupling due to the package is also included at the top level simulation. The top level schematic of whole system is shown in Fig. 99. The layout parasitics of connections between blocks are modeled as a pure capacitance, RC or RLC network depending on the frequency of operation and length of connection. The ADC clock network is modeled as RLC network, since the clock signal travels from synthesizer to I and Q ADCs. Although clock is at 528 MHz, it includes also higher order harmonics due to its squarewawe shape. On the other hand, the connections between baseband blocks and mixer are modeled as a capacitance, since the blocks are next to each other and frequency of operation is low.

Since whole system is simulated at time-domain, AC analysis does not give mean-

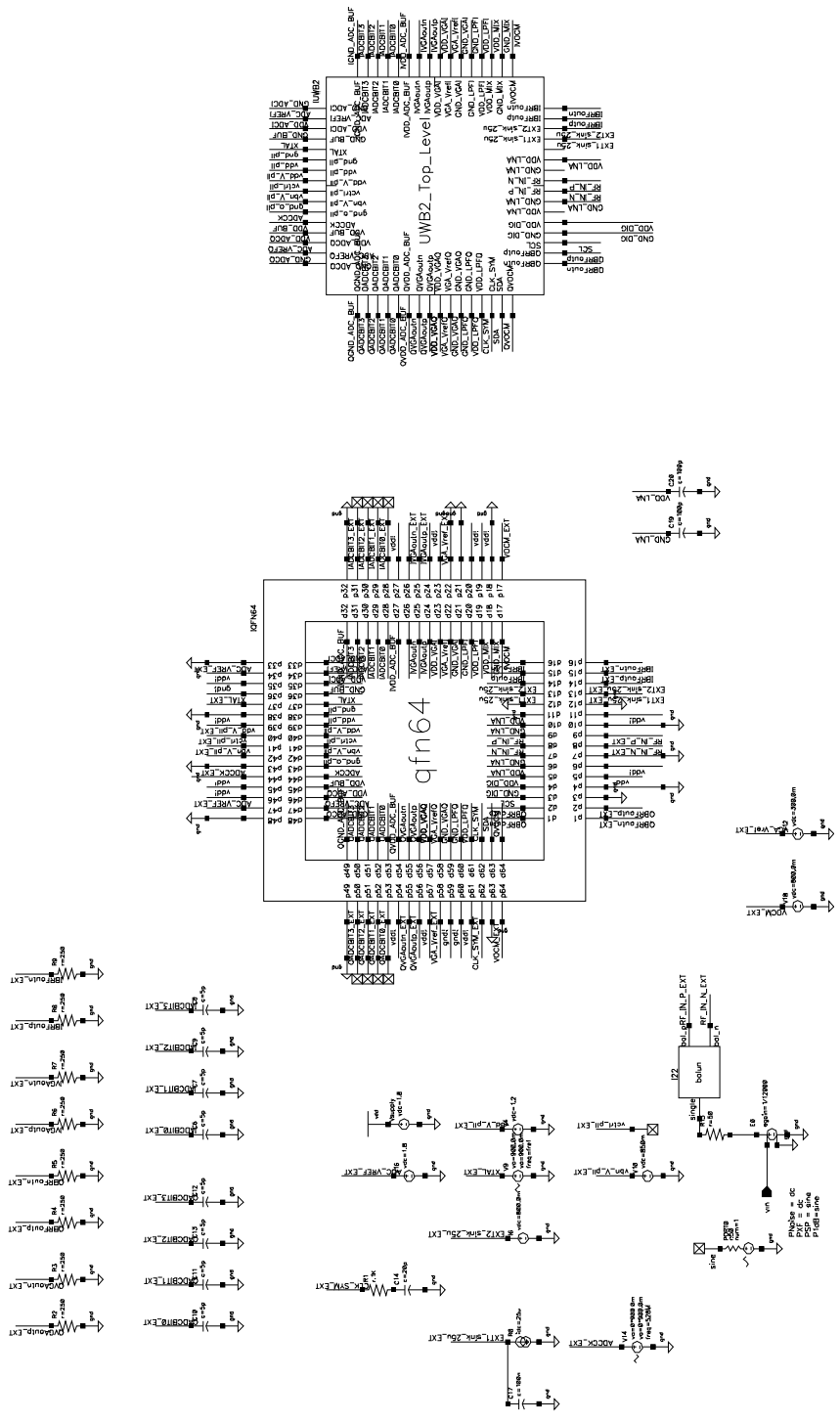

Fig. 98. Top Level Simulation Setup.

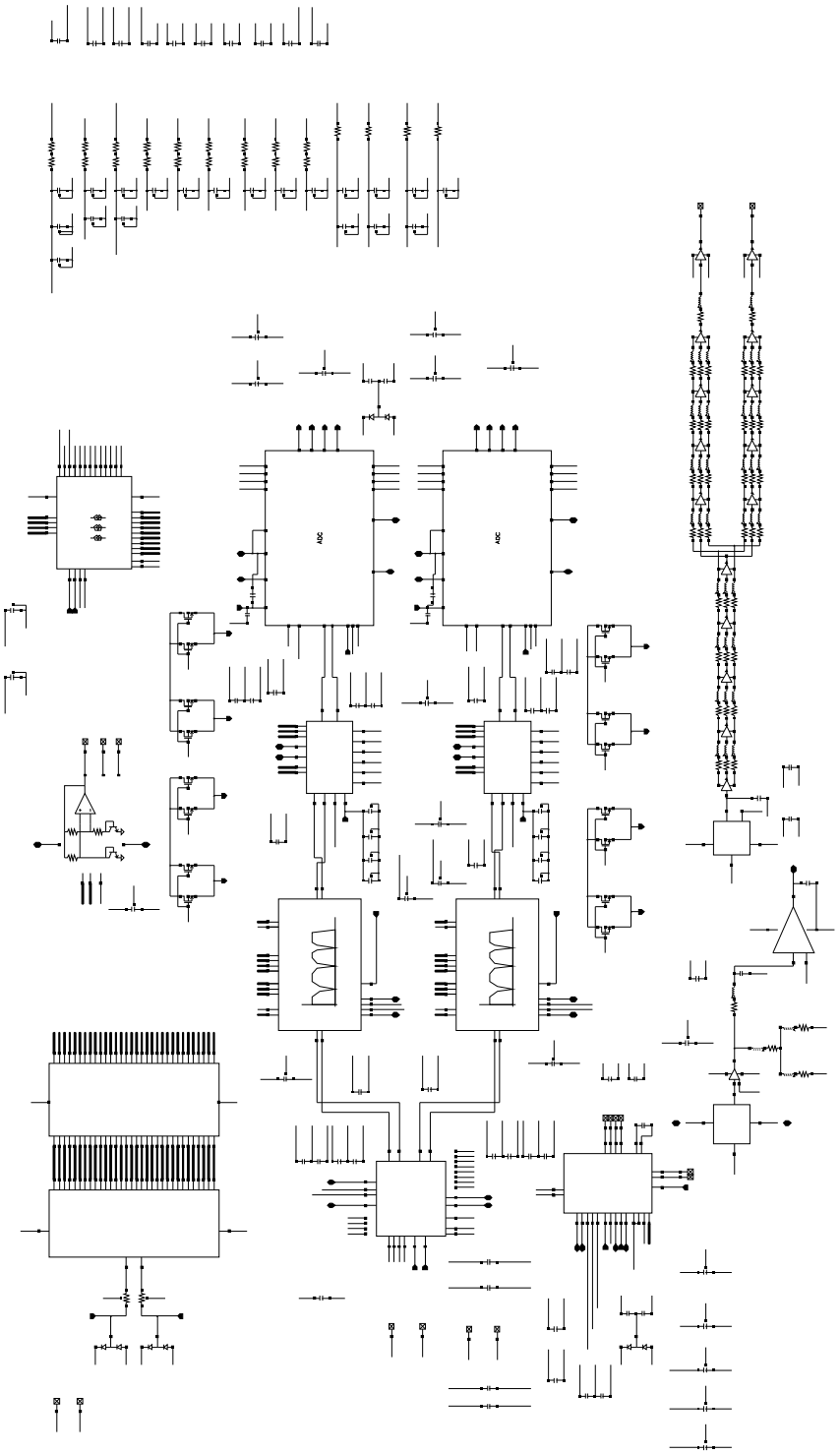

Fig. 99. Top Level Schematic with Estimated Parasitics.

ingful results. In Spice, there are two types of time-domain simulators. One is the classical transient analysis used for transient behavior, and the other is periodic steady-state analysis (PSS). PSS analysis tries to find the steady-state solution of the circuit and has convergence problems if the circuit is too large. PSS can also perform noise analysis to determine noise for mixers and oscillators. The whole UWB system with package and layout parasitics does not converge during PSS analysis. Therefore, it is not possible to verify noise response at the very top level. Transient analysis does not try to find steady state solution and has not convergence problems as PSS analysis. However, it does not simulate noise. Therefore, the linearity performance of whole system is verified with transient analysis.

To determine the second and the third order intercept points, the input power is swept. However, this requires multiple simulations with various input powers. Moreover, these simulations can not catch the interaction between the tones of MB-OFDM signal. Therefore, a missing tone power ratio test is performed. The signal is generated with sum of multiple sources. Then, this signal is applied to balun and the spectrum at the input of every block is calculated in Matlab. Since Cadence requires number of FFT points to be a power of two, it is not possible to calculate the spectrum in Cadence. The spectrum at the mixer input is shown in Fig. 100. Since the receiver is zero-IF, there is only one side visible at the low-pass filter input as shown in Fig. 101. The spectrum at the input of the variable gain amplifier and the analog-to-digital converter are shown in Figs. 102 and 103, respectively. Simulation results indicate that MTPR does not change in the receiver chain. Therefore, the linearity is limited by LNA. The MTPR at ADC input is 20.33 dB, which is 4 dB better than behavioral simulations.

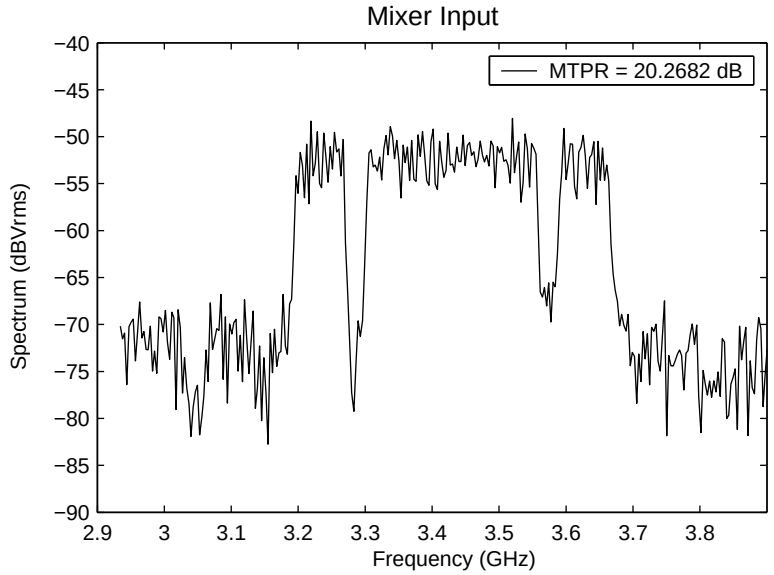

Fig. 100. Mixer Input Spectrum.

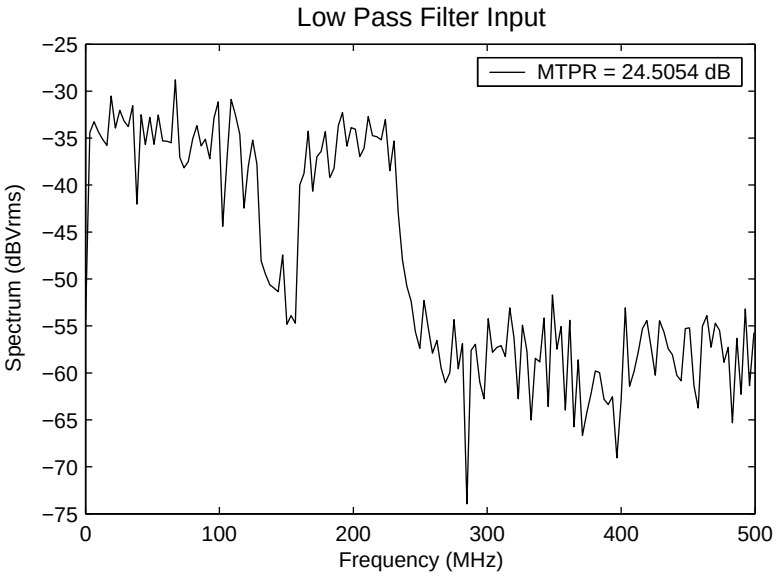

Fig. 101. Low-Pass Filter Input Spectrum.

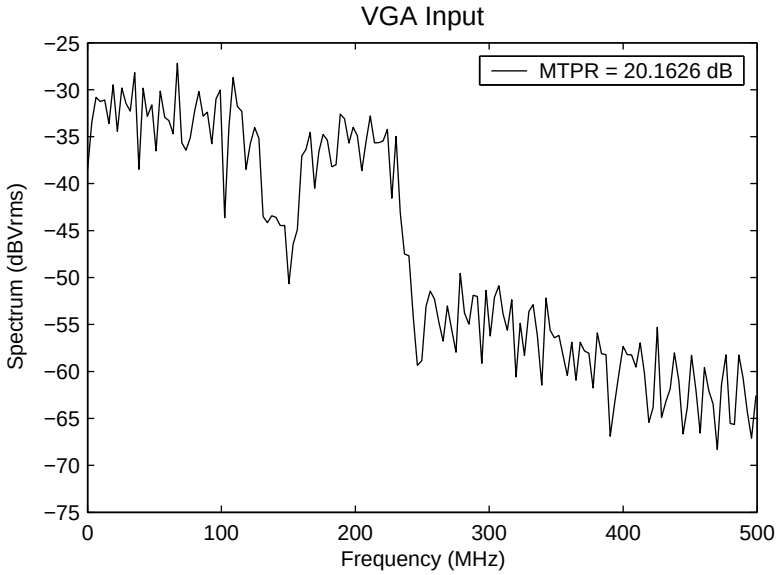

Fig. 102. Variable Gain Amplifier Input Spectrum.

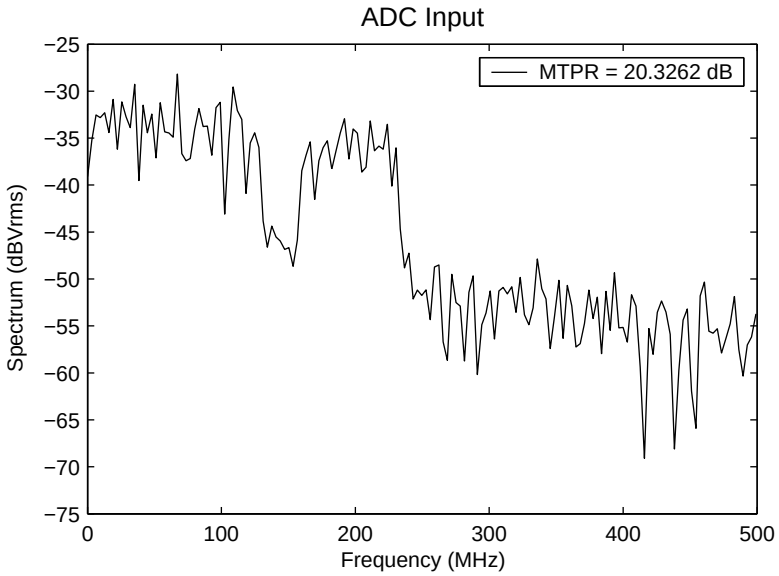

Fig. 103. Analog-to-Digital Converter Input Spectrum.

D. NBI Simulations

The IEEE 802.15 group issued the selection criteria of the UWB systems in the presence of interference [14]. According to the IEEE 802.15.3a physical selection criteria, the system must satisfy a packet error rate (PER) less than 8% for 1024 byte packets, when the interference power is at least 3 dB higher than the desired signal at a power 6 dB higher than the sensitivity level.

The performance of the adaptive NBI suppression is tested for the maximum mandatory data rate (200 Mb/s) of the proposal. The tests are evaluated for additive white Gaussian noise channel and four different multi-path channel realizations defined in [34]. Signal level is set to 6 dB higher than the sensitivity level for all simulations.

The overall simulation setup is depicted in Fig. 104. The randomly generated binary data is first coded using a convolutional encoder and tones are generated. After applying tone and symbol interleaving, QPSK modulation is performed and OFDM symbols are generated by inverse fast fourier transform (IFFT). Before upconversion, zero-padded cyclic prefix is added. The carrier frequency ω_c is switched to a different sub-band for every symbol according to the frequency hopping pattern. Since the interference is added at RF, it appears only in one sub-band. The received data is downconverted and out-of band signals are removed using a low-pass filter. Then the in-band interference is suppressed by tunable notch filter. VGA, ADC and AGC are used to quantize the signal and to set its level to maximize the dynamic range at the FFT input. The zero-padded cyclic prefix is removed by overlap-and-add technique before FFT. In the simulations the NBI is detected ideally, therefore, the initial performance degradation due to the notch filter tuning algorithm is not taken into account. This is a reasonable assumption, since the degradation effects only first

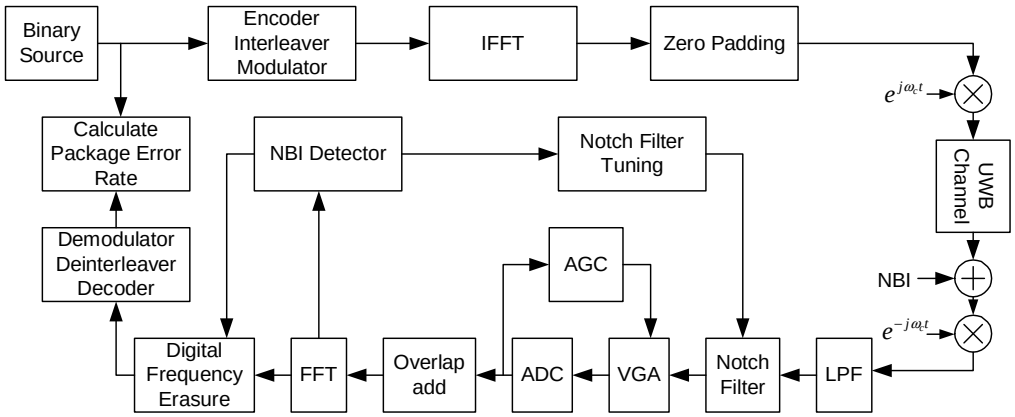

Fig. 104. Overall Simulation Setup.

couple of symbols. When the filter performance is learned by the algorithm, the notch filter will be tuned at the first couple of iterations. The tones affected by interference are then erased, since they are not reliable anymore. Finally, the data is recovered by demodulating, deinterleaving and decoding. The packet error rate is calculated by comparing the generated data with the recovered one.

The ADC number of bits is calibrated to ensure that the effect of the quantization noise is added into the simulations. Since the UWB signal's PAR is 9 dB, the optimum ADC number of bits is between 4 and 5 according to the Table X. The simulation results shown in Fig. 105 indicate that using 5 bit instead of 4 bit increases the performance only slightly. Therefore, ADC is selected as 4-bit.

Two different interference suppression schemes were tested. In the first scheme the notch filter is tuned to the interference frequency and kept on for all sub-bands. The other scheme is based on turning the filter on only during the sub-band that is affected by interference. Since the filter is off during the other sub-bands, a performance improvement is expected compared to the other scheme.

The baseband signal in the presence of interference is shown in Fig. 106. A notch filter with 4 MHz bandwidth can not reduce the interference properly as shown in

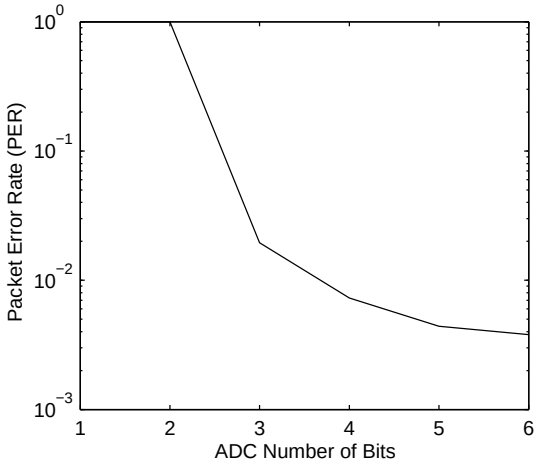

Fig. 105. Packet Error Rate (PER) vs. ADC Number of Bits.

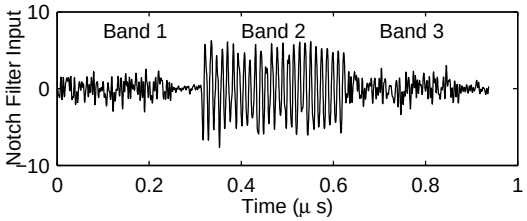

Fig. 106. Time-domain Waveform before the Notch Filter.

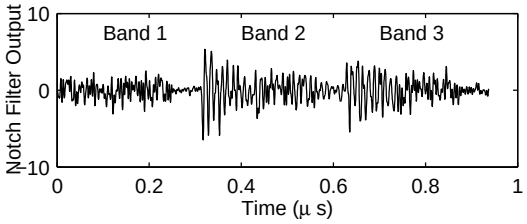

Fig. 107. Time-domain Waveform after the Notch Filter with 4 MHz Bandwidth.

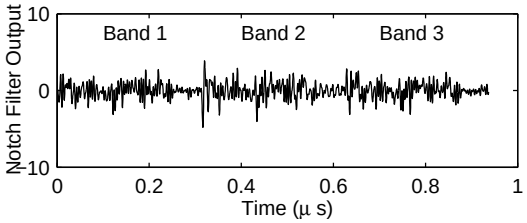

Fig. 108. Time-domain Waveform after the Notch Filter with 40 MHz Bandwidth.

Fig. 107. Moreover, the notch filter also creates ringing at the adjacent sub-band if the filter is not turned off during the adjacent sub-band. In Fig. 108, the same interference level is used but the bandwidth increased to 40 MHz. The ringing is reduced for the sub-band affected by interference and the adjacent sub-band even if the filter is on all the time.

The bandwidth of the filter is swept from 4 MHz to 100 MHz, and the resulting package error rate is shown in Figs. 109 and 110 for the first and second scheme, respectively. The optimum bandwidth is 30 MHz for the first scheme, but it is not a strong optimum point. The bandwidth between 20 MHz to 40 MHz almost gives the same performance. Therefore the sensitivity of the system performance regarding to the bandwidth is low. The optimum bandwidth is also increased as SIR decreases. The reason is that at low SIR levels, the settling of the filter degrades the performance. At higher SIR levels, the optimum bandwidth reduces, because the ringing is a less serious problem and smaller bandwidth will not attenuate the tone adjacent to the interference frequency. For the second scheme, there is no strong optimum value. Above 50 MHz, the PER is almost constant for low SIR levels. The performance degradation due to the attenuation of adjacent tones is more visible for high SIR.

The overall performance improvement is determined for AWGN and multi-path channels. The multi-path channels are separated according to their delay variation. CM1, CM2, CM3 and CM4 are very low, low, typical and very high multi-path channels, respectively. Since each multi-path channel realization has 100 different paths, the simulations are performed for every path and the PER is averaged to obtain the overall PER.

The filter bandwidth is selected as 30 MHz for the first scheme and 50 MHz for the second scheme. In order to determine the filter performance at high SIR, the notch filter is not turned off, when the interference power is low. In AWGN channel

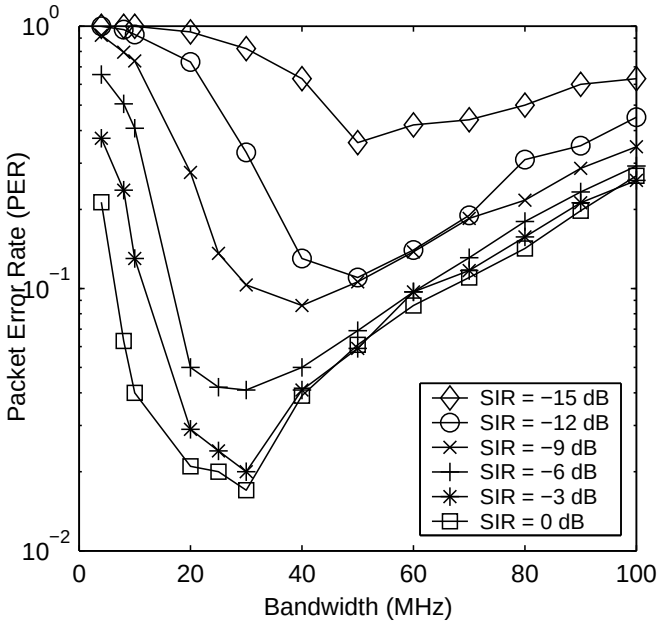

Fig. 109. Packet Error Rate (PER) vs. Notch Filter Bandwidth (scheme 1).

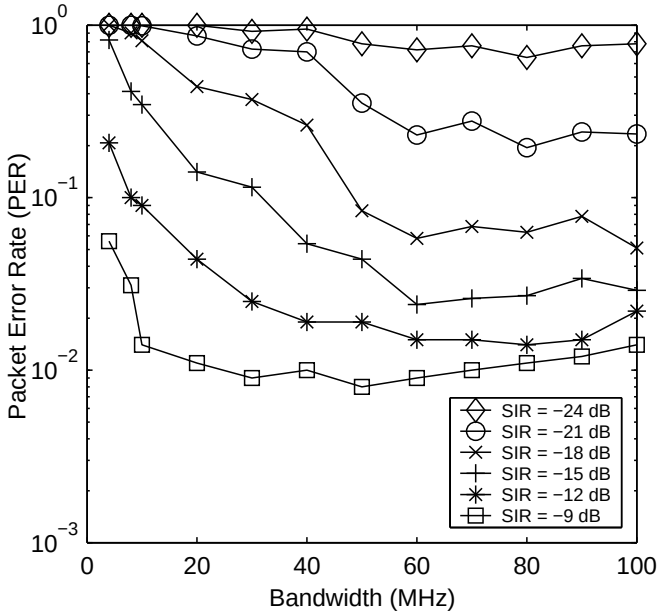

Fig. 110. Packet Error Rate (PER) vs. Notch Filter Bandwidth (scheme 2).

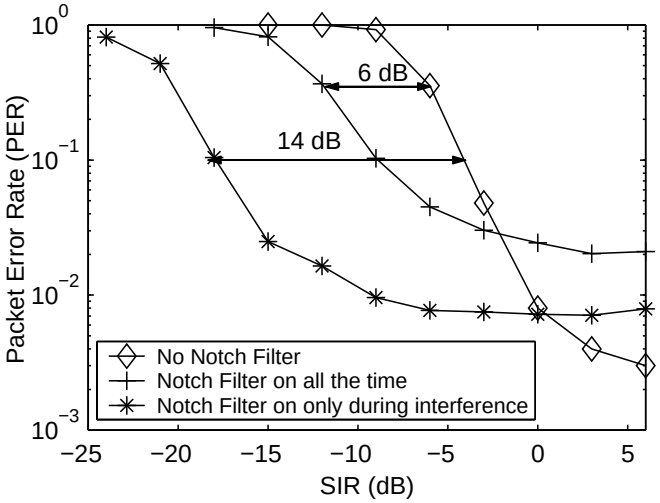

Fig. 111. PER vs. SIR in AWGN Channel.

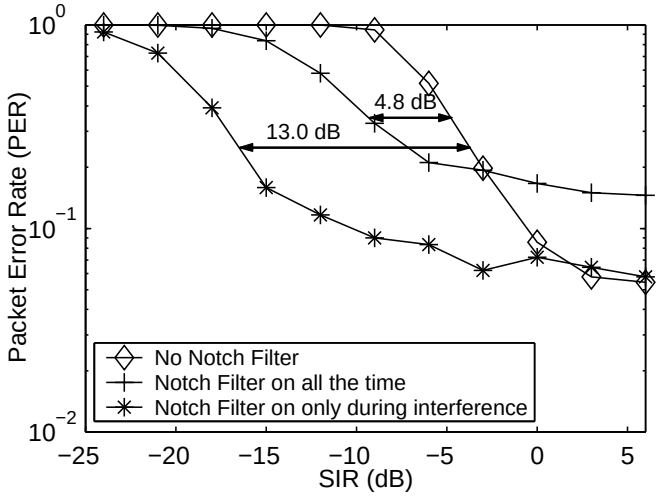

Fig. 112. PER vs. SIR in CM1 Channel.

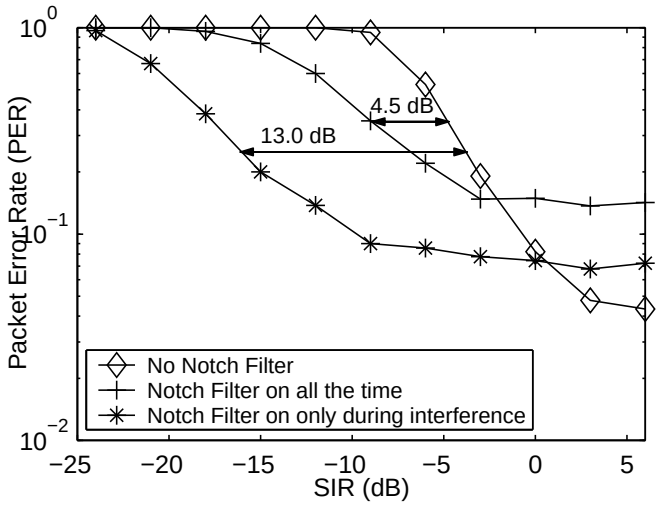

Fig. 113. PER vs. SIR in CM2 Channel.

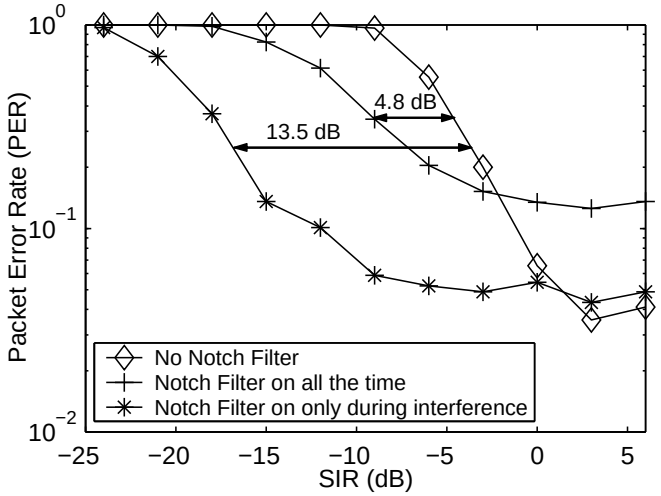

Fig. 114. PER vs. SIR in CM3 Channel.

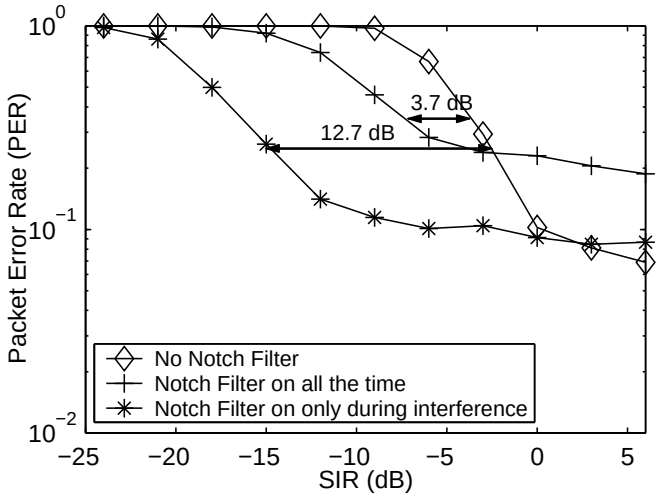

Fig. 115. PER vs. SIR in CM4 Channel.

shown in Fig. 111, the signal-to-noise ratio improvement is 6 dB and 14 dB for first and second schemes, respectively. The improvement decreases for multi-path channels as indicated on the Figs. 112–115.

The threshold to activate the suppression scheme is the SIR level when the PER with notch filter equals to the PER without notch filter. The simulation results indicate that the threshold for switching on the filter is −2 dB SIR, when the filter is on all the time, and 0 dB, when the filter is on only during the interference exists in the baseband. Since the threshold is −2 dB or 0 dB SIR, the interference detection is performed by comparing the interference level with spectrum density of the received signal.

CHAPTER VIII

CONCLUSION

In this dissertation, a MB-OFDM UWB receiver with narrowband interference suppression was presented. The suppression was performed in analog domain prior to ADC using a tunable notch filter. Most of the published interference suppression schemes have been proposed for spread spectrum systems and based on removing NBI in the digital domain. Since frequency hopping systems have been instantaneously narrow-band, research on interference rejection for frequency hopping systems was limited. However, MB-OFDM is a wideband frequency hopping system and utilized instantaneously 528 MHz band. This huge bandwidth makes it susceptible to NBI.

In Chapter II, MB-OFDM UWB proposal was discussed and its parameters related to this work were summarized. The sensitivity of MB-OFDM was also derived using communication theory. It has also been shown that the digital baseband of the proposed MB-OFDM UWB system was compatible with MB-OFDM standard. The background of receivers with emphasis on zero-IF receivers was recapitulated in Chapter III. The issues of zero-IF architecture were presented and potential solutions were discussed. Noise, linearity and simulation techniques were discussed in Chapter IV. Since integrated circuits are designed in voltage domain, the noise equations have been rewritten in noise voltage spectral density and voltage gain. It has been shown that single and two tone tests were not adequate to capture the effect of nonlinearity on the multi-tone signal. Therefore, MTPR has been used to quantify linearity of individual blocks in receive chain. Since noise and nonlinearity simulations require spectrum analysis a systematical approach for spectrum analysis has been presented. Following noise and linearity, two approaches based on summation of sinusoidal sources and filtering Gaussian source, was presented to generate desired

phase noise response. It has been found that filtering the Gaussian noise is faster but less accurate than summation of sinusoidal sources.

The design of MB-OFDM UWB receiver with interference suppression was discussed in Chapter V. In the first section, MB-OFDM receiver design was presented. First, required gain, noise figure and dynamic range were calculated. Out-of band interferences were analyzed and it has been found that 802.11a interference determined the order of low-pass filter in the baseband. It has been found that the linearity of overall system might limit maximum signal-to-noise ratio, since the intermodulation products of OFDM tones were in the band. System level simulations indicated minimum -15 dBVrms IIP3 and IIP2 were required for proper operation. Maximum tolerable gain and phase imbalances were also determined by system level simulations and found as 2 dB and 10 degrees. Since every block had a finite cut-off frequency, the overall frequency response was determined not only by low-pass filter but also other blocks, such as variable gain amplifier. It has been found that other block's 3-dB frequency should be at least 420 MHz in order to guarantee that cut-off frequency is determined by low-pass filter. The advantage of huge bandwidth was that the out-of band blockers are at least 264 MHz away from local oscillator. Since the phase noise of oscillator at 264 MHz offset has been very low, the adjacent blocker was not downconverted into desired channel. Since max SNR was limited by ADC's quantization noise, phase noise should be less than -85 dBc/Hz at 100KHz in order to not limit maximum SNR. The quantization noise was calculated by integrating the quantization noise at each step due to multi tone nature of OFDM signal. For optimum performance at least 4-bit ADC was required. Once system level requirements were determined, overall gain, noise and linearity was distributed across the receive chain using spreadsheet. The NBI suppression scheme was presented in the second section. Since NBI has appeared as spikes in frequency domain, FFT processor was

used to locate it. It was showed that NBI could be detected by comparing the spike level with predetermined level, if signal-to-interference level is below 0 dB. Different approximations and orders of notch filters were investigated and it was found second order filter gives minimum complexity and settling time. Notch bandwidth was optimized to minimize overall packet-error-rate. It has been found that optimum bandwidth was a function of interference level and received signal-to-noise ratio.

Package modeling and circuit level implementations were discussed in Chapter VI. The package and bondwire parasitics were analyzed separately. The inductance of package pins has been negligible and their capacitances dominated package parasitics. On the other hand, inductance of bondwires was dominant and determined the total inductance between the chip and the external world. Bondwire parasitics were found to be dependent on the pad location, and they were extracted using 3-D electromagnetic simulator. The extraction data was used to optimize pad locations. To minimize the number of pins for controllability, a digital control block was also added. This block allowed increased observability without increasing number of pins. Bias current for individual blocks was generated internally using a novel current reference generator.

In Chapter VII, the experimental and simulation results were discussed. The current reference was characterized between 20°C and 100°C. The measured current deviation was less than ±100 nA. Whole system was also simulated at behavioral and transistor level. The simulated noise figure of the whole receiver was 5.8 dB, which was very close to the spreadsheet value. IIP2 and IIP3 were 15.15 dBVrms and -5 dBVrms, respectively. Two different NBI suppression scheme was tested. In the first scheme the notch filter was on all the time. The other scheme was based on turning on the notch filter only during the sub-band that has been affected by NBI. The notch filter was optimized for minimum package-error-rate. The optimum bandwidth was

30 MHz for first scheme. Second scheme did not show strong optimum point and the performance did not change above 50 MHz notch bandwidth. Simulation results indicated that the signal-to-noise ratio has been improved 6 dB for the first scheme and 14 dB for the second scheme.

The proposed MB-OFDM UWB solution was implemented using TSMC 0.18μm CMOS process. The results indicate significant performance improvement in the presence of NBI for low signal-to-interference ratio. As a future work, the suppression scheme might be implemented in narrowband frequency hopping systems, where NBI could degrade performance.

REFERENCES

[1] Federal Communications Commission, "Part 15 - radio frequency devices," Tech. Rep., Aug. 2003, http://www.access.gpo.gov/nara/cfr/waisidx_06/47cfr15_06.html.

[2] R. Fisher, R. Kohno, H. Ogawa, H. Zhang, K. Takizawa, and et al., "DS-UWB physical layer submission to 802.15 task group 3a," Working draft proposed standard, July 2004, ftp://ftp.802wirelessworld.com/15/.

[3] A. Batra, J. Balakrishnan, A. Dabak, R. Gharpurey, J. Lin, and et al., "Multi-band OFDM physical layer proposal," Working draft proposed standard, Sept. 2004, ftp://ftp.802wirelessworld.com/15/.

[4] Myricom Inc., "Test report for the lan interface card, m3f2-pcixe-2," Tech. Rep., Jan. 2004, http://www.myri.com/myrinet/regulatory/M3F2-PCIXE-2.pdf.

[5] "Reply comments of time domain corporation in the matter of revision of part 15 of the fcc's rules regarding ultra-wideband transmission systems," Tech. Rep., Time Domain Corporation, Feb. 1999.

[6] Laurence B. Milstein, "Interference rejection techniques in spread spectrum communications," *Procedings of the IEEE.*, vol. 76, pp. 657–671, June 1988.

[7] J. D. Laster and J. H. Reed, "Interference rejection in digital wireless communications," *IEEE Signal Processing Magazine*, vol. 14, pp. 37–62, May 1997.

[8] Frank M. Hsu and Arthur M. Giordano, "Digital whitening techniques for improving spread-spectrum communications performance in the presence of narrow-band jamming and interference," *IEEE Transaction on Communications*, vol. 26, pp. 209–216, Feb. 1978.

[9] Maurice J. Bouvier, "The rejection of large interferers in spread spectrum systems," *IEEE Transaction on Communications*, vol. 26, pp. 254–256, Feb. 1978.

[10] Laurence B. Milstein and Pankaj K. Das, "An analysis of a real-time transform domain filtering digital communication system-part i: Narrow-band interference rejection," *IEEE Transaction on Communications*, vol. 28, pp. 816–824, June 1980.

[11] Naoki Kurita, Iwao Sasae, and Shinsaku Mori, "Suppression of narrow-band interference in ffh systems by hard-limited combining receiver using transversal filters," in *IEEE Int'l Conf. on Selected Topics in Wireless Communications.*, June 1992, pp. 445–448.

[12] Ronald A. Iltis, James A. Ritchey, and Laurence B. Milstein, "Interference rejection in ffh systems using least squares estimation techniques," *EEE Transaction on Communications.*, vol. 38, pp. 2174–2183, Dec. 1990.

[13] Reza Pasand, John Nielsen, and Abu Sesay, "UWB receiver based on filter bank architecture for suppression of narrowband interference noise," in *MILCOM 2004*, Oct. 2004, pp. 579–585.

[14] J. Ellis, K. Siwiak, and R. Roberts, "P802.15.3a alt phy selection criteria," Tech. Rep., IEEE, Dec. 2002.

[15] J. G. Proakis, *Digital Communications*, McGraw-Hill, New York, NY, fourth edition, 2001.

[16] J. K. Omura and B. K. Levitt, "Code error probability evaluation for antijam communication systems," *IEEE Transaction on Communications*, vol. 30, pp. 896–903, May 1982.

[17] Edwin H. Armstrong, "The super-heterodyne - its origin, development, and some recent improvements," *Proceedings of the IRE*, vol. 12, pp. 539–552, Oct. 1924.

[18] Behzad Razavi, "Design considerations for direct-conversion receivers," *IEEE Transactions on Circuit and Systems*, vol. 6, pp. 428–435, June 1997.

[19] K. Anvari, M. Kaube, and B. Hriskevich, "Performace of a direct conversion receiver with $\pi/4$-dqpsk modulated signal," in *Proc. IEEE Vehicular Tech. Conf.*, May 1991, pp. 822–827.

[20] H. T. Friis, "Noise figure of radio receivers," *Proc/ IRE*, vol. 32, pp. 419–422, July 1944.

[21] Ali Hajimiri and Thomas H. Lee, *The Design of Low Noise Oscillators*, Kluwer Academic Publishers, Norwell, MA, first edition, 1999.

[22] José Carlos Pedro and Nuno Borges de Carvalho, "On the use of multitone techniques for assessing rf components' intermodulation distortion," *IEEE Transactions on Microwave Theory and Techniques*, vol. 47, pp. 2393–2402, December 1999.

[23] Stephen A. Maas, *Nonlinear microwave circuits*, Artech House, Inc., Norwood, MA, 1th edition, 1988.

[24] J. G. Proakis and D. G. Manolakis, *Digital Signal Processing*, Prentice Hall, New Jersey, third edition, 1996.

[25] M. L. Schiff, "Spectral analysis using digital fft techniques," *SystemView Times*, vol. 2, April 1997.

[26] R. J. van de Plassche, *CMOS Integrated Analog-to-Digital and Digital-to-Analog Converters*, Springer, New York, second edition, 2003.

[27] D. F. Elliott and K. R. Rao, *Fast Transforms Algorithms, Analyses, Applications*, Academic Press, Orlando, FL, first edition, 1982.

[28] L. B. Jackson, *Signals, Systems, and Transforms*, Addison-Wesley Publishing Company, New Jersey, first edition, 1991.

[29] B. Liu, *Digital Filters and The Fast Fourier Transform*, Halsted Press, New York, first edition, 1975.

[30] N. Jeremy Kasdin, "Discrete simulation of colored noise and stochastic processes and $1/f^{\alpha}$ power law noise generation," *The Proceedings of the IEEE*, vol. 83, pp. 802–827, May 1995.

[31] A. Moschitta and D. Petri, "Stochastic properties of quantization noise in memoryless converters affected by integral nonlinearity," *IEEE Transaction on Instrumentation and Measurement*, vol. 52, pp. 1302–1307, Aug. 2003.

[32] Myricom Inc., "Test report for the lan switch, m3-clos-encl," Tech. Rep., Nov. 2004, http://www.myri.com/myrinet/regulatory/M3-CLOS-ENCL.pdf.

[33] M. Dirjish, "Cabinets, enclosures, & backplanes-no housing shortage for the electronics market," *Electronic Design*, Nov. 2003.

[34] Andreas F. Molisch, "P802.15.4a channel model subgroup final report," Tech. Rep., IEEE, Sept. 2004.

[35] Andreas F. Molisch, "P802.15.4a channel model subgroup final report," Tech. Rep., IEEE, Sept. 2004.

[36] Theodore L. Deliyannis, Yichuang Sun, and J. Kel Fidler, *Continuous-Time Active Filter Design*, CRC Press, New York, NY, first edition, 1999.

[37] EIA/JEDEC, "Bond wire modeling standard," June 1997.

[38] D. Hilbiber, "A new semiconductor voltage standard," *ISSCC Dig. Of Tech. Papers*, vol. 83, pp. 32–33, May 1964.

[39] A. P. Brokaw, "A simple three-terminal IC bandgap reference,," *IEEE J. Solid-State Circuits*, vol. SC-9, pp. 388–393, Dec 1974.

[40] C. H. Lee and H. J. Park, "All-cmos temperature independent current reference,," *Electronics Letters*, vol. 32, Jul 1996.

[41] Behzad Razavi, *Design of Analog CMOS Integrated Circuits*, McGraw-Hill, New York, NY, first edition, 2001.

APPENDIX A

VERILOG CODE OF DIGITAL CONTROL BLOCK

```
// Verilog HDL for "UWB", "I2C" "behavioral"

‘define TRUE  1’b1
‘define FALSE  1’b0

//STATE Definitions
‘define S0 2’d0
‘define S1 2’d1
‘define S2 2’d2

module I2Cext (SCL, SDA, DATAout0, DATAout1, DATAout2, DATAout3,
DATAout4, DATAout5, DATAout6, DATAout7, DATAout8, DATAout9,
DATAout10, DATAout11, DATAout12, DATAout13, DATAout14, DATAout15,
DATAout16, DATAout17, DATAout18, DATAout19, DATAout20, DATAout21,
DATAout22, DATAout23, DATAout24, DATAout25, DATAout26, DATAout27,
DATAout28, DATAout29, DATAout30, DATAout31, psupa, nsupa);

input SCL, SDA, psupa, nsupa;
output [7:0] DATAout0, DATAout1, DATAout2, DATAout3, DATAout4;
output [7:0] DATAout5, DATAout6, DATAout7, DATAout8, DATAout9;
output [7:0] DATAout10, DATAout11, DATAout12, DATAout13, DATAout14;
output [7:0] DATAout15, DATAout16, DATAout17, DATAout18, DATAout19;
output [7:0] DATAout20, DATAout21, DATAout22, DATAout23, DATAout24;
output [7:0] DATAout25, DATAout26, DATAout27, DATAout28, DATAout29;
output [7:0] DATAout30, DATAout31;

reg [7:0] DATAout0, DATAout1, DATAout2, DATAout3, DATAout4;
reg [7:0] DATAout5, DATAout6, DATAout7, DATAout8, DATAout9;
reg [7:0] DATAout10, DATAout11, DATAout12, DATAout13, DATAout14;
reg [7:0] DATAout15, DATAout16, DATAout17, DATAout18, DATAout19;
reg [7:0] DATAout20, DATAout21, DATAout22, DATAout23, DATAout24;
reg [7:0] DATAout25, DATAout26, DATAout27, DATAout28, DATAout29;
reg [7:0] DATAout30, DATAout31;

reg [2:0] STATE;
reg START, STOP;
reg [12:0] TMPREG;
reg [4:0] i;

//STOP
always @(posedge SDA or posedge START or negedge SCL)
begin
  if (START == ‘TRUE)
```

```
  STOP =  ‘FALSE;
  else if (SCL == 1’b0)
    STOP =  ‘FALSE;
  else
    STOP =  ‘TRUE;
end

//START
always @ (negedge SDA or negedge SCL)
begin
  if (SCL == 1’b0)
    START= ‘FALSE;
  else
    START= ‘TRUE;
end

//STATES
always @(posedge SCL or posedge STOP or posedge START)
begin
  if (START == ‘TRUE)
    begin
      i=5’d0;
      STATE=‘S1;
    end
  else if (STOP == ‘TRUE)
    begin
      i=5’d0;
      STATE=‘S0;
    end
  else
    begin
      case (STATE)
        ‘S0:   begin
            i=5’d0;
            STATE=‘S0;
            DATAout0=DATAout0;
            DATAout1=DATAout1;
            DATAout2=DATAout2;
            DATAout3=DATAout3;
            DATAout4=DATAout4;
            DATAout5=DATAout5;
            DATAout6=DATAout6;
            DATAout7=DATAout7;
            DATAout8=DATAout8;
            DATAout9=DATAout9;
            DATAout10=DATAout10;
            DATAout11=DATAout11;
            DATAout12=DATAout12;
            DATAout13=DATAout13;
            DATAout14=DATAout14;
            DATAout15=DATAout15;
```

```
    DATAout16=DATAout16;
    DATAout17=DATAout17;
    DATAout18=DATAout18;
    DATAout19=DATAout19;
    DATAout20=DATAout20;
    DATAout21=DATAout21;
    DATAout22=DATAout22;
    DATAout23=DATAout23;
    DATAout24=DATAout24;
    DATAout25=DATAout25;
    DATAout26=DATAout26;
    DATAout27=DATAout27;
    DATAout28=DATAout28;
    DATAout29=DATAout29;
    DATAout30=DATAout30;
    DATAout31=DATAout31;
    TMPREG=13'd0;
  end
`S1:   begin
    case(i)
    0: begin TMPREG[0] = SDA; i=5'd1; STATE=`S1; end
    1: begin TMPREG[1] = SDA; i=5'd2; STATE=`S1; end
    2: begin TMPREG[2] = SDA; i=5'd3; STATE=`S1; end
    3: begin TMPREG[3] = SDA; i=5'd4; STATE=`S1; end
    4: begin TMPREG[4] = SDA; i=5'd5; STATE=`S1; end
    5: begin TMPREG[5] = SDA; i=5'd6; STATE=`S1; end
    6: begin TMPREG[6] = SDA; i=5'd7; STATE=`S1; end
    7: begin TMPREG[7] = SDA; i=5'd8; STATE=`S1; end
    8: begin TMPREG[8] = SDA; i=5'd9; STATE=`S1; end
    9: begin TMPREG[9] = SDA; i=5'd10; STATE=`S1; end
    10: begin TMPREG[10] = SDA; i=5'd11; STATE=`S1; end
    11: begin TMPREG[11] = SDA; i=5'd12; STATE=`S1; end
    12: begin TMPREG[12] = SDA; i=5'd0; STATE=`S2; end
    endcase
  end
`S2:  begin
    case (TMPREG[4:0])
    5'd0:begin DATAout0[7:0]=TMPREG[12:5]; end
    5'd1:begin DATAout1[7:0]=TMPREG[12:5]; end
    5'd2:begin DATAout2[7:0]=TMPREG[12:5]; end
    5'd3:begin DATAout3[7:0]=TMPREG[12:5]; end
    5'd4:begin DATAout4[7:0]=TMPREG[12:5]; end
    5'd5:begin DATAout5[7:0]=TMPREG[12:5]; end
    5'd6:begin DATAout6[7:0]=TMPREG[12:5]; end
    5'd7:begin DATAout7[7:0]=TMPREG[12:5]; end
    5'd8:begin DATAout8[7:0]=TMPREG[12:5]; end
    5'd9:begin DATAout9[7:0]=TMPREG[12:5]; end
    5'd10:begin DATAout10[7:0]=TMPREG[12:5]; end
    5'd11:begin DATAout11[7:0]=TMPREG[12:5]; end
    5'd12:begin DATAout12[7:0]=TMPREG[12:5]; end
    5'd13:begin DATAout13[7:0]=TMPREG[12:5]; end
```

```
    5'd14:begin DATAout14[7:0]=TMPREG[12:5]; end
    5'd15:begin DATAout15[7:0]=TMPREG[12:5]; end
    5'd16:begin DATAout16[7:0]=TMPREG[12:5]; end
    5'd17:begin DATAout17[7:0]=TMPREG[12:5]; end
    5'd18:begin DATAout18[7:0]=TMPREG[12:5]; end
    5'd19:begin DATAout19[7:0]=TMPREG[12:5]; end
    5'd20:begin DATAout20[7:0]=TMPREG[12:5]; end
    5'd21:begin DATAout21[7:0]=TMPREG[12:5]; end
    5'd22:begin DATAout22[7:0]=TMPREG[12:5]; end
    5'd23:begin DATAout23[7:0]=TMPREG[12:5]; end
    5'd24:begin DATAout24[7:0]=TMPREG[12:5]; end
    5'd25:begin DATAout25[7:0]=TMPREG[12:5]; end
    5'd26:begin DATAout26[7:0]=TMPREG[12:5]; end
    5'd27:begin DATAout27[7:0]=TMPREG[12:5]; end
    5'd28:begin DATAout28[7:0]=TMPREG[12:5]; end
    5'd29:begin DATAout29[7:0]=TMPREG[12:5]; end
    5'd30:begin DATAout30[7:0]=TMPREG[12:5]; end
    5'd31:begin DATAout31[7:0]=TMPREG[12:5]; end
    endcase
    i=5'd0;
    STATE=`S0;
  end
default:begin
    i=5'd0;
    STATE=`S0;
    DATAout0=DATAout0;
    DATAout1=DATAout1;
    DATAout2=DATAout2;
    DATAout3=DATAout3;
    DATAout4=DATAout4;
    DATAout5=DATAout5;
    DATAout6=DATAout6;
    DATAout7=DATAout7;
    DATAout8=DATAout8;
    DATAout9=DATAout9;
    DATAout10=DATAout10;
    DATAout11=DATAout11;
    DATAout12=DATAout12;
    DATAout13=DATAout13;
    DATAout14=DATAout14;
    DATAout15=DATAout15;
    DATAout16=DATAout16;
    DATAout17=DATAout17;
    DATAout18=DATAout18;
    DATAout19=DATAout19;
    DATAout20=DATAout20;
    DATAout21=DATAout21;
    DATAout22=DATAout22;
    DATAout23=DATAout23;
    DATAout24=DATAout24;
    DATAout25=DATAout25;
```

```
            DATAout26=DATAout26;
            DATAout27=DATAout27;
            DATAout28=DATAout28;
            DATAout29=DATAout29;
            DATAout30=DATAout30;
            DATAout31=DATAout31;
            TMPREG=13'd0;
          end
        endcase
    end
end
endmodule
```

APPENDIX B

DIGITAL CONTROL REGISTERS

Table XXI. UWB1 Digital Control Registers.

Address		Default Value	Operation
00000	Bit 7 - Bit 0	0010 0010	Control pins for bandgap reference. Sets the bandgap voltage
00001	Bit 7	1	PLL I channel VCO output
	Bit 6	1	PLL Q channel VCO output
	Bit 5	1	PLL I channel Mixer output
	Bit 4	1	PLL Q channel Mixer output
	Bit 3	0	Power Down for bandgap set 0 for normal operation
	Bit 2 - Bit 0	100	Set the resistor of current source of bandgap. Lower this value to increase the resistance value which results in decrease of the current reference.
00010	Bit 7 - Bit 6	N/A	Not Used
	Bit 5	0	Power Down for LPF set 0 for normal operation
	Bit 4 - Bit 0	10101	Set the cutoff frequency of LPF

Table XXI. Continued.

Address		Default Value	Operation
00011	Bit 7 - Bit 0	0000 0000	1st bandpass of Band Reject Filter notch frequency
00100	Bit 7 - Bit 0	0000 0000	2nd bandpass of Band Reject Filter notch frequency
00101	Bit 7 - Bit 0	0000 0000	3rd bandpass of Band Reject Filter notch frequency
00110	Bit 7	N/A	Not Used
	Bit 6	1	PLL control switch
	Bit 5	1	Sets symbol clock source 1: Turns on internal source. 0: Turns on external source.
	Bit 4	1	PLL set
	Bit 3	0	PLL reset
	Bit 2	0	PLL 792
	Bit 1	0	PLL 264-
	Bit 0	1	PLL 264+
00111	Bit 7	0	ADC power down set 0 for normal operation
	Bit 6	0	ADC clock source 0: uses external clock 1: uses internal clock
	Bit 5 - Bit 0	11 1111	VGA Gain settings 11 1111: highest gain 00 0000: lowest gain

Table XXI. Continued.

Address		Default Value	Operation
01000	Bit 7	1	Current Generator TEST1 1 : uses EXT1 pin as a current source 0: applies internal current source to EXT1 pin
	Bit 6	1	Current Generator TEST2 1 : uses EXT2 pin as a current source 0: applies internal current source to EXT2 pin
	Bit 5 - Bit 4	00	LNA current source
	Bit 3 - Bit 2	00	Mixer current source
	Bit 1 - Bit 0	00	LPF current source
01001	Bit 7 - Bit 6	00	BRF current source
	Bit 5 - Bit 4	00	PLL1 current source
	Bit 3 - Bit 2	00	PLL2 current source
	Bit 1 - Bit 0	00	PLL3 current source
01010	Bit 7 - Bit 6	00	ADC current source
	Bit 5 - Bit 4	00	VGA current source
	Bit 3 - Bit 2	00	VGA exp ctrl
	Bit 1 - Bit 0	00	VGA bias ctrl

Table XXI. Continued.

Address		Default Value	Operation
01011	Bit 7 - Bit 4	0000	ADC bias p
	Bit 3 - Bit 0	0000	ADC bias n
01100	Bit 7 - Bit 0	0000 0000	BRF f_range
01101	Bit 7 - Bit 0	N/A	Not Used
01110	Bit 7 - Bit 4	0011	LNA bias
	Bit 3	N/A	Not Used
	Bit 2	0	Mixer power down
			0: normal operation
	Bit 1	0	LNA power down
			0: normal operation
	Bit 0	0	LNA Gain
			0 = high gain
			1 = low gain
01111	Bit 7 - Bit 4	0011	Mixer bias p
	Bit 3 - Bit 0	0011	Mixer bias n
10000	Bit 7 - Bit 6	01	VGA 1st stage common mode set
	Bit 5	1	VGA 1st stage p offset pd
	Bit 4 - Bit 3	11	VGA 1st stage p offset control
	Bit 2	11	VGA 1st stage n offset pd
	Bit 1 - Bit 0	11	VGA 1st stage n offset control

Table XXI. Continued.

Address		Default Value	Operation
10001	Bit 7 - Bit 6	01	VGA 2nd stage common mode set
	Bit 5	1	VGA 2nd stage p offset pd
	Bit 4 - Bit 3	11	VGA 2nd stage p offset control
	Bit 2	11	VGA 2nd stage n offset pd
	Bit 1 - Bit 0	11	VGA 2nd stage n offset control
10010	Bit 7 - Bit 6	01	VGA 3rd stage common mode set
	Bit 5	1	VGA 3rd stage p offset pd
	Bit 4 - Bit 3	11	VGA 3rd stage p offset control
	Bit 2	11	VGA 3rd stage n offset pd
	Bit 1 - Bit 0	11	VGA 3rd stage n offset control
10011	Bit 7	N/A	Not used
	Bit 5 - Bit 4	001	BRF Filt_1_sel
	Bit 3	N/A	Not used
	Bit 2 - Bit 0	000	BRF Filt_2_sel
10100	Bit 7	0	BRF BP Control
	Bit 6 - Bit 4	001	BRF Clock Control
	Bit 3	N/A	Not used
	Bit 2 - Bit 0	000	BRF Filt_3_sel

Table XXI. Continued.

Address		Default Value	Operation
10101	Bit 7 - Bit 0	N/A	Not Used
10110	Bit 7 - Bit 0	N/A	Not Used
10111	Bit 7 - Bit 0	N/A	Not Used
11000	Bit 7 - Bit 0	N/A	Not Used
11001	Bit 7 - Bit 0	N/A	Not Used
11010	Bit 7 - Bit 0	N/A	Not Used
11011	Bit 7 - Bit 0	N/A	Not Used
11100	Bit 7 - Bit 0	N/A	Not Used
11101	Bit 7 - Bit 0	N/A	Not Used
11110	Bit 7 - Bit 0	N/A	Not Used
11111	Bit 7 - Bit 0	N/A	Not Used

APPENDIX C

MATLAB CODE TO GENERATE MTPR TEST SIGNAL

```
%Baseband signal

clear all;

%System Specification
IIP2=20; %in dBVrms
IIP3=0; %in dBVrms

%Calculate System Parameters
a1=1;
a2=-a1/10^(IIP2/20); %IIP2
a3=-4*a1/(3*10^(IIP3/10)); %IIP3

%Create Amplitudes
A=ones(1,128/2);
%set DC to zero
A(1)=0;
%Missing tone numbers
b=40:50;
A(b)=0;

df=528e6/128;
fs=528e6;
N=fs/df;

f=0:df:fs/2-df;
t=1/fs:1/fs:1/df;

k=1;
NPRtest=2;
while NPRtest > 1,
    PARtest=2;
       while PARtest > 1,
            phsig=rand(1,N/2)*2*pi;
            signal=0;
            for i=1:N/2,
                signal=signal+A(i)*sin(2*pi*f(i)*t+phsig(i));
            end
            PAR=20*log10(max(abs(signal))/std(signal));
            if PAR < 8.99 || PAR > 9.01
                PARtest=0;
            end
        end
```

```
        %Save Signal
        for i=1:N
            signalM(k,i)=signal(i);
        end

        %Set input peak to peak 1
        input=signal/max(abs(signal))/2;

        %Calculate spectrum at the output
        out=a1*input+a2*input.^2+a3*input.^3;
        fouttmp=fft(out)*2/N;
        fout=fouttmp(1:N/2);

        %Calculate distortion products density in the missing band
        Pfout=abs(fout).^2;
        Dmis=sum(Pfout(b))/length(b);
        %Calculate tone density in the band
        Dtone=(sum(Pfout(2:(b(1)-1)))...
        +sum(Pfout((b(length(b))+1):N/2)))/(N/2-length(b));
        NPR=10*log10(Dtone/Dmis);

        disp(sprintf('NPR = %0.5g dB', NPR));

        NPRM(k)=NPR;
        k=k+1;

        if k > 1000
            NPRtest=0;
        end
end

%Select the signal with worst NPR
WNPRi=find(NPRM==min(NPRM));
for i=1:N,
    signal(i)=signalM(WNPRi,i);
end

%File Operations
FID=fopen('source.in','w');
fprintf(FID,'simulator lang=spectre\n');
for i=2:N/2/2,
fprintf(FID,...
'IS%d (1 0) isource dc=0 type=sine ampl=%d freq=%6.0f ...
sinephase=%6.20f\n',i,A(i),f(i),phsig(i)*180/pi);
end
fprintf(FID,'RL1 (1 0) resistor r=1\n');
fprintf(FID,'EBUF (vin 0 1 0) vcvs gain=%1.20f\n'...
,-1/max(abs(signal))/2);
fclose(FID);
```

```
%Calculate & Print Information
input=signal/max(abs(signal))/2;

fsignaltmp=fft(input)*2/N;
fsignal=fsignaltmp(1:N/2);

disp(sprintf('Worst Case NPR = %0.5g dB', NPRM(WNPRi)));

out=a1*input+a2*input.^2+a3*input.^3;
fouttmp=fft(out)*2/N;
fout=fouttmp(1:N/2);

%Plot Signals
figure(1);
plot(1e9*t,input);
fig1xlabel=xlabel('Time (ns)');
fig1ylabel=ylabel('Amplitude');

figure(2);
plot(1e-6*f,20*log10(abs(fsignal)));
xlabel('Frequency (MHz)');
ylabel('Amplitude');

figure(3);
plot(1e-6*f,20*log10(abs(fout)));
xlabel('Frequency (MHz)');
ylabel('Amplitude');

[fig4]=figure(4);
hist(NPRM,10);
xlabel('MBT (dB)');
ylabel('Number of Occurrence');
```

APPENDIX D

MATLAB CODE TO GENERATE PACKAGE INPUT FILE

```
%generate input file for fasthenry
%based on jesd59 standard

clear all;

%enter die height (in mm)
h2=0.25;
%enter bondwire heigth (in mm)
h1=0.15;

%enter bondwire parameters
sigma=1e-3/22.14e-9; %1/mm/Ohm
bondR=2.54e-2; %(in mm) 1 mil diameter
w=(bondR/2)*sqrt(pi);
h=(bondR/2)*sqrt(pi);

%enter pin locations (x,y) (in mm)
pin=[-3.75,-4.475;...       %1
        -3.25,-4.475;...    %2
        -2.75,-4.475;...    %3
        -2.25,-4.475;...    %4
        -1.75,-4.475;...    %5
        -1.25,-4.475;...    %6
        -0.75,-4.475;...    %7
        -0.25,-4.475;...    %8
        0.25,-4.475;...     %9
        0.75,-4.475;...     %10
        1.25,-4.475;...     %11
        1.75,-4.475;...     %12
        2.25,-4.475;...     %13
        2.75,-4.475;...     %14
        3.25,-4.475;...     %15
        3.75,-4.475;...     %16
        4.475,-3.75;...     %17
        4.475,-3.25;...     %18
        4.475,-2.75;...     %19
        4.475,-2.25;...     %20
        4.475,-1.75;...     %21
        4.475,-1.25;...     %22
        4.475,-0.75;...     %23
        4.475,-0.25;...     %24
        4.475,0.25;...      %25
        4.475,0.75;...      %26
```

```
        4.475,1.25;...      %27
        4.475,1.75;...      %28
        4.475,2.25;...      %29
        4.475,2.75;...      %30
        4.475,3.25;...      %31
        4.475,3.75;...      %32
        3.75,4.475;...      %33
        3.25,4.475;...      %34
        2.75,4.475;...      %35
        2.25,4.475;...      %36
        1.75,4.475;...      %37
        1.25,4.475;...      %38
        0.75,4.475;...      %39
        0.25,4.475;...      %40
        -0.25,4.475;...     %41
        -0.75,4.475;...     %42
        -1.25,4.475;...     %43
        -1.75,4.475;...     %44
        -2.25,4.475;...     %45
        -2.75,4.475;...     %46
        -3.25,4.475;...     %47
        -3.75,4.475;...     %48
        -4.475,3.75;...     %49
        -4.475,3.25;...     %50
        -4.475,2.75;...     %51
        -4.475,2.25;...     %52
        -4.475,1.75;...     %53
        -4.475,1.25;...     %54
        -4.475,0.75;...     %55
        -4.475,0.25;...     %56
        -4.475,-0.25;...    %57
        -4.475,-0.75;...    %58
        -4.475,-1.25;...    %59
        -4.475,-1.75;...    %60
        -4.475,-2.25;...    %61
        -4.475,-2.75;...    %62
        -4.475,-3.25;...    %63
        -4.475,-3.75;...    %64
    ];

%enter pad locations (x,y)
pad=[-1.539,-1.936;...      %1
        -1.377,-1.936;...   %2
        -1.215,-1.936;...   %3
        -1.053,-1.936;...   %4
        -0.891,-1.936;...   %5
        -0.729,-1.936;...   %6
        -0.405,-1.936;...   %7
        -0.081,-1.936;...   %8
        0.081,-1.936;...    %9
        0.405,-1.936;...    %10
```

```
0.729,-1.936;...    %11
0.891,-1.936;...    %12
1.053,-1.936;...    %13
1.215,-1.936;...    %14
1.377,-1.936;...    %15
1.539,-1.936;...    %16
1.936,-1.539;...    %17
1.936,-1.377;...    %18
1.936,-1.215;...    %19
1.936,-1.053;...    %20
1.936,-0.891;...    %21
1.936,-0.729;...    %22
1.936,-0.405;...    %23
1.936,-0.081;...    %24
1.936,0.081;...     %25
1.936,0.405;...     %26
1.936,0.729;...     %27
1.936,0.891;...     %28
1.936,1.053;...     %29
1.936,1.215;...     %30
1.936,1.377;...     %31
1.936,1.539;...     %32
1.539,1.936;...     %33
1.377,1.936;...     %34
1.215,1.936;...     %35
1.053,1.936;...     %36
0.729,1.936;...     %37
0.567,1.936;...     %38
0.243,1.936;...     %39
0.081,1.936;...     %40
-0.243,1.936;...    %41
-0.405,1.936;...    %42
-0.729,1.936;...    %43
-0.891,1.936;...    %44
-1.053,1.936;...    %45
-1.215,1.936;...    %46
-1.377,1.936;...    %47
-1.539,1.936;...    %48
-1.936,1.539;...    %49
-1.936,1.377;...    %50
-1.936,1.215;...    %51
-1.936,1.053;...    %52
-1.936,0.891;...    %53
-1.936,0.729;...    %54
-1.936,0.405;...    %55
-1.936,0.081;...    %56
-1.936,-0.081;...   %57
-1.936,-0.405;...   %58
-1.936,-0.729;...   %59
-1.936,-0.891;...   %60
-1.936,-1.053;...   %61
```

```
        -1.936,-1.215;...   %62
        -1.936,-1.377;...   %63
        -1.936,-1.539;...   %64
    ];

%enter angle (alpha)
alpha=[80;80;80;80;80;80;80;80;...
    80;80;80;80;80;80;80;80;...
    80;80;80;80;80;80;80;80;...
    80;80;80;80;80;80;80;80;...
    80;80;80;80;80;80;80;80;...
    80;80;80;80;80;80;80;80;...
    80;80;80;80;80;80;80;80;...
    80;80;80;80;80;80;80;80;...
];

%Check parameters
pinsize=size(pin);
padsize=size(pad);
anglesize=size(alpha);

if pinsize(1)~=anglesize(1) || padsize(1)~=anglesize(1) ...
    error('Number of pins and pads must equal to the ...
number of angles');
end
for i=1:anglesize(1),
    if pin(i,1)==pad(i,1) && pin(i,2)==pad(i,2) ...
        error('Pin and Pad should have differen coordinates');
end
end

%calculate parameters
for i=1:anglesize(1),

    if pin(i,1)~=pad(i,1) && pin(i,2)~=pad(i,2)
        d=sqrt((pad(i,1)-pin(i,1)).^2+(pad(i,2)-pin(i,2)).^2);
        a=atan((pad(i,2)-pin(i,2))/(pad(i,1)-pin(i,1)));
        d1=h1*cot(alpha(i,1)*pi/180);
        d2=h1*cot(alpha(i,1)*pi/180)+d/8;
        x1(i,:)=[pad(i,1),pad(i,2),h2];

        if pad(i,1) > pin(i,1)
            x2(i,1)=-cos(a)*d1+pad(i,1);
            x2(i,2)=-sin(a)*d1+pad(i,2);
            x3(i,1)=-cos(a)*d2+pad(i,1);
            x3(i,2)=-sin(a)*d2+pad(i,2);
        else
            x2(i,1)=cos(a)*d1+pad(i,1);
            x2(i,2)=sin(a)*d1+pad(i,2);
            x3(i,1)=cos(a)*d2+pad(i,1);
            x3(i,2)=sin(a)*d2+pad(i,2);
```

```
        end

        x2(i,3)=h1+h2;

        x3(i,3)=h1+h2;

        x4(i,:)=[pin(i,1),pin(i,2),0];

    elseif pin(1)==pad(1)
        d=abs(pin(i,2)-pad(i,2));
        d1=h1*cot(alpha(i,1)*pi/180);
        d2=h1*cot(alpha(i,1)*pi/180)+d/8;
        x1(i,:)=[pad(i,1),pad(i,2),h2];

        x2(i,1)=pad(i,1);
        x2(i,2)=pad(2)+sign(pin(2)-pad(2))*d1;
        x2(i,3)=h1+h2;

        x3(i,1)=pad(i,1);
        x3(i,2)=pad(i,2)+sign(pin(i,2)-pad(i,2))*d2;
        x3(i,3)=h1+h2;

        x4(i,:)=[pin(1),pin(2),0];

    else
        d=abs(pin(i,1)-pad(i,1));
        d1=h1*cot(alpha(i,1)*pi/180);
        d2=h1*cot(alpha(i,1)*pi/180)+d/8;
        x1(i,:)=[pad(i,1),pad(i,2),h2];

        x2(i,1)=pad(i,1)+sign(pin(i,1)-pad(i,1))*d1;
        x2(i,2)=pad(i,2);
        x2(i,3)=h1+h2;

        x3(i,1)=pad(i,1)+sign(pin(i,1)-pad(i,1))*d2;
        x3(i,2)=pad(i,2);
        x3(i,3)=h1+h2;

        x4(i,:)=[pin(i,1),pin(i,2),0];
    end
end


%create file
FID=fopen('qfn64.inp','w');
fprintf(FID,'*fasthenry test file\n');
fprintf(FID,'.Units mm\n');
fprintf(FID,'*Frequency range of interest\n');
fprintf(FID,'.freq fmin=1e9 fmax=10e9 ndec = 1\n');
for i=1:anglesize(1),
fprintf(FID,'Nbw_%d_0 x=%6.20f y=%6.20f z=%6.20f\n',...
```

```
i,x1(i,1),x1(i,2),x1(i,3));
fprintf(FID,'Nbw_%d_1 x=%6.20f y=%6.20f z=%6.20f\n',...
i,x2(i,1),x2(i,2),x2(i,3));
fprintf(FID,'Nbw_%d_2 x=%6.20f y=%6.20f z=%6.20f\n',...
i,x3(i,1),x3(i,2),x3(i,3));
fprintf(FID,'Nbw_%d_3 x=%6.20f y=%6.20f z=%6.20f\n',...
i,x4(i,1),x4(i,2),x4(i,3));
fprintf(FID,'Ebw_%d_0 Nbw_%d_0 Nbw_%d_1 w=%6.20f h=%6.20f ...
sigma=%6.20f nwinc=1 nhinc=1\n',i,i,i,w,h,sigma);
fprintf(FID,'Ebw_%d_1 Nbw_%d_1 Nbw_%d_2 w=%6.20f h=%6.20f ...
sigma=%6.20f nwinc=1 nhinc=1\n',i,i,i,w,h,sigma);
fprintf(FID,'Ebw_%d_2 Nbw_%d_2 Nbw_%d_3 w=%6.20f h=%6.20f s ...
igma=%6.20f nwinc=1 nhinc=1\n',i,i,i,w,h,sigma);
end
for i=1:anglesize(1),
fprintf(FID,'.External Nbw_%d_0 Nbw_%d_3\n',i,i);
end
fprintf(FID,'.end\n');
fclose(FID);
```

APPENDIX E

AUTOMATIC GAIN CONTROL MATLAB CODE

```
function [agccontrol] = agcdecide(rms)
%AGC Lookup Table
%LNA 2 gain settings 0dB and 33dB => LNActrl = 1 or 2
%VGA 51 gain settings between 0dB and 50dB => VGActrl = 1 to 51
RMSfin=0.5/(10^(9/20));
RMS=rms(1);
Gainpre=20*log10(rms(2));
checkstart=rms(3);
checkmode=rms(4);
count=rms(5);
preRMSsum=rms(6);
if checkstart == 1
    RMSnor=RMS/(10^(Gainpre/20));
    if RMSnor < RMSfin/(10^(75/20))
        Gain=75;
        mode=1;
    else
        if checkmode == 1 % 11 mode
            error=[abs((10.^((0:83)/20))*RMSnor-RMSfin)];
            Gain=find(error==min(error))-1;
            mode=1;
            count=0;
            if abs(Gain-Gainpre) <2
                Gain=Gainpre;
                mode=2;
                count=0;
            end
        else
            if count == 10
                RMSnor=sqrt(RMSnor.^2+preRMSsum.^2)/sqrt(11);
                error=[abs((10.^((0:83)/20))*RMSnor-RMSfin)];
                Gain=find(error==min(error))-1;
                mode=2;
                preRMSsum=0;
                count=0;
                if abs(Gain-Gainpre) <2
                    Gain=Gainpre;
                    mode=2;
                end
                if abs(Gain-Gainpre) >6
                    Gain=Gainpre;
                    mode=1;
                end
```

```
            else
                Gain=Gainpre;
                count=count+1;
                preRMSsum=sqrt(preRMSsum.^2+RMSnor.^2);
                mode=2;
            end
        end
    end
else
    Gain=Gainpre;
    mode=1;
    count=0;
    preRMSsum=0;
end

if Gain < 33
    LNActrl=0;
    VGActrl=Gain;
else
    LNActrl=33;
    VGActrl=Gain-33;
end

agccontrol=[10^(LNActrl/20) 10^(VGActrl/20) mode count preRMSsum];
```

VITA

Burak Kelleci received the B.S. and M.Sc. degrees in electrical and communication engineering from Istanbul Technical University, Istanbul, Turkey, in 1998 and 2001, respectively. Between 2002 and 2007, he worked toward the Ph.D. degree at Texas A&M University, College Station, in the Analog and Mixed Signal Center (AMSC). From 1998 to 2000, he was with ITU ETA Foundation ASIC Design Center, Istanbul, Turkey as a Design Engineer. In 2000, he joined Alcatel-Teletas Microelectronic Design Center as a RFIC Design Engineer. During the summer of 2004, he worked at Conexant in the System on Chip Group. He is currently employed by Texas Instruments, Dallas. His current research interests include analog and mixed signal circuits and systems, wireless communication systems, and high-frequency circuit design. He can be reached through the Department of Electrical and Computer Engineering, Texas A&M University, College Station, TX.